Summer 8-13-2021

Cardio-Renal Syndrome Type 2: The Role of Cardiac Spinal Afferent Reflex

Zhiqiu Xia
University of Nebraska Medical Center

Cardio-Renal Syndrome Type 2:
The Role of Cardiac Spinal Afferent Reflex

by

Zhiqiu Xia

A DISSERTATION

Presented to the Faculty of the University of Nebraska Graduate College

in Partial Fulfillment of the Requirements

for the Degree of Doctor of Philosophy

Cellular and Integrative Physiology

Graduate Program

Under the Supervision of Professor Hanjun Wang

University of Nebraska Medical Center

Omaha, Nebraska

August 2021

Supervisory Committee:

Irving H. Zucker, Ph.D.	Steven J. Lisco, M.D.
Steven C. Sansom, Ph.D.	Wallace B. Thoreson, Ph.D.

ACKNOWLEDGEMENTS

I would like to start with the most invaluable person to the completion of my doctoral degree, my mentor, Dr. Hanjun Wang. Thank you for all the guidance, and support and being a wonderful advisor throughout the past five years. The commitment and enthusiasm of science has always inspired me. I wish to extend my deepest gratitude to my supervisory committee, Dr. Irving Zucker, who always provides important perspectives in my research and career goal; Dr. Steven Lisco, who offers clinical perspectives all the time; Dr. Steven Sansom, who offers excellent scientific insight into the pathology of kidney diseases; Dr. Wallace Thoreson for valuable input related to neuronal regulation. Thank you all for your valuable time, perspectives, and expertise that help continually refine my research in every committee meeting and correspondence. I am sincerely grateful to have you as my committee, and you all have been a wonderful influence on me.

I gratefully acknowledge the contributions of Dr. Erika Boesen for teaching me about GFR measurement and histological analysis. I am also thankful to Dr. Matthew Zimmerman, who is always approachable and guides me throughout the whole training since my first day in the IPMM program.

I recognize and thank every current and past member of Dr. Wang's and Dr. Zucker's labs. I would like to thank Tara Rudebush, for the help with animal management. I would like to thank Bryan Hackfort for the help with echocardiography. I would like to thank Kaye Talbitzer for her help with all the rat surgeries of myocardial infarction.

I would like to thank the office staff in the Department of Cellular and Integrative Physiology and Anesthesiology for their effort with all the administrative work.

Special thanks to Dr. Carver David and Kelly Swoboda for their tremendous support and understanding.

And most of all, I would like to thank my family and my friends, for their unconditional support, patience, and believing in me. This journey would not have been possible without them.

ABSTRACT

Cardio-Renal Syndrome Type 2: The Role of Cardiac Spinal Afferent Reflex

Zhiqiu Xia, University of Nebraska Medical Center, 2021

Supervisor: Hanjun Wang, M.D.

Cardio-renal syndrome type 2 (CRS type 2) is defined as a chronic cardiovascular disease, usually chronic heart failure (CHF), resulting in chronic kidney disease. We hypothesized that the cardiac spinal afferent reflex (CSAR), a cardiogenic sympatho-excitatory reflex mediated by cardiac spinal afferents plays a critical role in the development of CRS type 2. We examined the effects of acute activation and chronic ablation of the CSAR on renal blood flow (RBF), renal vascular resistance (RVR), central venous pressure (CVP), renal function and renal histology in sham and myocardial infarction (MI)-induced CHF rats. RNA sequencing analysis (RNA-Seq) and validation by real-time PCR in renal tissues were used to identify the potential molecular mechanisms underlying the effects of the CSAR on renal function in CHF. We found that acute CSAR activation increased RVR to a greater extent in CHF rats compared to sham rats. Chronic CSAR ablation with the epicardial application of a selective afferent neurotoxin resiniferatoxin (RTX) at the time of myocardial infarction (MI), in part, restored RBF and reduced RVR in CHF rats. Furthermore, epicardial RTX largely prevented the development of renal dysfunction 4-5 months post-MI. RNA-Seq analysis showed that renal injury, inflammatory, hypoxia, and apoptotic genes were significantly upregulated in the renal tissue of CHF rats, which was largely restored by RTX. Renal congestion as indexed by increased CVP in CHF+vehicle rats was significantly attenuated by epicardial RTX. These data suggest that CSAR ablation by epicardial RTX has a selective protective effect on renal proximal tubular damage in the setting of CHF by partially restoring renal cortical blood flow and ameliorating renal congestion. In addition, CSAR ablation by intra-stellate ganglia (SG) injection 4 weeks after MI had similar renal protective effects on

renal tubular damage in CHF rats, suggesting a translational potential of CSAR ablation in the post-MI state. To examine whether renal denervation (RDN) mimics the beneficial effects of CSAR ablation in CHF, unilateral RDN was performed in CHF rats. We observed that unilateral RDN mitigated renal dysfunction, by preventing the deterioration of glomerular filtration rate (GFR) and by attenuation of the gene expression of kidney damage marker. Unilateral RDN also improved the cardiac function of CHF rats. On the other hand, we carried out a systematic analysis of clinical trials to assess the effectiveness and risks of bilateral RDN in patients with CHF with reduced ejection fraction. Our calculation showed that RDN significantly improved the symptoms of CHF as evidenced by decreases in New York Heart Association (NYHA) class and increased six-minute walk distances. This meta-analysis also showed echocardiographic improvements in left ventricular function and congestion after RDN, suggesting that these echocardiographic improvements could drive symptomatic improvement. Moreover, RDN decreased systolic and diastolic blood pressure (BP) as well as heart rate (HR) without affecting renal function. In summary, the current study suggests that both CSAR ablation and RDN may have translational potential in the treatment of patients with CRS type 2.

TABLE OF CONTENTS

LIST OF FIGURES

LIST OF TABLES

LIST OF ABBREVIATIONS

ACEI	angiotensin-converting enzyme inhibitor
Actb	actin beta
Adra1d	alpha-1d adrenergic receptor
ATF3	activating transcription factor 3
AKI	acute kidney injury
Ang II	angiotensin II
ANS	autonomic nervous system
ANTHEM-HF	Autonomic Neural Regulation Therapy of Enhance Myocardial Function in Heart Failure
AP	arterial pressure
ARB	angiotensin II receptor blocker
Atf3	activating transcription factor 3
Avpr2	arginine vasopressin receptor 2
BAT	baroreflex activation therapy
BK	bradykinin
BP	blood pressure
BUN	blood urea nitrogen
CHF	chronic heart failure
Chk1	Checkpoint Kinase 1

CI	confidence interval
CKD	chronic kidney disease
CRS	cardio-renal syndrome
CSAR	cardiac spinal afferent reflex
CSAR	cardiac spinal afferent reflex
CVD	cardiovascular disease
CVP	central venous pressure
CVP	central venous pressure
DBP	diastolic blood pressure
DRG	dorsal root ganglia
EF	ejection fraction
Epo	erythropoietin
FITC	fluorescein isothiocyanate
FS	fractional shortening
GFR	glomerular filtration rate
GO	gene ontology
HF	Heart failure
HFpEF	heart failure with preserved ejection fraction
HFrEF	heart failure with reduced ejection fraction
Hif1a	hypoxia-inducible factor 1 alpha

Hif3a	hypoxia-inducible factor 3 alpha
HK-2	human proximal tubule cells
Hmox1	heme oxygenase 1
HR	heart rate
HR	heart rate
IL-12	interleukin 12
Il1b	interleukin 1 beta
Il6	interleukin 6
iNos	inducible nitric oxide synthases
INOVATE-HF	Increase of Vagal Tone in Congestive Heart Failure
IQR	interquartile range
KIM-1	kidney injury molecule-1
LAD	and left atrium diameter
LVEDD	left ventricular end-diastolic diameter
LVEDP	left ventricular end-diastolic pressure
LVEF	left ventricular ejection fraction
LVESD	left ventricular end-systolic diameter
LVESP	left ventricular end-systolic pressure
MAP	mean arterial pressure
MD	mean difference

MI	myocardial infarction
MOOSE	Meta-Analyses of Observational Studies in Epidemiology
NE	norepinephrine
NECTAR-HF	Neural Cardiac Therapy for Heart Failure
Ngal	neutrophil gelatinase-associated lipocalin
NOS	Newcastle-Ottawa Scale
NT-pro BNP	N-terminal-pro b-type natriuretic peptide
NYHA	New York Heart Association
PAS	periodic acid-Schiff
PRISMA	Preferred Reporting Items for Systematic Reviews and Meta-Analyses
RAAS	renin-angiotensin-aldosterone system
RBF	renal blood flow
RBF	renal blood flow
RDN	renal denervation
RNA-Seq	RNA sequencing
RSNA	renal sympathetic nerve activity
RT-PCR	real time quantitative polymerase chain reaction
RTX	resiniferatoxin
RVR	renal vascular resistance
RVR	renal vascular resistance

SBP	systolic blood pressure
SD	standard deviation
SNS	sympathetic nervous system
STAT3	Signal Transducer and Activator of Transcription-3
TIM-1	T-cell immunoglobulin and mucin-containing molecule
Tnfa	tumor necrosis factor alpha
TRPV1	transient receptor potential vanilloid 1
URDN	unilateral renal denervation group
VNS	vagal nerve stimulation

INTRODUCTION

Chronic heart failure

Heart failure (HF) is defined as the inability of the heart to meet the requirement of tissues due to reduced contractile and/or filling function. Typical symptoms and signs of HF include dyspnea, exercise intolerance, leg swelling, and pulmonary congestion. Chronic heart failure (CHF) is one of the leading causes of death in the U.S. In addition to patient mortality and morbidity and lost productivity, the economic toll of treating this disease is enormous.[1]

Heart failure is divided into acute and chronic. Acute HF can result from abrupt worsening of chronic HF or de novo HF. On the other hand, CHF is usually caused by coronary artery disease, hypertension, valvular disease, myocarditis, congenital heart diseases, and infiltrative diseases. Based on the left ventricular ejection fraction (LVEF), CHF can be divided into two categories, which are HF with preserved ejection fraction (HFpEF) and HF with reduced ejection fraction (HFrEF). HFpEF is characterized by a normal LVEF and evidence of abnormal diastolic function, usually with LV concentric hypertrophy. HFrEF is characterized by systolic dysfunction, usually with LV eccentric remodeling. In HFrEF, LVEF is less than 40%. New York Heart Association (NYHA) Functional Classification describes the symptom severity of HF (**Table 1**).

Current pharmacological therapy for HF involves inhibition of renin-angiotensin-aldosterone system (RAAS) and sympathetic nervous system. In spite of the fact that the use of β-adrenergic blocking agents, angiotensin-converting enzyme inhibitor (ACEI) and angiotensin II receptor blockers (ARB) have been highly effective in slowing the progression of the disease and reducing mortality, there remains an extremely high mortality and morbidity rate for patients diagnosed with CHF.[2-4] Diuretics are one of the basic drugs used for heart failure treatment to ameliorate fluid retention. However, chronic use of diuretics along the progression of CHF lead to diuretic

resistance. Cardiac remodeling, renal dysfunction and increased sympathetic outflow have been demonstrated to be independent predictors of poor prognosis in patients with CHF.[5-10]

Table 1. New York Heart Association (NYHA) functional classification

NYHA class	**Symptoms**
I	No limitation in any physical activity
II	Mild limitation with normal activity
III	Marked limitation during daily activity, comfortable only at rest
IV	Severe limitations and symptoms even at rest, quite uncomfortable with any physical activity

Cardio-renal syndrome type 2

Renal dysfunction is highly prevalent among HF patients and is an independent prognostic factor in diastolic and systolic HF.[11, 12] The term cardio-renal syndrome (CRS) implies the interdependency of the heart and the kidneys.[6, 13-16] Based on primary failing organs and acuteness, CRS is divided into five subtypes. Types 1 and 2 describe acute and chronic cardiovascular disease (CVD) leading to acute kidney injury (AKI) or chronic kidney disease (CKD). Types 3 and 4, describe AKI and CKD, respectively leading primarily to HF. Finally, CRS type 5 describes a systemic insult to both heart and the kidneys, such as sepsis, where both organs are injured simultaneously in patients with previously normal heart and kidney function at baseline.

The current study focused on the neural mechanisms underlying CRS Type 1 and 2. The traditional dogma of how renal dysfunction develops in HF is that it results in large degree from heart failure-induced hypoperfusion of the kidneys. In addition, renal dysfunction in heart failure is now also thought to develop as a result of increased cardiac congestion, increased right atrial pressure and increased central venous pressure (CVP), which results in the development of renal venous hypertension, renal venous congestion, increased renal fibrogenesis, and eventually the loss of renal function. Renal venous congestion and loss of renal function in combination with (neuro)hormonal responses and potentially altered intra-abdominal and/or intrasplanchnic pressures which may contribute to fluid overload and increased venous return in a vicious cycle.

Many kidney damage biomarkers have been intensively investigated in the setting of CHF. KIM-1 and NGAL were shown to be associated with long-term mortality and recurrent heart failure hospitalization. These two biomarkers are more prevalent with the increase in the severity of New York Heart Association (NYHA) class, indicating that renal injury may contribute to the progression and development of the CRS.[17, 18] KIM-1, also known as T-cell immunoglobulin and mucin-containing molecule (TIM-1), is a type 1 cell membrane glycoprotein composed of an extracellular portion, transmembrane domain, and intracellular portion. KIM-1 is expressed at a

low level in normal kidneys, but in damaged kidneys, in both acute and chronic settings, it is specifically upregulated in injured proximal tubular cells. The cleaved ectodomain of KIM-1 excreted into urine makes it a noninvasive, specific and sensitive proximal tubular damage indicator while NGAL, another commonly used kidney damage marker, reflects both proximal tubular and distal tubular injury.

Medical therapy is divided into several classes of agents that have favorable effects on both the heart and the kidneys in the setting of CRS management. In general, evidence strongly supports the use of ACEI in both heart failure and renal disease. For those with ACEI intolerance, ARB play an important therapeutic role. However, despite early enthusiasm with dual therapy, the use of ACEI and ARBs together has resulted in an unfavorable risk/benefit ratio with higher rates of acute kidney injury, hyperkalemia, and hypotension.[19] Considerable effort has also been undertaken to understand the range of metabolic perturbations that occur in CKD and evaluation of modifications for renal and cardiac outcomes. However, to date, modifications of a single factor such as hemoglobin, parathyroid hormone, or reduction in oxidative stress have resulted in no demonstrable benefit for outcomes in the CRS leading to cessation of clinical development for these agents.[20-22] Therefore, it is critical to discover novel mechanisms underlying renal dysfunction in CHF and develop alternative effective therapies. In this dissertation, we promote the idea and provide evidence for direct neural crosstalk between the heart and kidney specifically through cardiac spinal afferents that contribute to the pathological development of renal dysfunction in the post (MI)/CHF state.

Autonomic modulation of cardiovascular system

The autonomic nervous system (ANS), which includes sympathetic and parasympathetic systems, plays a critical role in maintaining the homeostasis of the heart and vascular system in HF. In the failing heart, long-term overactivation of sympathetic system and attenuation of parasympathetic systems contribute to progression of cardiac dysfunction and neurohormonal dysregulation. Due to side effect and lack of specificity of current pharmacological strategies of CHF, there is an increasing interest in nonpharmacological approaches of ANS modulation for heart failure.

Baroreflex activation therapy (BAT)

The carotid baroreflex plays a critical role in the regulation of hemodynamics to maintain maintaining blood pressure and heart rate within a narrow physiologic range.[23-28] In the setting of CHF, the sensitivity of the normal inhibitory function of carotid baroreceptors is reduced , resulting in uninhibited sympathetic outflow.[29] Baroreceptor stimulation to treat CHF has been shown to be promising in initial human evaluation and animal studies.[25, 26] In a dog model of coronary microembolization-induced heart failure, baroreflex stimulation reduced plasma norepinephrine, reduced interstitial fibrosis and cardiomyocyte hypertrophy resulting in improvement in global LV function.[30] Currently, Barostim Neo System is the only FDA approved autonomic device to treat HFrEF.[29] In 2014, a small, single-center observational study by Gronda et al. showed improvement in baroreflex sensitivity, LVEF, NYHA class, quality of life and 6 min walk distance.[31] A larger randomized trial which included 146 patients with NYHA class III HF with LVEF $\leq$ 35% demonstrated that at the 6-month follow-up, BAT was associated with statistically significant improvement in 6 min hall walk distance and quality-of-life score, and NYHA functional class, and significant reduction in N-terminal-pro b-type natriuretic peptide (NT-pro BNP), suggesting that BAT has potential value in the treatment of CHF.[32] BAT protocols (unilateral or bilateral,

stimulation parameters), and selection of appropriate patients with CHF require future investigation by larger, prospective studies.

Cardiac spinal afferent denervation

Cardiac spinal afferents, whose cell bodies are located in the thoracic dorsal root ganglia (DRG), transmit the sensation of cardiac nociception to the spinal cord and up to the central nervous system through the sympathetic pathway when there is cardiac injury including myocardial ischemia, and CHF.[33, 34] In conditions of cardiac injury, bradykinin (BK), adenosine, and other substances released from the heart stimulate the afferent nerves resulting in increased sympathetic outflow, blood pressure (BP) and heart rate (HR).[34-37] Cardiac spinal afferents subserve dual functions; pain sensation during ischemia and both acute and chronic sympatho-excitation. Ablation of certain nociceptive neurons, while retaining all other sensory modalities and motor function, represents a new therapeutic approach to controlling severe pain/sensory dysfunction while avoiding off-target side effects. Transient receptor potential vanilloid 1 (TRPV1) is a nonselective cation channel with high calcium conductance expressed on peripheral and central terminals of small-diameter sensory neurons. Administration of the ultra-potent TRPV1 agonist, resiniferatoxin (RTX) to neuronal perikarya or nerve terminals induces calcium cytotoxicity and selective lesioning of the TRPV1-expressing nociceptive primary afferent population.[38, 39] This selective neural ablation has been coined "molecular neurosurgery" and has the advantage of sparing motor, proprioceptive, and other somatosensory functions that are important for coordinated movement, performing activities of daily living, and maintaining quality of life. We have successfully used the RTX chemoablation strategy to determine the role of these afferents on cardiac remodeling, sympatho-excitation, baroreflex function in the post MI/CHF state by selective ablation of cardiac spinal afferents.[33, 35, 40]

In the past two decades, studies from our laboratories have focused on a role of cardiac spinal afferents that mediate a sympatho-excitatory reflex in CHF.[41-45] These afferents are silent in the

normal state. Our studies and those of others have demonstrated that stimulation of these afferents increase sympathetic outflow, BP and HR and to decrease baroreflex sensitivity in a chronic manner in the CHF state.[41-47] We have also demonstrated that the discharge of cardiac spinal afferents is increased, and cardiac reflex responses are exaggerated in CHF, suggesting that these afferents are sensitized and are tonically active in CHF. More recently we published new evidence showing that chronic and selective ablation of cardiac TRPV1-positive afferents with the potent neurotoxin, RTX prevented the exaggerated renal and cardiac sympatho-excitation in rats with MI-induced CHF.[33, 35] These data strongly suggest that selective CSAR ablation may be clinically beneficial to the heart and kidneys in the setting of CHF.

Renal denervation

RDN is a minimally invasive endovascular procedure that is originally performed to treat resistant hypertension. Radiofrequency energy is applied using a specialized catheter throughout the length of renal arteries to damage both afferent and efferent renal nerves that traverse the renal arteries.[48] This procedure is well tolerated without significant side effects. Recently several randomized clinical studies have shown that RDN effectively reduces blood pressure compared regardless of the use of antihypertensives.[49-51] In addition, other cardiovascular diseases including CHF has also been proposed to be an indication for RDN.

Excessive activation of sympathetic nervous system in the setting of CHF is the main contributor to progressive cardiorenal syndrome associated with poor prognosis.[52-54] In the setting of CHF, increased renal efferent nerve activity induces renal vasoconstriction leading to renal hypoperfusion, which induces renin release, RAAS activation, sodium and water retention. [55, 56] Therefore, interventional procedure to downregulate adverse sympathetic signaling offers supplemental therapy for CHF patients who do not adhere to or respond well to contemporary pharmacotherapy.[57] Nonhuman animal models of HF demonstrated that surgical RDN improved cardiac function, improved renal blood flow, ameliorates renal damage, suppresses the

overactivation of RAAS, and increases sodium and water excretion, suggesting beneficial effects of RDN on chf.[55, 56, 58-66] Previous studies indicated that bilateral RDN improve exercise tolerance, attenuated the LV structural maladaptation and improved quality of life in patients with HF. [67-71] However, there have been no large, randomized controlled trials to evaluate the effects of RDN on renal function in the setting of CHF.

Vagal nerve stimulation (VNS)

VNS have shown beneficial effects in CHF because vagal nerves are responsible for regulation of cardiac contractility and sinus rate.[72, 73] In addition, VNS has also been used to stimulate vagal afferents for the treatment of several neurological diseases including migraine, depression, and seizures.[74-76] Animal studies of CHF showed that VNS was associated with improvement in ventricular contractility, improvement in heart rate variability and baroreflex sensitivity, attenuation of increased plasma norepinephrine (NE), anti-inflammatory effects and improved survival. [77-79] Three large clinical studies, ANTHEM-HF (Autonomic Neural Regulation Therapy of Enhance Myocardial Function in Heart Failure), NECTAR-HF (Neural Cardiac Therapy for Heart Failure), and INOVATE-HF (Increase of Vagal Tone in Congestive Heart Failure) demonstrate significant improvements in quality of life and improvement in NYHA class. However, the conclusions were not consistent in terms of significant improvement in LV contractility.[80-82] Overall, to improve the efficacy of VNS in HF, laterality (right versus left stimulation), stimulation methods (timing, frequency, intensity), choice of fibers (afferent versus efferent vagal fibers) are worth considering for further investigation.

Spinal cord stimulation (SCS)

SCS has been used in clinics to treat chronic pain and angina symptoms in patients with severe coronary artery disease.[83, 84] In addition, more and more evidence suggests that SCS has a cardioprotective effect probably through enhancement of the parasympathetic system.[85] In several

large animal models of heart failure, SCS significantly improved LVEF and decreased the incidence of ventricular arrhythmias.[86, 87] . In the SCS HEART first in-human study, Tse et al. investigated the effects of thoracic SCS in patients with NYHA class III HF and reduced LVEF (20%-35%). Their results demonstrated that thoracic SCS could improve HF symptoms, quality of life, LV contraction and remodeling in patients with severe systolic HF.[88] The mechanism underlying the regulatory role of SCS in autonomic tone is still unclear. Long-term safety, proper population of HF for SCS treatment and optimization of current procedure warrant further assessment in larger randomized controlled studies.

Hypothesis and specific aims

CRS type 2 is defined as a chronic cardiovascular disease (CVD), usually chronic heart failure (CHF), resulting in chronic kidney disease (CKD). We hypothesized that the CSAR, a cardiogenic sympatho-excitatory reflex mediated by cardiac spinal afferents plays a critical role in the development of CRS type 2. To address the hypothesis, we examined the effects of CSAR ablation on renal hemodynamics, and renal function in CHF rats. RNA sequencing analysis (RNA-Seq) and validation by real-time PCR in renal tissues were used to identify the potential molecular mechanisms underlying the effects of the CSAR on renal function in CHF. In addition, whether RDN mimics the beneficial effects of CSAR ablation on renal perfusion and renal function in CHF rats was examined. We also carried out a systematic analysis of clinical trials to evaluate bilateral RDN in patients with CHF with reduced ejection fraction.

Specific aims in this dissertation are summarized below.

Aim 1: To investigate the role of the CSAR in mediating the pathological development of renal impairment in rats with CRS type 2.

Aim 2: To examine the effect of renal denervation on changes in kidney damage and inflammation in rats with CHF.

Aim 3: To assess the effectiveness and risks of bilateral RDN in patients with chronic HFrEF.

CHAPTER 1: CARDIAC SYMPATHETIC AFFERENT DENERVATION ATTENUATS RENAL DYSFUNCTION IN RATS WITH CARDIO-RENAL SYNDROME TYPE 2

Introduction

CHF is a serious and debilitating disease associated with high morbidity and mortality and affects over six million Americans with over 660,000 new diagnoses each year[89]. About half of CHF patients also exhibit chronic renal dysfunction, prolonging hospitalization with a poor prognosis.[90] CRS describe the complex and bidirectional interaction between the heart and kidneys in acute and chronic conditions. Cardio-renal syndromes are divided into five categories, among which CRS types 1 and 2 involve acute and chronic CVD scenarios leading to acute kidney injury (AKI) or CKD. Insufficient renal perfusion due to impaired cardiac function, previously thought to be a primary hemodynamic precipitant in the development of renal dysfunction in CRS type 1 and 2, fails to explain the worsening renal function observed clinically [91]. In addition, venous congestion, and other major pathophysiological mechanisms, such as neurohormonal dysregulation, inflammation, and oxidative stress, also exert deleterious effects on both the heart and the kidneys.[90] However, the upstream factors that drive these changes in the setting of CHF are not completely understood.

The cardiac spinal afferent reflex (CSAR) is a pathological sympatho-excitatory reflex which is normally silent but becomes activated in CVD including hypertension, acute myocardial ischemia and congestive heart failure.[33, 42] Previous work from this laboratory confirmed the presence of tonically active cardiac afferent reflexes in rats with CHF that contribute to exaggerated cardiac and renal sympatho-excitation.[33, 42, 92] Chemical ablation of cardiac spinal afferents by epicardial application of RTX,[93] an ultrapotent analog of capsaicin which is capable of inducing rapid degeneration of transient receptor potential cation channel subfamily V member 1 (TRPV1)-expressing afferent neurons and fibers resulted in the attenuation of exaggerated renal and cardiac

sympatho-excitation and amelioration of adverse ventricular remodeling after myocardial infarction.[35] However, whether selective CSAR ablation offers beneficial effects on the CRS type 2 is unknown. The primary aim of this study was to investigate the role of the CSAR in mediating the pathological development of renal impairment in CRS type 2.

Methods

Rat model of chronic heart failure

All animal experiments was approved by the Institutional Animal Care and Use Committee of the University of Nebraska Medical Center and performed in accordance with the National Institutes of Health's *Guide for the Care and Use of Laboratory Animals*. Experiments were performed on adult, male, 400-500g Sprague-Dawley rats purchased from the Charles River Laboratories. Animals were housed on-site and given a one-week acclimation period prior to experimentation. Food and water were supplied *ad libitum*, and rats were on 12 hour light/dark cycles. The overall experimental protocol is outlined in **Figure 1**.

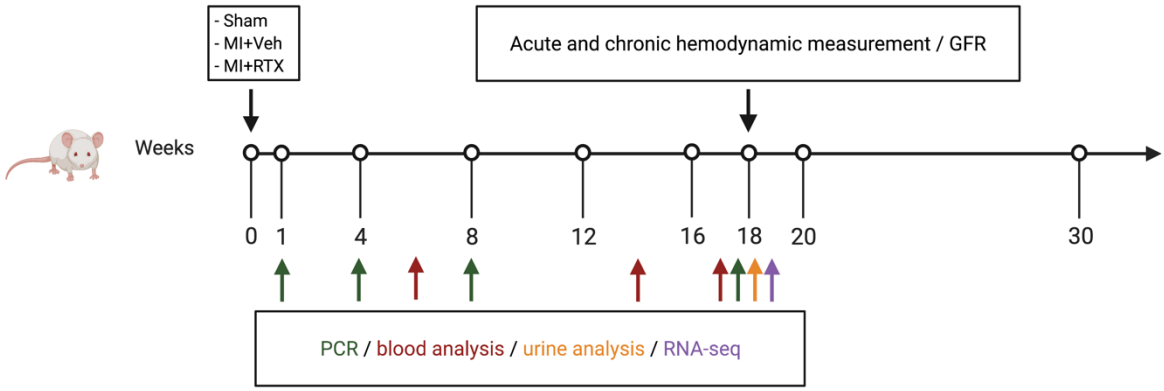

Figure 1. Schematic diagram of study design in Chapter 1.

Myocardial infarction (MI)-induced CHF was produced by coronary ligation as previously described.[35] Briefly, rats were anesthetized with 2-3% isoflurane-oxygen mixture during the surgical procedure with positive pressure mechanical ventilation at a rate of 60 breaths per min. A left thoracotomy was performed through the fifth intercostal space to expose the heart. The left anterior descending coronary artery was ligated with a 6-0 silk suture. The thorax was closed and intrapleural pressure was re-established. Buprenorphine (0.05 mg/kg, SC) was given once following surgery and on post-operative day 1 and 2 for alleviation of pain. Cardiac function including ejection fraction (EF) and fractional shortening (FS) were measured using high frequency echocardiography (VEVO 3100, Visual Sonics, Inc., Toronto, Ontario, Canada). At the terminal experiments, rat infarct size was determined as previously described.[35] The rats (n=16) with less than 15% infarct size were considered as mild infarction and excluded from this study.

Chronic cardiac sympathetic afferent desensitization by RTX

In a subgroup of the rats that were assigned to receive MI procedures, the epicardial application of resiniferatoxin (RTX, 50 μg/ml) was performed to desensitize the CSAR by afferent ablation as previously described.[35] Resiniferatoxin (Sigma-Aldrich, St Louis, MO, USA; 50 μg/ml) was painted twice on the entire surface of the left and right ventricles with a small brush just prior to coronary artery ligation. Vehicle (2 ml of ethanol mixed with 18 ml of Tween in isotonic saline) was painted on the ventricles as a control. The dose of RTX was determined in a previous study[35] in which we found nearly complete ablation of TRPV1-expressing cardiac nerve endings on the surface of the rat heart. The same dose of RTX also abolished functional activation of the CSAR by epicardial application of exogenous BK (10 μg/ml).[35]

Hemodynamic, renal blood flow measurements and activation of the CSAR

In acute terminal experiments, rats were anesthetized with urethane (800 mg/kg I.P.) and α-chloralose (40 mg/kg I.P.). The rat was ventilated artificially with room air supplemented with

100% oxygen. A heating pad was used to maintain body temperature at approximately 37°C during the experiment. Left ventricular end-diastolic pressure (LVEDP) and left ventricular end-systolic pressure (LVESP) were measured using a Millar catheter (SPR 524; size, 3.5-Fr; Millar Instruments, Houston, TX, USA) that was placed though the right carotid artery into the left ventricle. Arterial pressure (AP) and mean arterial pressure (MAP) were recorded when the Millar catheter was pulled back into the aorta. Heart rate (HR) and MAP were derived from the AP pulse using LabChart 7.1 software and a PowerLab model 16S (ADInstruments, Colorado Springs, CO, USA) data acquisition system. A polyethylene catheter was placed in the right jugular vein for intravenous injections. After jugular vein cannulation, the cervical vagi were sectioned bilaterally in order to isolate the CSAR from vagally mediated reflexes. A perivascular flow probe (0.5 VB587; Transonic Systems Inc., NY, USA), connected to a flow meter (T106, small animal flow meter; Transonic Systems Inc.), was placed around the left renal artery to allow continuous recording of renal blood flow (RBF) both at rest and during CSAR activation. Renal vascular resistance (RVR) was calculated as MAP/RBF. To activate the CSAR, a left thoracotomy was performed through the fourth intercostal space, and the heart was exposed. A square of filter paper (3 mm × 3 mm) saturated with BK (10 μg/ml) was applied to the anterior surface of the left ventricle to activate regional cardiac spinal afferents in vagotomized rats. Hemodynamic changes were continuously recorded before and after the BK application. At the end of the experiment, the rat was euthanized with an overdose of saturated potassium chloride.

Central venous pressure (CVP) measurements

The CVP was measured in the conscious state utilizing the radiotelemetry technique. Under 2% isoflurane anesthesia, the rat was placed in the supine position. After making a 10 - 15 mm incision in the frontal neck area, the right external jugular vein was identified and dissected. The catheter tip of a telemetry unit (PA-C10, Data Science International; St Paul, MN) was inserted into the jugular vein and further advanced into the caudal vena cava to the right atria level. The

telemetry unit was then secured to connective tissue with a 4-0 suture and buried under the skin in back neck area. Three days after surgery, the CVP was continuously recorded for 24 hours at a sampling rate of 1 kHz using a PowerLab data acquisition system with LabChart 7 software (model 8S, ADInstruments; Colorado Springs, CO). The final CVP was obtained by averaging 24-hour values.

GFR measurement

Glomerular filtration rate (GFR) was measured using fluorescein isothiocyanate (FITC)-inulin (Sigma, St Louis, MO) at 16-18 weeks post MI. Rats were anesthetized with urethane (800 mg/kg I.P.) and α-chloralose (40 mg/kg I.P.), and then ventilated with room air supplemented with 100% oxygen. A heating table was used to maintain body temperature at 37°C throughout the experiment. A catheter was placed though the right carotid artery into the left ventricle for blood sample collection (**Figure 2**). A polyethylene catheter was placed in the right jugular vein for intravenous administration of FITC-inulin. A bolus dose of 8 mg/mL of FITC-inulin was initially administered followed by constant infusion of 4 mg/mL at 50uL/min. A catheter was placed into the bladder via a suprapubic incision and urine was collected continuously. The FITC-inulin concentration in urine and plasma were measured using a fluorescence microplate reader at 480 nm excitation and 520 nm emission. Below is the formula used for calculation of GFR.

$$\text{GFR} = \frac{\text{Urine flow rate } \times \text{Urine inulin concentration}}{\text{Plasma inulin concentration}}$$

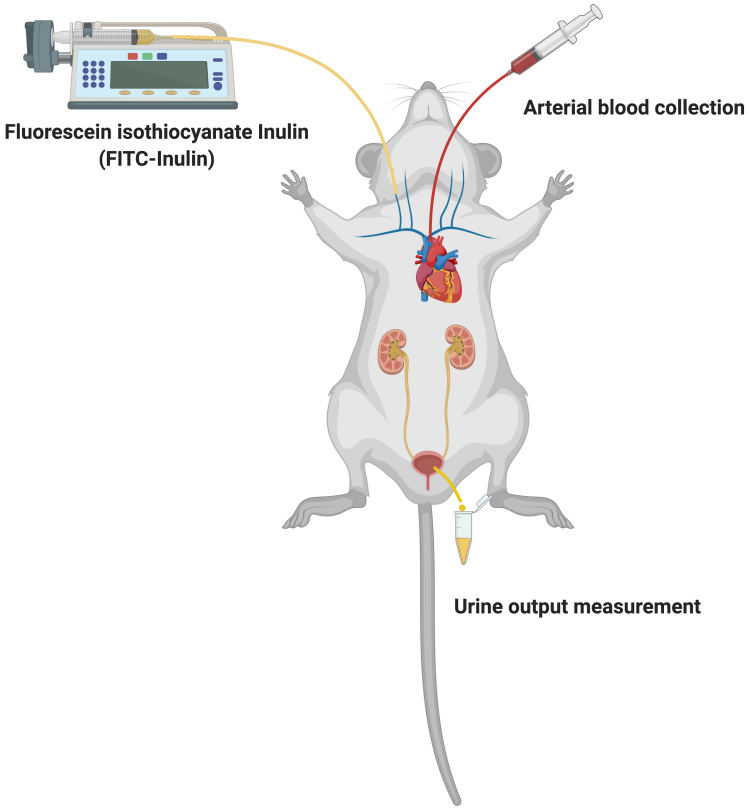

Figure 2. Schematic of GFR measurement.

Renal function measurement

A blood sample of ~100 μL was obtained from the rat tail veins at various time points after MI or sham surgery. These were 6-8, 12-14, and 16-18 weeks. Renal function was evaluated by measuring 1) potassium, 2) creatinine, and blood urea nitrogen (BUN) using iSTAT analysis (Abbott, Chicago, IL, USA).

Urinary KIM-1 and albumin measurement

Twenty-four-hour urine was collected in metabolic cages, followed by centrifugation to remove any particulates and then stored at -80°C. Urinary osmolality was measured with a Vapro Pressure Osmometer (D.A.I. Scientific Equipment, Inc., Mundelein, IL, USA). Urinary kidney injury molecule-1 (KIM-1) levels were measured by using Rat TIM-1/KIM-1/HAVCR Immunoassay (R&D Systems, Inc., Minneapolis, MN, USA) according to the manufacturer's instructions. Urinary albumin concentration was measured by the Physiology Core Laboratory at the Medical College of Wisconsin.

Kidney histological evaluation

The kidneys from Sham, CHF+Vehicle and CHF+RTX rats at ~4 months post-MI were fixed in 4% paraformaldehyde solution, embedded in paraffin, cut into 5 μm serial sections, and stained with Masson trichrome or periodic acid-Schiff (PAS) staining by the tissue core facility at the University of Nebraska Medical Center. In order to evaluate tubular injury, ten high powered (20X) fields (five cortical fields and five medullary fields) of PAS stained kidney sections were randomly selected per rat, and the percentage area of tubules that were classified as normal, dilated, containing casts, or necrotic was calculated by overlaying a 10 x 10 grid of points on each image, similar to the method described in the previous study.[94] The Masson trichrome-positive area or PAS-positive area relative to the whole area (10 cortical fields and 10 medullary fields per rat) was analyzed using Image J software (NIH, Bethesda, MD, USA). In addition, Masson trichrome

stained sections were scored semiquantitatively using the following scale: Score 0: no fibrosis; Score 1: < 25% fibrotic tubules; Score 2: 25%-50% fibrotic tubules; Score 3: 50%-75% fibrotic tubules; Score 4: > 75% fibrotic tubules.

RNA sequencing

The Qiagen miRNeasy kit was used to isolate total RNA from homogenized kidney tissue from sham, CHF+Vehicle, and CHF+RTX rats according to the manufacturer's instructions. RNAseq libraries were prepared from 500 ng total RNA for each sample using the NEBNext Ultra RNA Library Prep Kit for Illumina with the NEBNext Poly(A) mRNA Magnetic Isolation Module following manufacturers recommended protocol.

Trimming low-quality ends from reads, and adapter trimming was performed using cutadapt.[95] Reads were mapped against the genome reference mm10 using STAR aligner v2.3.0.[96] Aligned reads were further filtered to exclude transcripts for which the maximum number of reads for all samples was > 40 reads to eliminate noise and genes with low read counts. Raw sequencing data were submitted to the NCBI sequence read archive (SRA, Accession: SRP101707; Samples: SAMN06560417, SAMN06560429-51; BioProject: PRJNA378728).

Differential expression analyses and pathway enrichment analyses

The read count data were exported to DESeq2v1.18.1[97] to identify differentially expressed genes using the negative binomial distribution from normalized read count data. Pairwise comparisons were made between sham and CHF+Vehicle, sham and CHF+RTX, and CHF+Vehicle and CHF+RTX. A gene was considered significantly differentially expressed if its corresponding FDR corrected P value[98] was ≤0.05, and if it had a log2 fold change equal to or greater than 1.5. Gene annotation enrichment analysis of differentially regulated proteins to identify known functions, pathways, and networks effected was performed using Ingenuity Pathway Analysis (IPA) (Ingenuity Systems; Mountain View, CA, USA). The significance was set at a *P*-

value of 0.05. Network representations of enriched pathways and gene ontology (GO) terms associated with the biological process were graphically represented using ClueGO cytoscape plug-in.[99] Clustered heat map of differentially expressed genes was plotted using the heatmap.2 function of the R package gplots (https://cran.r-project.org/web/packages/gplots/).[100]

Real time quantitative PCR (RT-PCR)

Kidney tissues were harvested and dissected into cortex and medulla at different time points (1 week, 4 weeks, 8 weeks, and 18 weeks post-MI), and then small pieces of the kidney cortex and medulla from sham, CHF+Vehicle, and CHF+RTX were frozen at -80°C, from which RNA was purified by using the RNeasy Mini RNA purification kit (Qiagen, Germantown, MD, USA). cDNA was generated from RNA using the QuantiTect Reverse Transcription Kit (Qiagen, Germantown, MD, USA), according to the manufacturer's instructions. For the measurements of the mRNA expression of kidney injury molecule-1 (*Kim-1*), neutrophil gelatinase-associated lipocalin (*Ngal*), interleukin 1 beta (*Il1b*), interleukin 6 (*Il6*), and other genes, RT-PCR was performed by using the QuantiFast SYBR Green PCR Kit (Qiagen, Germantown, MD, USA). Primer sequences for RT-PCR are listed in **Table 2**. Reaction conditions were decided according to the manufacturer's instructions. The Ct (threshold cycle) values of the target gene amplifications were normalized to those of the actin beta (*Actb*). Each biological replicate was measured with three technical replicates, and fold change was calculated using the $2-\Delta\Delta CT$ method. Primers were designed and synthesized by Integrated DNA Technologies (Coralville, IA, USA) based on published sequences (http://www.ncbi.nlm.nih.gov).

Table 2. Primer sequences for RT-PCR

Genes	Primer sequences
Kim1	**Forward:** 5'-GCC TGG AAT CAC ACT GTA AG-3' **Reverse:** 5'-GCA ACG GAC ATG CCA ACA TAG-3'
Ngal	**Forward:** 5'-CGA ATG CGG TCC AGA AAG A-3' **Reverse:** 5'-GAG GAT GGA AGT GAC GTT GTA G-3'
Il6	**Forward:** 5'-TCC TAC CCC AAC TTC CAA TGC TC-3' **Reverse:** 5'-TTG GAT GGT CTT GGT CCT TAG CC-3'
Il1b	**Forward:** 5'-CAC CTC TCA AGC AGA GCA CAG-3' **Reverse:** 5'-GGG TTC CAT GGT GAA GTC AAC-3'
Actb	**Forward:** 5'-ACA GGA TGC AGA AGG AGA TTA C-3' **Reverse:** 5'-ACA GTG AGG CCA GGA TAG A-3'
Tnfa	**Forward:** 5'-AAA TGG GCT CCC TCT ATC AGT TC-3' **Reverse:** 5'-TCT GCT TGG TGG TTT GCT ACG AC-3'
iNos	**Forward:** 5'-TGG AGC GAG TTG TGG ATT G-3' **Reverse:** 5'-CCT CTT GTC TTT GAC CCA GTA G-3'

Epo	**Forward:** 5’-CCA GAG AGT CTT CAG CTT CAT ATA G-3’ **Reverse:** 5’-TCT GGA GGC GAC ATC AAT TC-3’
Hif1a	**Forward:** 5’-TCC ATT ACC TGC CTC TGA AAC-3’ **Reverse:** 5’-CTC TGG GCT TGA CTC TAA CTT C-3’
Hif3a	**Forward:** 5’-CAT GGC TTA CCT GTC GGA AA-3’ **Reverse:** 5’-CTT GGT CAC AGG GAT GGA TAA A-3’
Atf3	**Forward:** 5’-GAG ATG CGG TCC AGA GTA TTT C-3’ **Reverse:** 5’-TCG GAT TGA ACA CTG AGG ATT T-3’
Hmox1	**Forward:** 5’-GAT GGC CTC CTT GTA CCA TAT C-3’ **Reverse:** 5’-AGC TCC TCA GGG AAG TAG AG-3’
Avpr2	**Forward:** 5’-GCT CTT CAT CTT TGC TCA GCG T-3’ **Reverse:** 5’-TCC AGG TGA CAT AGG CAC GAA-3’

Kim1, kidney injury molecule-1; Ngal, neutrophil gelatinase-associated lipocalin; Il6, interleukin 6; Il1b, interleukin 1 beta; Actb, actin beta; Tnfa, tumor necrosis factor alpha; iNos, inducible nitric oxide synthases; Epo, erythropoietin; Hif1a, hypoxia-inducible factor 1 alpha; Hif3a, hypoxia-inducible factor 3 alpha; Atf3, activating transcription factor 3; Hmox1, heme oxygenase 1; Avpr2, arginine vasopressin receptor 2.

Survival analysis

Survival was monitored from 1-week post-MI through study endpoint (up to six months). The condition of each rat was monitored and recorded every day. Acute death occurring within 1week after MI was not included in the survival analysis.

Intra-stellate injection of RTX

Rat model of chronic heart failure

Experiments were performed on adult, male, 400-500g Sprague-Dawley rats purchased from the Charles River Laboratories. The overall experimental protocol for intra-stellate injection of RTX is outlined in **Figure 3**. Myocardial infarction (MI)-induced CHF was produced by coronary ligation as previously described.[35] Four weeks after MI procedure, these rats were randomized to either bilateral intra-stellate injection of RTX (MI+SG RTX group) or sham surgery group (MI group). Intra-stellate injection of RTX was done as previous described.[101] Briefly, rats were mechanically ventilated with 3% isoflurane-oxygen mixture. The internal thoracic and costocervical arteries were exposed, medially to the origins of which stellate ganglion is located. Then, RTX (5μl, 50 mg/ml) was injected into the left and right stellate ganglia over 30s.

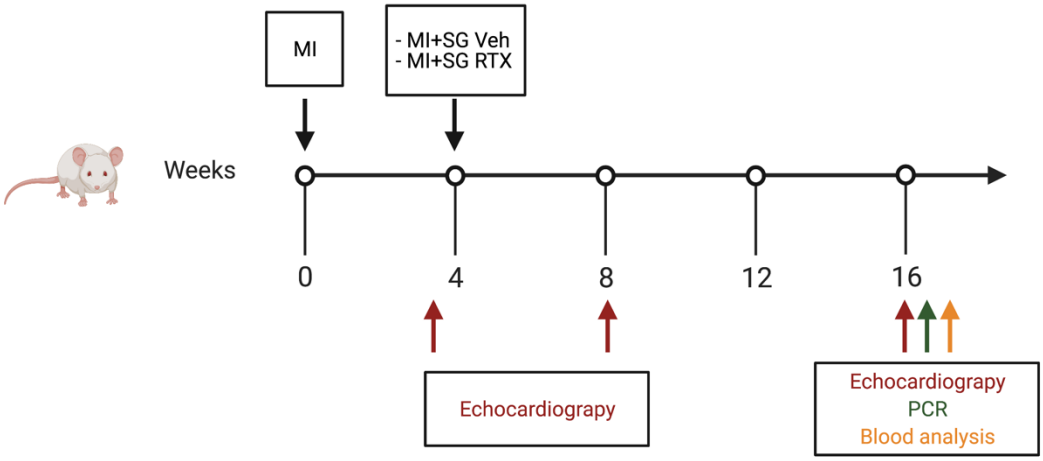

Figure 3. Schematic diagram of study design for intra-stellate injection of RTX.

Surgical preparation for the validation of SG injection of RTX

Rats were anesthetized with urethane (800 mg/kg ip) and a-chloralose (40 mg/kg ip). AP, MAP, and HR were measured as described above in the section of CSAR ablation. RSNA was recorded as previously described.[102]

Activation of cardiac spinal afferents

Topical application of BK was used to activate cardiac spinal afferents as described in our precious study.[40] The chest was opened through the fourth intercostal space. To activate cardiac spinal afferents, a square of filter paper (3×3mm) saturated with BK (10 μg/mL; Sigma Aldrich) was applied randomly to the surface of left ventricular free wall of the heart. Hemodynamics and RSNA were continuously recorded. After the responses peaked, the heart was rinsed three times with 10 mL of warm normal saline. Twenty minutes were allowed to elapse between subsequent stimulations, to allow MAP, HR, and RSNA to return and stabilize at control levels.

Statistics

All data are expressed as the mean ± standard deviation (SD). Differences between groups were determined by a two-way ANOVA followed by Tukey's post hoc test. Changes in cardiac function before and after epicardial application of BK were determined by Student's paired t-test. Survival data between vehicle-treated and RTX-treated rats were calculated as Kaplan-Meier plots and the Log-rank (Mantel-Cox) test. P-value < 0.05 was considered statistically significant.

Results

Baseline hemodynamics

Echocardiographic and hemodynamic measurements in all groups are summarized in **Table 3** for rats that had blood chemistry measurements (i.e. iSTAT) and **Table 4** for those rats where we examined the acute activation of the CSAR. CHF+Vehicle rats exhibited increased heart weights, heart weight, and lung weight to body weight ratios and LVEDP compared with sham rats, which were all attenuated by RTX application. CHF+Vehicle rats had reduced ejection fraction (EF), fractional shortening (FS), and LVESP compared with sham rats. EF, FS, LVESP, and infarct sizes of CHF+Vehicle and CHF+RTX were comparable. The infarct sizes of rats with CHF at different time points were comparable (1 wk-post MI, infarct size 46.9 ± 5.2%; 4 wk-post MI, infarct size 45.4 ± 3.8%; 8 wk-post MI, infarct size 43.5 ± 3.8%; 18 wk-post MI, infarct size 44.5 ± 3.4%; CHF+RTX 18 wk-post MI, infarct size 44.2 ± 2.6%). These data are consistent with our previous findings, suggesting that cardiac sympathetic afferent ablation provides cardiac protection to heart failure.[35]

Table 3. Hemodynamic and morphological data in sham, CHF+Vehicle and CHF+RTX rats that received iSTAT measurements

Parameters	Sham (n=8)	CHF+Vehicle (n=14)	CHF+RTX (n=8)
Body weight, g	486 ± 41	499 ± 66	476 ± 40
Heart weight, mg	1355 ± 113	2103 ± 246 *	1608 ± 176 *†
HW/BW, mg/g	2.8 ± 0.3	4.3 ± 0.6 *	3.4 ± 0.5 *†
WLW/BW, mg/g	4.1 ± 0.8	8.8 ± 2.1 *	5.8 ± 1.0 *†
LVESP, mmHg	134.8 ± 6.4	109.2 ± 12.9 *	113.6 ± 11.7 *
LVEDP, mmHg	2.9 ± 2.1	23.8 ± 9.6 *	10.4 ± 2.9*†
EF, %	72.9 ± 2.9	36.4 ± 6.6 *	34.9 ± 7.4 *
FS, %	43.0 ± 2.8	18.1 ± 3.7 *	17.8 ± 3.9 *
Infarct size, %	0	43.1 ± 6.2 *	42.8 ± 3.8*

Values are mean ± SD. BW, body weight; HW, heart weight; WLW, wet lung weight; LVESP, left ventricle end-systolic pressure; LVEDP, left ventricle end-diastolic pressure; EF, ejection fraction; FS, fractional shortening. *P<0.05 vs. sham. †, P<0.05 vs. CHF+Vehicle.

Table 4. Baseline hemodynamic and morphological data in sham, CHF+Vehicle and CHF+RTX rats prior to acute activation of cardiac sympathetic afferent reflex with bradykinin

Parameters	Sham (n=8)	CHF+Vehicle (n=7)	CHF+RTX (n=7)
Body weight, g	463 ± 25	469 ± 31	460 ± 13
Heart weight, mg	1188 ± 105	2086 ± 236 *	1471 ± 231 *†
HW/BW, mg/g	2.6 ± 0.2	4.4 ± 0.3 *	3.2 ± 0.5 *†
WLW/BW, mg/g	4.2 ± 0.3	8.6 ± 0.9 *	4.4 ± 0.2 †
LVESP, mmHg	135.5 ± 7.6	110.1 ± 8.0 *	118.9 ± 12.3 *
LVEDP, mmHg	3.5 ± 1.5	19.4 ± 3.2 *	8.8 ±3.4 *†
EF, %	73.5 ± 2.5	43.6 ± 4.5 *	40.9± 3.2 *
FS, %	43.1 ± 2.4	22.0± 2.6 *	21.1 ± 2.6 *
Infarct size, %	0	43.0± 4.0 *	46.0± 1.3*

Values are mean ± SD. BW, body weight; HW, heart weight; WLW, wet lung weight; LVESP, left ventricle end-systolic pressure; LVEDP, left ventricle end-diastolic pressure; EF, ejection fraction; FS, fractional shortening. *P<0.05 vs. sham. †, *P*<0.05 vs. CHF+Vehicle.

Blood analysis data

We investigated the point at which CHF rats developed the CRS and renal dysfunction post-MI. At various time points (6-8 weeks, 12-14 weeks, and 16-18 weeks post-MI), blood samples from sham, CHF+Vehicle, and CHF+RTX rats were collected to evaluate renal function. Blood analysis of creatinine, BUN, potassium, and other parameters are summarized in **Table 5**. In CHF+Vehicle rats, we did not see any significant difference in BUN, creatinine, or potassium compared with sham rats until 16-18 weeks post-MI, suggesting that CHF+Vehicle rats developed CRS type 2 four months after MI. Interestingly, BUN, creatinine, and potassium of RTX-treated CHF rats were comparable to those of sham rats. Compared with the sham, CHF+Vehicle rats exhibited decreased urine output and increased urinary osmolality **(Figure 4 A and 1B**). Animals treated with RTX exhibited significantly increased urine output and decreased osmolality in comparison with CHF+Vehicle rats.

Table 5. Blood analysis in sham, CHF+Vehicle, and CHF+RTX rats

Parameters	Sham (n=8)			CHF+Vehicle (n=14)			CHF+RTX (n=8)		
	6-8 w	12-14 w	16-18 w	6-8 w	12-14 w	16-18 w	6-8 w	12-14 w	16-18 w
Na, mM	140.8±1.1	140.6±0.9	140.9±1.1	140.1±1.8	138.6±1.8	140.7±0.9	139.9±1.3	137.7±1.4	140.8±0.7
K, mM	4.10±0.19	4.03±0.23	4.00±0.16	4.23±0.28	4.14±0.29	4.71±0.25*	4.14±0.22	4.07±0.16	4.19±0.26†
Cl, mM	102.3±2.1	101.8±2.2	102.5±2.5	101.5±1.8	101.5±1.3	102.5±3.1	102.1±1.6	102.3±1.0	101.9±1.5
iCa, mM	1.23±0.09	1.22±0.13	1.20±0.07	1.31±0.09	1.32±0.03	1.23±0.06	1.21±0.07	1.25±0.07	1.19±0.05
TCO_2, mM	25.4±4.0	25.5±3.8	25.9±3.3	26.2±1.7	26.3±1.6	26.1±3.0	25.6±2.2	26.4±1.8	25.4±1.5
BUN, mg/dL	20.3±1.6	21.3±1.3	21.6±2.2	22.2±2.5	22.9±2.6	30.9±5.6*	21.8±2.3	21.6±1.8	25.8±2.8†
Crea, mg/dL	0.53±0.14	0.54±0.13	0.56±0.09	0.43±0.22	0.47±0.09	0.71±0.18*	0.43±0.19	0.36±0.12	0.55±0.11†
HCt, %PCV	48.8±3.2	49.3±3.8	49.0±3.3	46.9±3.1	45.7±2.4	51.7±6.2	46.6±4.2	43.7±1.8	52.5±1.9
Hb, g/dL	16.2±1.7	16.9±1.2	16.7±1.1	16.4±0.9	15.5±0.8	17.5±2.2	15.7±0.9	14.5±0.4	17.9±0.6
AnGap	17.5±3.9	17.8±3.1	17.8±3.3	16.3±2.4	15.9±2.2	17.6±2.5	13.3±1.9	12.7±1.8	18.6±1.4

Values are mean ± SD. Na, sodium; K, potassium; Cl, chloride; iCa, ionized calcium; TCO2, total carbon dioxide; BUN, blood urea nitrogen; Crea, creatinine; HCt, hematocrit; Hb, hemoglobin; AnGap, anion gap. CSAR ablation by RTX prevents the renal dysfunction measured by blood creatinine, BUN and potassium in CHF rats. *P<0.05 vs. 6-8 w or 12-14w. †, P<0.05 vs. CHF+Vehicle.

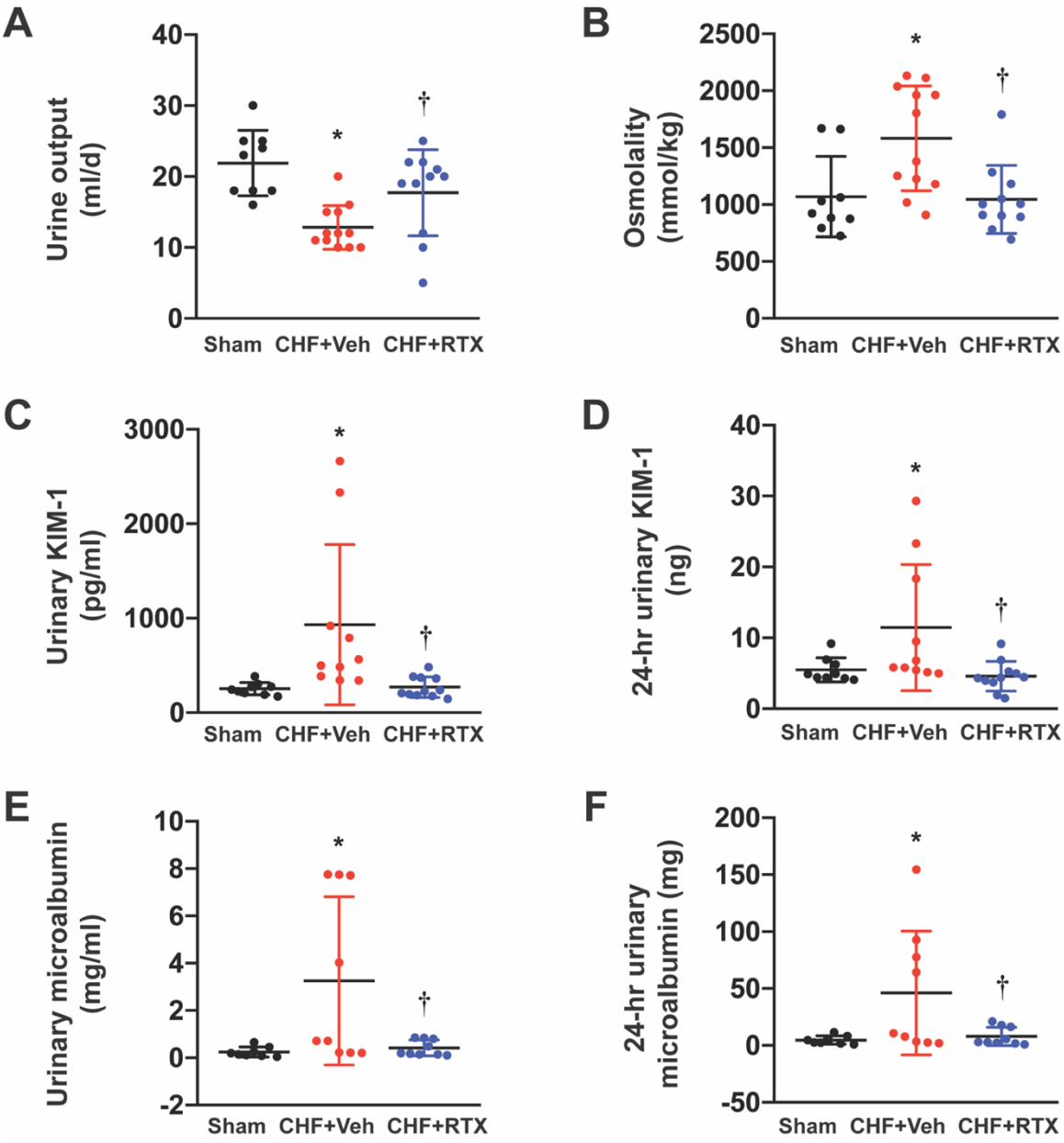

Figure 4. CSAR ablation by RTX prevents renal dysfunction as measured by (A) urine output, (B)urinary osmolality, (C, D) urinary KIM-1 and (E, F) microalbuminuria in CHF rats. Sham group, n=9 for A-D, n=8 for E, F; CHF+Veh group, n=12 for A, B, n=10 for C, D, n=9 for E, F; CHF+RTX group, n=11 for A-D, n=9 for E, F. KIM-1, kidney injury molecule-1. *P<0.05 vs. Sham. †, P<0.05 vs. CHF+Vehicle.

Urinary KIM-1

KIM-1, a sensitive proximal tubular injury biomarker, is expressed at a very low level in normal kidneys but is highly expressed in damaged and ischemic kidneys. It has been shown that high urinary concentration of KIM-1 is associated with increased mortality in CHF.[17] We found that in CHF rats urinary KIM-1 concentration and 24-hour KIM-1 excretion was markedly increased compared with those of sham rats. Cardiac spinal afferent ablation by RTX significantly decreased urinary KIM-1 concentration and 24-hour KIM-1 excretion in CHF rats (**Figure 4 C, D**).

Urinary albuminuria

Urinary albuminuria, which is defined as urinary albumin excretion ranging from 30 to 300 mg/d or 20 to 200 ug/min, results from damage to the glomerular barrier and/or reduced reabsorption of the proximal tubules to filtered albumin. Several studies confirm that microalbuminuria is an independent risk factor of cardiovascular and renal mortality.[103] In comparison with sham rats, the average urinary microalbumin concentration and 24-hour microalbumin excretion in CHF+Vehicle rats was significantly higher and was normalized in CHF+RTX rats (**Figure 4 E, F**).

Kidney histological examination

Histological examination showed that compared with sham rats, there were more dilated tubules, more cast-filled tubules, and more necrotic tubules in the renal cortex and medulla of the rats with CHF, which were all reduced by RTX (**Figure 5 A, B**). Masson trichrome analysis demonstrated that there was substantial fibrosis in the cortex and medulla of CHF rats. However, RTX significantly decreased collagen deposition in the kidneys of CHF rats (**Figure 5 C, E**). In addition, PAS staining analysis showed that the thickening of glomerular basement membranes were observed in CHF rats, which was also attenuated by CSAR ablation (**Figure 5 D**).

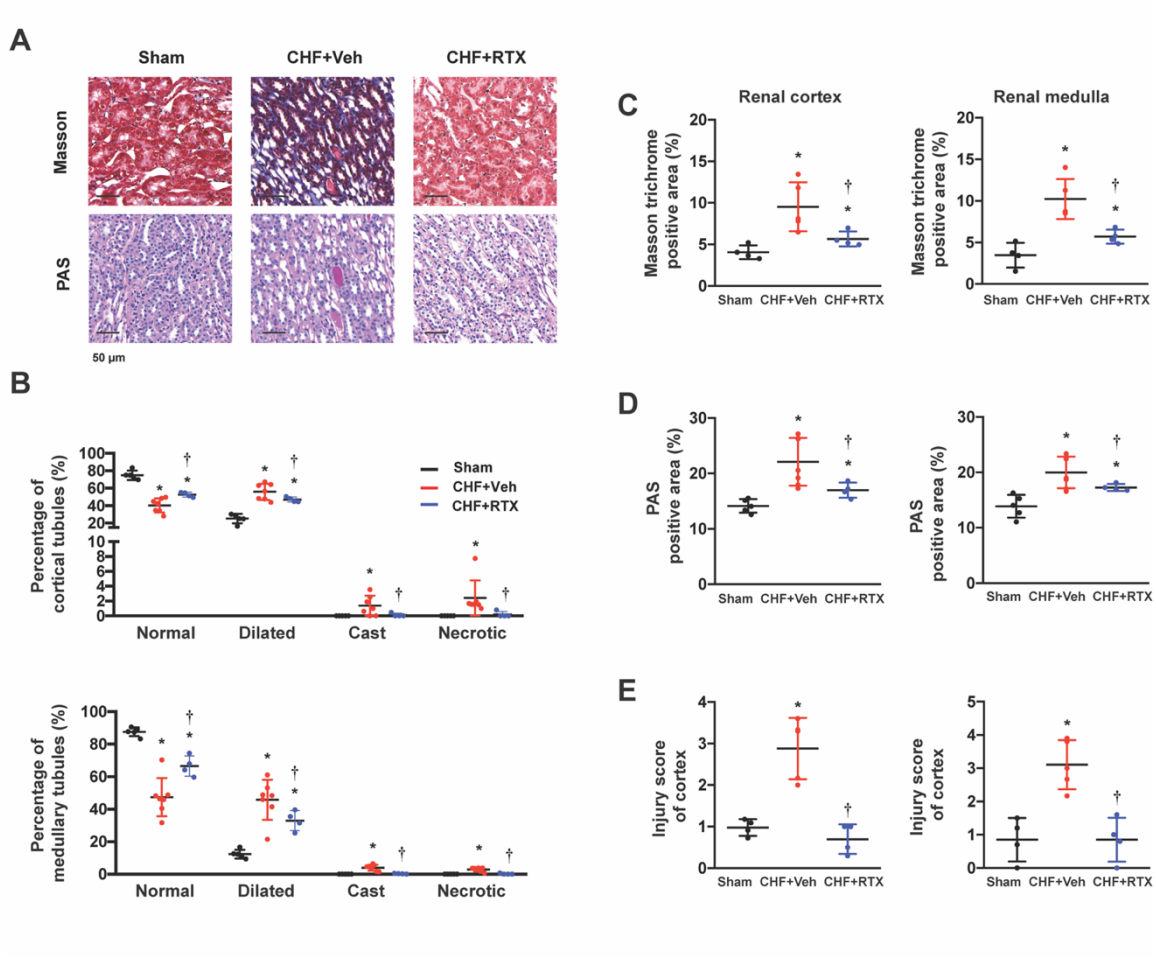

Figure 5. CSAR ablation by RTX reduced renal fibrosis and tubular injury in CHF rats. A. Representative images of Masson trichrome staining and PAS staining in both renal cortex and medulla from Sham, CHF+Vehicle, and CHF+RTX rats. Scale bar, 50 μm. B. Percentages of renal tubular profiles categorized as normal, dilated, cast-filled, or necrotic in the cortex and medulla. C. Quantitative analysis for Masson trichrome positive area. D. Quantitative analysis for PAS positive area. E. Scores of tubular injury. For Masson trichrome staining, Sham group, n=4; CHF+Veh group, n=5; CHF+RTX group, n=4. For PAS staining, Sham group, n=5; CHF+Veh group, n=7; CHF+RTX group, n=4. PAS staining, periodic acid-Schiff staining. *P<0.05 vs. Sham. †, P<0.05 vs. CHF+Vehicle.

GFR measurement

To further evaluate kidney function, GFR values were measured at 16-18 weeks post MI. Compared with sham animals, the GFR of CHF+Sham animals was significantly reduced at 16-18 weeks post MI, which was improved by epicardial application of RTX (**Figure 6**).

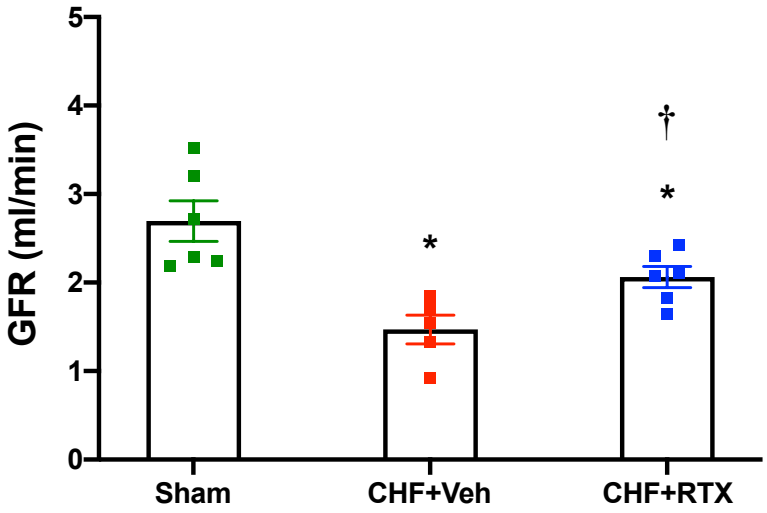

Figure 6. Epicardial application of RTX ameliorated renal dysfunction in chronic heart failure. CHF, chronic heart failure. *P<0.05 vs. Sham. †P<0.05 vs. CHF+Sham.

RNA sequencing analysis

To further investigate the pathophysiological mechanisms of CRS type 2, RNA sequencing of the whole kidneys was performed in sham, CHF+Vehicle, and CHF+RTX rats. Sequencing of these transcriptomes yielded more than one hundred million, 75-mer single end high quality reads from a total of 11 samples (five replicates for sham, and three replicates each for CHF+Vehicle and CHF+RTX). The average number of raw reads per sample was 21 million. The average mapping percentage of the raw reads to the reference transcripts was 50%.

Of the 394 genes differentially expressed between sham and CHF+Vehicle rats, the majority (n = 359) were upregulated in CHF+Vehicle (**Table 6**, **Figure 7**). KIM-1 and another global renal injury marker, neutrophil gelatinase-associated lipocalin (NGAL), have been shown to be associated with long-term mortality and recurrent heart failure hospitalization.[17, 18] The RNA-Seq shows that gene expression of Kim-1 (Havcr1) was increased by ~104 fold, and Ngal (Lcn2) was increased by ~36 fold in whole-kidney tissues of CHF+Vehicle rats compared to sham rats, confirming the occurrence of renal damage in CHF rats ~18 weeks post-MI. In addition, RNA-Seq demonstrated that gene expression of the pro-inflammatory cytokine, Il6 was significantly upregulated by ~ 40-fold at 18 weeks post-MI. Expression of genes related to cell death and survival, such as interleukin 24 (Il24) and nephroblastoma overexpressed (Nov) were increased by ~ 55 fold and ~ 4 fold, respectively, suggesting that renal cell death contributes to the development of renal failure in the setting of CRS type 2. Interestingly, two hypoxia-related genes, receptor-type tyrosine-protein phosphatase zeta (Ptprz1) and hypoxia-inducible factor 3 alpha (Hif3a) were also upregulated by ~ 6 and ~ 7 fold, respectively, suggesting that hypoxia may exist in the kidneys of CHF+Vehicle rats.

Table 6. Differentially expressed genes between CHF+Veh and Sham

Gene	log2 Fold Change	P value	P adj	Direction
Prss22	8.0	2.08E-07	1.09E-05	up
Tgm1	7.2	1.43E-08	1.19E-06	up
Fosl1	7.2	2.55E-09	2.63E-07	up
Lypd8	7.2	2.14E-05	0.00047	up
Havcr1	6.7	9.03E-15	3.26E-12	up
Il1r2	6.3	4.97E-09	4.76E-07	up
Fgb	6.1	5.56E-11	8.36E-09	up
Csf3	6.1	4.87E-05	0.000885	up
Ugt1a2	5.9	8.05E-08	4.95E-06	up
Il24	5.8	1.4E-05	0.000341	up
Hmox1	5.8	4.15E-09	4.02E-07	up
Serpina3n	5.7	1.83E-12	4.13E-10	up
Mfsd2a	5.7	3.94E-06	0.000125	up
Vgf	5.6	2.6E-06	9.18E-05	up
LOC298795	5.6	1.69E-12	3.9E-10	up
Igfbp1	5.4	3.76E-17	2.55E-14	up
Il6	5.3	1.44E-05	0.000348	up
Atf3	5.3	8.67E-38	9.39E-34	up
Lcn2	5.2	5.03E-14	1.6E-11	up
Rasd1	5.0	6.53E-17	3.93E-14	up
Slc7a11	5.0	3.63E-08	2.5E-06	up
Fgg	5.0	1.36E-10	1.78E-08	up
Trim15	4.9	1.5E-05	0.000359	up
Lamc2	4.8	8.18E-15	3.05E-12	up
Trib3	4.8	5.04E-06	0.000152	up
Socs3	4.8	4.1E-23	6.34E-20	up
Trpv6	4.7	6.18E-09	5.8E-07	up
Adamts4	4.6	5.81E-10	6.84E-08	up
Rnd1	4.6	2.61E-16	1.41E-13	up
PVR	4.5	1.03E-11	1.82E-09	up
Fosb	4.5	4.03E-06	0.000127	up
Btg2	4.5	5.89E-14	1.75E-11	up
Angptl4	4.4	1.25E-08	1.04E-06	up
Chac1	4.4	2.25E-06	8.13E-05	up
Cdkn1a	4.4	2.09E-20	2.84E-17	up
Cxcl10	4.4	4.43E-12	9.04E-10	up
Fga	4.3	1.07E-08	9.02E-07	up
Lif	4.3	4.61E-07	2.21E-05	up

Glycam1	4.3	3.46E-12	7.21E-10	up
Cxcl2	4.2	0.00029	0.003489	up
Nfil3	4.2	3.18E-18	2.87E-15	up
Arid5a	4.2	3.54E-17	2.55E-14	up
Cyp3a9	4.1	1.9E-06	7.02E-05	up
Bcat1	4.1	6.74E-12	1.28E-09	up
Cldn4	3.9	1.26E-10	1.68E-08	up
S100a8	3.9	2.63E-06	9.23E-05	up
RGD1564664	3.9	2.36E-10	2.93E-08	up
Cxcl1	3.9	1.11E-10	1.5E-08	up
Cbarp	3.7	3.77E-14	1.28E-11	up
Myc	3.7	6.52E-28	1.77E-24	up
Pcsk1	3.6	4.07E-08	2.74E-06	up
Cfd	3.5	1.6E-06	6.11E-05	up
Epo	3.5	0.002794	0.017913	up
Lexm	3.5	0.00017	0.002307	up
Cebpd	3.5	5.91E-24	1.07E-20	up
Clcf1	3.5	1.2E-12	2.88E-10	up
Serpine1	3.5	6.41E-14	1.83E-11	up
Bdkrb2	3.5	8.02E-10	8.96E-08	up
B4galnt4	3.5	1.8E-07	9.74E-06	up
Il23a	3.4	5.89E-05	0.001015	up
Apold1	3.4	1.14E-19	1.37E-16	up
Tnfrsf12a	3.3	6.31E-08	4E-06	up
Nfkbiz	3.3	1.14E-13	3.08E-11	up
Tubb6	3.3	4.1E-09	4E-07	up
Birc3	3.3	3.43E-14	1.2E-11	up
Cyp3a9	3.3	1.87E-07	1.01E-05	up
Ptx3	3.3	5.78E-05	0.001004	up
A2m	3.3	0.000181	0.002411	up
Map3k6	3.2	1.64E-12	3.87E-10	up
Rgs1	3.2	5.88E-16	3.03E-13	up
Osmr	3.2	3.15E-13	8.13E-11	up
Spp1	3.2	4.58E-18	3.82E-15	up
Sphk1	3.1	4.75E-11	7.36E-09	up
Gadd45b	3.1	2.18E-10	2.77E-08	up
Maff	3.0	1.07E-15	5.04E-13	up
Nr4a3	3.0	6.63E-12	1.28E-09	up
Cebpb	3.0	7.31E-19	7.92E-16	up
Hbegf	3.0	7.49E-11	1.07E-08	up
LOC684871	3.0	8.58E-14	2.38E-11	up

Pcsk2	3.0	0.001479	0.011343	up
Lax1	2.9	0.000186	0.002468	up
S100a9	2.9	1.22E-07	7.01E-06	up
Gpnmb	2.9	8.92E-09	7.92E-07	up
Socs1	2.9	2.28E-08	1.74E-06	up
Tmem252	2.8	3.57E-15	1.43E-12	up
Sds	2.8	3.14E-06	0.000105	up
Anxa8	2.8	6.77E-05	0.001123	up
Tgif1	2.8	4.64E-15	1.79E-12	up
Srxn1	2.8	1.33E-05	0.000327	up
Klf6	2.8	1.02E-12	2.5E-10	up
Zfp36	2.8	2.55E-17	1.98E-14	up
Ctgf	2.7	5.66E-07	2.62E-05	up
Hif3a	2.7	0.003665	0.021595	up
Upp1	2.7	3.41E-10	4.15E-08	up
Ucma	2.7	8.3E-07	3.48E-05	up
Dusp2	2.7	6.75E-05	0.001121	up
Dmbt1	2.7	3.77E-07	1.86E-05	up
Edn1	2.6	6.91E-09	6.34E-07	up
Slc16a3	2.6	5.67E-10	6.74E-08	up
Csrnp1	2.6	2.68E-15	1.11E-12	up
Timp1	2.6	9.46E-11	1.3E-08	up
Chi3l1	2.6	0.00121	0.009754	up
Kng1l1	2.6	3.97E-05	0.000761	up
Il1rn	2.6	1.83E-08	1.44E-06	up
Gdf15	2.5	1.43E-31	6.16E-28	up
Ccnf	2.5	5.22E-05	0.000931	up
Selp	2.5	0.000283	0.003427	up
Fam46b	2.5	0.000786	0.007096	up
Ptprz1	2.5	3.73E-06	0.000119	up
Lrg1	2.5	1.67E-07	9.32E-06	up
Rab7b	2.5	0.000105	0.001573	up
Fam167a	2.5	2.68E-08	2.01E-06	up
Itpkc	2.5	2.9E-08	2.15E-06	up
Krt18	2.5	1.95E-08	1.52E-06	up
Slc7a1	2.5	2.11E-08	1.62E-06	up
C4b	2.5	8.77E-17	5E-14	up
Gadd45a	2.5	2.76E-06	9.61E-05	up
Dusp1	2.5	6.27E-13	1.58E-10	up
Egr2	2.5	2.81E-05	0.00058	up
Hspa1a	2.4	3.46E-08	2.45E-06	up

Cyp11a1	2.4	0.001095	0.009025	up
Mt2A	2.4	3.32E-11	5.37E-09	up
Phlda1	2.4	9.3E-05	0.001433	up
Vtcn1	2.4	1.11E-07	6.49E-06	up
Gpx2	2.4	0.003266	0.019986	up
Crtac1	2.4	6.23E-06	0.000178	up
Fkbp5	2.4	2.7E-12	5.84E-10	up
Gem	2.3	5.71E-14	1.75E-11	up
Fam25a	2.3	0.000326	0.003771	up
Gprc5a	2.3	2.73E-09	2.77E-07	up
Clec10a	2.3	2.44E-06	8.67E-05	up
Arl4c	2.3	9.13E-12	1.7E-09	up
Fam129a	2.3	5.88E-11	8.64E-09	up
F2rl1	2.3	1.49E-08	1.22E-06	up
Car3	2.3	0.00343	0.020613	up
Ifnlr1	2.3	0.002596	0.016953	up
Afap1l2	2.3	1.08E-09	1.17E-07	up
Pou3f1	2.3	7.87E-08	4.87E-06	up
Map1b	2.3	9.59E-05	0.001465	up
Mex3b	2.3	5.05E-05	0.000911	up
Prg4	2.3	5.32E-07	2.48E-05	up
Slc7a5	2.3	9.97E-06	0.000262	up
LOC500300	2.3	4.7E-17	2.99E-14	up
Elf3	2.3	6.25E-09	5.8E-07	up
Inhbb	2.3	5.45E-11	8.31E-09	up
Pnrc1	2.3	1.78E-15	7.7E-13	up
Cd14	2.3	3.89E-09	3.87E-07	up
Fosl2	2.2	9.25E-12	1.7E-09	up
Nr4a1	2.2	0.000427	0.004598	up
Eid3	2.2	0.002491	0.016489	up
Ppp1r15a	2.2	1.41E-13	3.71E-11	up
Nyap1	2.2	3.23E-08	2.35E-06	up
Penk	2.2	0.003266	0.019986	up
Pla1a	2.2	9.47E-08	5.73E-06	up
Nfkbia	2.2	8.21E-28	1.78E-24	up
Hspa1b	2.2	1.05E-09	1.15E-07	up
Scel	2.2	3.42E-05	0.000679	up
Cd44	2.2	1.88E-11	3.27E-09	up
Plin2	2.2	6.82E-05	0.001123	up
Dusp5	2.2	4.48E-08	2.98E-06	up
Rhob	2.2	1.9E-11	3.27E-09	up

Sox9	2.2	1.34E-07	7.64E-06	up
Bcl3	2.2	5E-06	0.000151	up
Ier5	2.2	5.15E-12	1.02E-09	up
Akap12	2.2	2.28E-07	1.19E-05	up
Chka	2.2	1.62E-08	1.31E-06	up
Plk3	2.2	3.63E-08	2.5E-06	up
Col7a1	2.1	3.24E-05	0.000648	up
RT1-CE6	2.1	0.000307	0.003632	up
Gpr4	2.1	5.69E-07	2.62E-05	up
Lypd3	2.1	2.19E-06	7.93E-05	up
Ldlr	2.1	3.25E-08	2.35E-06	up
Nr4a2	2.1	7.6E-11	1.07E-08	up
S100b	2.1	0.000888	0.007721	up
S100a10	2.1	2.08E-09	2.17E-07	up
Pthlh	2.1	0.000136	0.001927	up
Mab21l3	2.1	6.22E-11	8.98E-09	up
Dyrk3	2.1	0.000178	0.002378	up
Gzmk	2.1	7.84E-05	0.001251	up
Spsb1	2.1	6.33E-07	2.84E-05	up
Gpsm1	2.1	4.55E-05	0.000842	up
Arntl	2.1	6.8E-05	0.001123	up
Clu	2.1	6.7E-10	7.8E-08	up
Tsc22d1	2.1	6.81E-10	7.85E-08	up
Tinagl1	2.0	6.32E-08	4E-06	up
Creb5	2.0	0.000677	0.006379	up
Fgl2	2.0	2.88E-07	1.44E-05	up
Cldn7	2.0	9.74E-08	5.86E-06	up
Uchl1	2.0	3.78E-05	0.000733	up
Runx1	2.0	9.81E-07	4.06E-05	up
Akr1b8	2.0	7.9E-05	0.001258	up
Epha2	2.0	1.09E-07	6.43E-06	up
Ier2	2.0	2.05E-10	2.65E-08	up
Klf4	2.0	2.07E-06	7.54E-05	up
Bhlha15	2.0	0.000824	0.007302	up
Gnat1	2.0	1.34E-05	0.000329	up
Arl4a	2.0	6E-14	1.75E-11	up
Bcl6	2.0	3.93E-11	6.25E-09	up
Adamts1	2.0	1.72E-08	1.37E-06	up
Cxcr4	2.0	1.08E-07	6.39E-06	up
Fcgr2b	2.0	9.21E-06	0.000247	up
Sh2b2	2.0	2.79E-05	0.000576	up

Rnf125	2.0	1.51E-05	0.000362	up
Tmbim1	2.0	1.45E-06	5.65E-05	up
Klf5	2.0	5.76E-07	2.64E-05	up
Junb	2.0	7.75E-08	4.82E-06	up
Fam84a	2.0	2.75E-07	1.39E-05	up
Ddit4l2	2.0	0.000413	0.004516	up
Plaur	2.0	0.000325	0.003771	up
Mt1a	1.9	2.14E-12	4.74E-10	up
Isg20	1.9	0.000183	0.002433	up
Pdk4	1.9	0.000645	0.006172	up
Gpr171	1.9	6.63E-16	3.26E-13	up
Il7	1.9	5.42E-06	0.00016	up
Mrc1	1.9	3.71E-06	0.000119	up
Sat1	1.9	2.41E-07	1.23E-05	up
Alox15	1.9	1.77E-07	9.71E-06	up
Sh2d2a	1.9	2.4E-05	0.000512	up
Ephb6	1.9	0.000814	0.007257	up
Slc5a3	1.9	2.31E-06	8.24E-05	up
Map3k8	1.9	3.98E-07	1.95E-05	up
P2ry10	1.9	7.95E-09	7.17E-07	up
Itgb3	1.9	1.76E-06	6.63E-05	up
Jun	1.9	5.18E-12	1.02E-09	up
Lgals3	1.9	1.13E-07	6.56E-06	up
Sbno2	1.9	3.99E-07	1.95E-05	up
Tnfrsf1b	1.9	3.52E-08	2.48E-06	up
Dusp8	1.9	8.03E-07	3.41E-05	up
Nov	1.9	0.000365	0.004109	up
Irf1	1.9	3.89E-05	0.000748	up
Slc20a1	1.9	4.31E-06	0.000134	up
Slfn2	1.8	2.34E-05	0.000503	up
Angptl8	1.8	0.006394	0.032455	up
Pdlim1	1.8	6.57E-06	0.000186	up
Tnfrsf1a	1.8	6.2E-08	3.97E-06	up
Il6r	1.8	1.02E-08	8.7E-07	up
RGD1305807	1.8	0.000372	0.004173	up
Ptges	1.8	4.93E-06	0.00015	up
Asns	1.8	2.58E-05	0.000542	up
Olr1	1.8	6.8E-06	0.000191	up
Mss51	1.8	5.2E-05	0.000931	up
Sema6b	1.8	1.17E-05	0.000295	up
Cyr61	1.8	3.2E-05	0.000642	up

Minpp1	1.8	3.7E-06	0.000119	up
Dnajb3	1.8	8.36E-06	0.000227	up
Cfi	1.8	9.89E-09	8.5E-07	up
Cd3eap	1.8	2.64E-05	0.000551	up
Tifa	1.8	1.94E-06	7.12E-05	up
Runx3	1.8	2.16E-05	0.000473	up
LOC100909675	1.8	1.02E-06	4.2E-05	up
A3galt2	1.8	8.12E-09	7.27E-07	up
Slfn13	1.8	1.16E-08	9.75E-07	up
Zdhhc18	1.8	5.98E-06	0.000171	up
Ace	1.8	4.41E-07	2.14E-05	up
Fcrl2	1.8	0.000199	0.002584	up
Rassf1	1.8	3.97E-09	3.91E-07	up
Oasl	1.8	0.000171	0.002316	up
Themis2	1.8	0.00049	0.005055	up
Phldb3	1.7	5.35E-07	2.49E-05	up
Guca2a	1.7	4.5E-14	1.48E-11	up
Gadd45g	1.7	0.001422	0.011037	up
Bcl2l11	1.7	9.43E-09	8.17E-07	up
RGD1311892	1.7	0.000123	0.001792	up
Grem2	1.7	3.15E-05	0.000638	up
Rprm	1.7	5.54E-06	0.000162	up
Bbc3	1.7	1.94E-05	0.000437	up
Cpne8	1.7	1.76E-06	6.63E-05	up
Tes	1.7	9.86E-08	5.9E-06	up
Vmp1	1.7	2.08E-08	1.61E-06	up
Lamb3	1.7	3.37E-05	0.000669	up
Slc16a5	1.7	6.78E-05	0.001123	up
Anxa2	1.7	6.26E-09	5.8E-07	up
Gch1	1.7	0.006682	0.03342	up
Tns4	1.7	0.000324	0.003771	up
Ppp2r3b	1.7	2.58E-05	0.000542	up
Cks2	1.7	0.000581	0.005718	up
Enc1	1.7	2.83E-06	9.78E-05	up
Elmsan1	1.7	7.97E-10	8.96E-08	up
Il17rb	1.7	1.44E-07	8.16E-06	up
Hmga1	1.7	6.32E-05	0.001072	up
Cited4	1.7	0.000569	0.005651	up
Dusp10	1.7	0.001182	0.009593	up
Fam227a	1.7	0.00045	0.004761	up
LOC100362783	1.7	0.001076	0.008909	up

Ifrd1	1.7	4.54E-07	2.18E-05	up
Map6	1.7	3.19E-06	0.000106	up
Etnk2	1.7	3.18E-05	0.00064	up
Gmnn	1.7	1.03E-05	0.000268	up
Ccnl1	1.7	1.78E-06	6.65E-05	up
Btg1	1.7	9.39E-09	8.17E-07	up
Pfkfb3	1.7	1.36E-10	1.78E-08	up
RGD1311946	1.6	2.44E-08	1.85E-06	up
Lcat	1.6	0.001535	0.011669	up
Fam110c	1.6	2.12E-06	7.72E-05	up
Pstpip1	1.6	1.05E-06	4.31E-05	up
Tuba1c	1.6	2.49E-05	0.000528	up
Hspb1	1.6	8.03E-05	0.001269	up
B4galt5	1.6	2.51E-05	0.000531	up
Tfpi2	1.6	0.001576	0.011884	up
Rhbdf2	1.6	3.03E-06	0.000102	up
Sgk1	1.6	3.68E-06	0.000119	up
Slc2a1	1.6	8.82E-05	0.001368	up
Agfg2	1.6	3.47E-08	2.45E-06	up
C1qb	1.6	5.71E-08	3.7E-06	up
Errfi1	1.6	4.98E-07	2.34E-05	up
Plk2	1.6	3.04E-08	2.23E-06	up
Efna1	1.6	4.49E-05	0.000837	up
Ier3	1.6	5.9E-11	8.64E-09	up
LOC302022	1.6	0.002789	0.017893	up
Snx20	1.6	6.31E-06	0.00018	up
Ager	1.6	0.007704	0.037258	up
Eno2	1.6	0.000454	0.00478	up
Kcnk1	1.6	7.14E-07	3.12E-05	up
B3galnt1	1.6	7.46E-05	0.001202	up
S100a11	1.6	7.12E-09	6.48E-07	up
Hk2	1.6	3.24E-07	1.62E-05	up
Plekhn1	1.6	0.001785	0.013021	up
Ren	1.6	0.002648	0.017231	up
Cd300a	1.5	0.000261	0.003224	up
Pla2g2a	1.5	0.001587	0.011939	up
Sdc4	1.5	8.67E-06	0.000234	up
Cnnm4	1.5	1.67E-07	9.32E-06	up
Art4	1.5	0.006989	0.034617	up
LOC498276	1.5	7.41E-06	0.000204	up
Kcnk5	1.5	5.98E-06	0.000171	up

Slc25a25	1.5	1.71E-31	6.16E-28	up
Cxcl14	1.5	0.000256	0.003179	up
Lama5	1.5	2.13E-05	0.00047	up
Ddit3	1.5	6.17E-05	0.001054	up
Slc1a5	1.5	5.93E-06	0.000171	up
Tubb2b	1.5	8.32E-07	3.48E-05	up
Ppl	1.5	1.98E-11	3.35E-09	up
Ddit4	1.5	1.03E-09	1.14E-07	up
Zyx	1.5	7.54E-07	3.24E-05	up
Cd276	1.5	8.45E-06	0.000229	up
Ch25h	1.5	2.8E-06	9.73E-05	up
Ambp	1.5	0.004426	0.024569	up
Tsc22d4	1.5	9.62E-07	3.99E-05	up
Prcp	1.5	0.001556	0.011773	up
Jund	1.5	2.2E-10	2.77E-08	up
Csdc2	1.5	0.002301	0.01564	up
Pik3r5	1.5	0.00036	0.004063	up
Wfikkn1	1.5	0.000662	0.006314	up
Tagln	1.5	5.87E-05	0.001015	up
Zfand2a	1.5	9.48E-06	0.000252	up
Rgs2	1.5	2.07E-09	2.17E-07	up
Zbtb16	1.5	3.67E-08	2.5E-06	up
Pkp1	1.5	0.000279	0.003401	up
Ccl19	1.5	0.000195	0.002554	up
C4a	1.5	4.34E-11	6.81E-09	up
Cnksr3	1.5	7.1E-07	3.11E-05	up
Pde10a	1.5	0.002476	0.016433	up
Gja1	1.5	5.72E-09	5.43E-07	up
Clec9a	1.5	0.003397	0.020508	up
RGD1305464	1.5	8.23E-07	3.47E-05	up
Lum	1.5	0.010996	0.047977	up
Zbtb42	1.5	1.14E-06	4.6E-05	up
Aen	1.5	9.44E-05	0.00145	up
Hspb7	1.5	0.00056	0.005599	up
Adcy1	-1.5	0.000859	0.007536	Down
Paqr7	-1.5	3.34E-06	0.00011	Down
A4galt	-1.5	2.67E-06	9.35E-05	Down
Slco1a1	-1.5	3.29E-06	0.000109	Down
Wscd1	-1.5	0.003579	0.021223	Down
Dleu7	-1.5	3.46E-08	2.45E-06	Down
Esm1	-1.6	3.18E-05	0.00064	Down

Hykk	-1.6	0.009393	0.042736	Down
RT1-T24-3	-1.7	0.002477	0.016433	Down
Cml1	-1.7	1.54E-06	5.89E-05	Down
RGD1559600	-1.7	0.004193	0.023734	Down
Pipox	-1.7	5.62E-05	0.000984	Down
Pdxp	-1.8	4.38E-08	2.93E-06	Down
Glyatl1	-1.8	5.74E-05	0.001	Down
Ihh	-1.8	1.43E-05	0.000346	Down
Sv2b	-1.8	0.000967	0.008224	Down
Snca	-1.9	0.007389	0.036061	Down
Zfp93	-1.9	0.000863	0.007548	Down
Tmem125	-1.9	0.001126	0.00923	Down
LOC367975	-2.0	0.000924	0.007933	Down
Rfx6	-2.0	4.31E-05	0.000814	Down
Sema5b	-2.0	0.001011	0.008521	Down
Mylk3	-2.0	0.004211	0.023811	Down
Gpr63	-2.2	6.98E-05	0.001144	Down
Slc16a14	-2.2	0.00043	0.004619	Down
LOC690918	-2.2	0.001223	0.009817	Down
Spata22	-2.4	9.65E-12	1.74E-09	Down
Prima1	-2.4	0.000333	0.003829	Down
Ptprq	-2.5	7.86E-06	0.000215	Down
Pcdh9	-2.5	0.010101	0.045108	Down
Ros1	-2.6	8.26E-08	5.05E-06	Down
Fam184b	-2.6	7.18E-07	3.12E-05	Down
Cyp8b1	-2.7	6.7E-05	0.001115	Down
Cyp2c11l	-3.9	2.16E-18	2.13E-15	Down
Hrasls	-4.0	0.010499	0.046275	Down

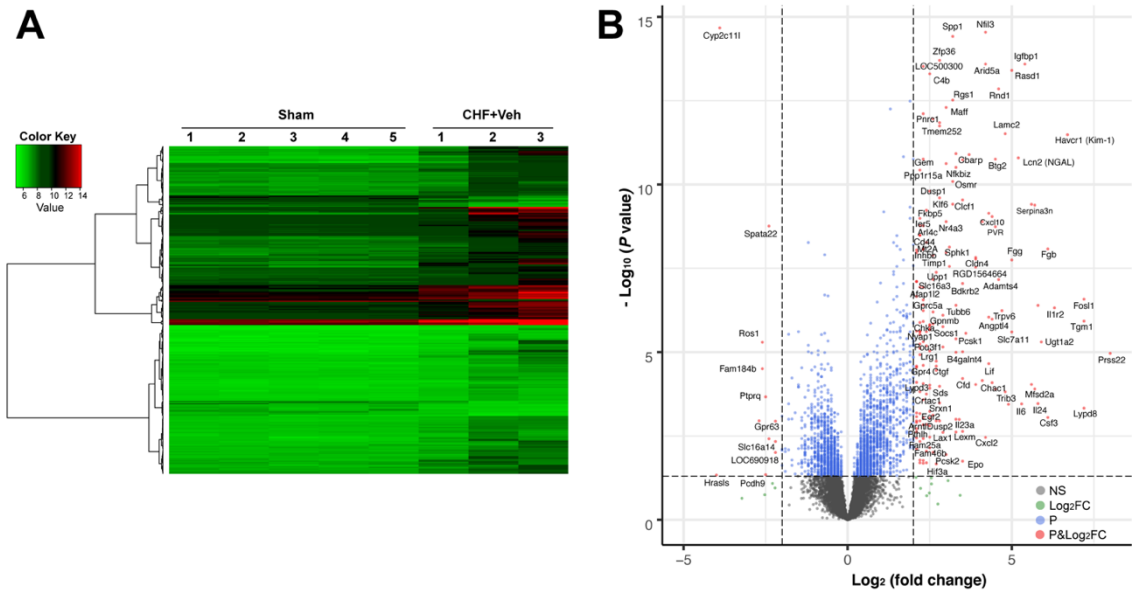

Figure 7. A. Heatmap of differentially expressed genes in kidneys of CHF+Vehicle rats when compared to sham. Genes were clustered according to their expression profile. Red representing higher level of expression and blue representing lower expression. Gene expression values were converted to z-scores to facilitate comparison, and for visual clarity. B. The volcano plot of differentially expressed genes between CHF and sham. The red dots represent differentially expressed genes with at least 1 log2 fold-change between CHF when compared to sham and Benjamini-Hochberg (BH) adjusted P-value <0.05; green and blue dots indicate genes with log2 fold change ≥1 or BH adjusted P-value ≤0.05 respectively. Grey dots indicate genes that did not meet the cutoff for fold change or P-value. Sham group, n=5; CHF+Veh group, n=3.

Significantly enriched Gene Ontology (GO) categories for differentially expressed genes between sham and CHF+Vehicle groups are shown in **Table 7** and in **Figure 8**. The MAPK signaling pathway, the pathway related to cytokine-cytokine receptor interaction, and tumor necrosis factor (TNF) signaling pathway were upregulated in the kidneys of CHF+Vehicle rats. In addition, hypoxia-inducible factor 1 (HIF-1) signaling and apoptosis-related pathways were also activated in CHF+Vehicle rats compared with sham, indicating that hypoxia and apoptosis occur and may also be involved in the development of kidney damage in CHF+Vehicle rats. IPA analysis (**Table 8**) identified the IL-6 signaling pathway to be enriched ($p = 4.48E-09$, overlap = 12.1%).

Table 7. Common differentially expressed genes

15 common elements in "Up(Sham/CHF+Veh)" and "Dn(CHF+Veh/CHF+RTX)"

Genes	Fold (CHF+Veh vs Sham)	Fold (CHF+RTX vs Sham)
Havcr1 (Kim1)	104.19	4.88
Il24	55.28	0.85
Cyp3a9	16.69	1.82
Adra1d	9.89	1.97
Gpnmb	7.32	1.16
Kng1ll	5.98	0.95
Ptprz1	5.68	1.26
C4b	5.54	1.03
Cd44	4.54	1.54
Alox15	3.76	1.08
Nov	3.61	1.07
Cfi	3.48	0.87
Fcrl2	3.38	1.09
Ccl19	2.77	0.67
Lum	2.75	0.60

5 common elements in "Dn(sham/CHF+Veh)" and "Up(CHF+Veh/CHF+RTX)"

Genes	Fold (CHF+Veh vs Sham)	Fold (CHF+RTX vs Sham)
Slco1a1	0.35	1.23
Spata22	0.19	0.59
Ptprq	0.18	1.00
Ros1	0.16	0.79
Cyp2c11l	0.07	0.75

3 common elements in "Up(Sham/CHF+Veh)" and "Up(CHF+Veh/CHF+RTX)"

Genes	Fold (CHF+Veh vs Sham)	Fold (CHF+RTX vs Sham)
Sds	7.03	37.22
Pou3f1	4.90	15.00
Gnat1	4.00	11.28

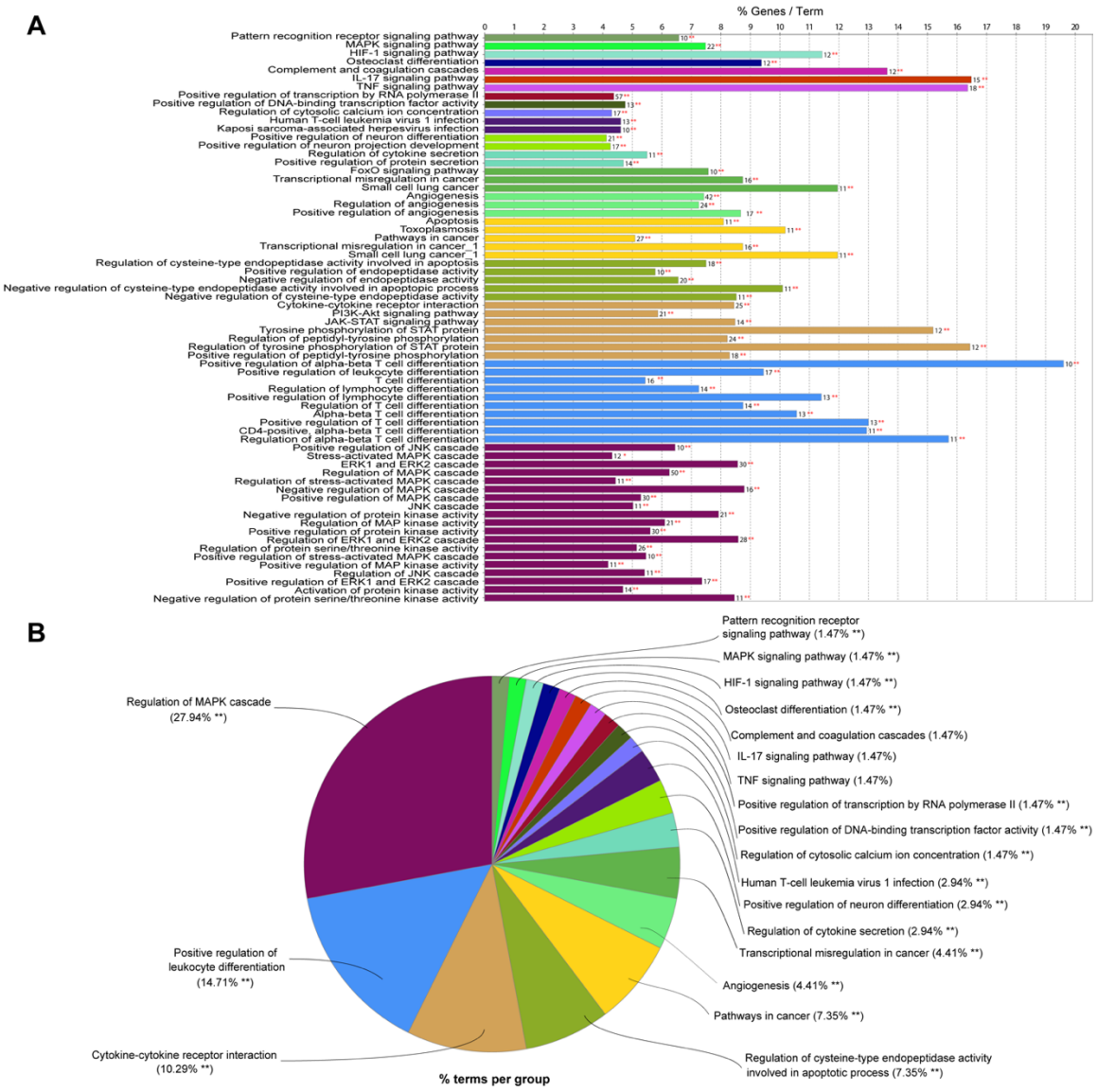

Figure 8. Gene Ontology (GO) analysis of differentially expressed genes in CHF+Vehicle when compared to sham performed using the Cytoscape plugin ClueGO. GO terms represented includes major functional category groupings for biological process and molecular function along with KEGG pathways. A. GO/pathway terms specific for the differentially expressed genes. The bars represent the number of highly expressed genes associated with the terms. B. An overview chart showing the percentage contribution of each enriched functional group, including specific terms for the differentially expressed genes in CHF when compared to sham. Sham group, n=5; CHF+Veh group, n=3.

Table 8. IPA Enriched Canonical pathways between CHF+ vehicle and sham

The significance values (p-value of overlap) for the canonical pathways are calculated by the right-tailed Fisher's Exact Test. The ratio is the number of molecules in a given pathway divided by the total number of molecules that make up that pathway and that are in the reference set. Z-scores indicate activity of a pathway. Positive Z-scores indicate activation,and negative z-score predicts overall decrease in activity.

Ingenuity Canonical Pathways	-log(B-H p-value)	Ratio	z-score	Molecules
Acute Phase Response Signaling	7.51	0.118	2.828	A2M,AMBP,C4A/C4B,CEBPB,FGA,FGB,FGG,HMOX1,IL1RN,IL6,IL6R,JUN,NFKBIA,OSMR,SERPINA3,SERPINE1,SOCS1,SOCS3,TNFRSF1A,TNFRSF1B
IL-6 Signaling	6.06	0.121	2.84	A2M,CD14,CEBPB,HSPB1,HSPB7,IL1R2,IL1RN,IL6,IL6R,JUN,NFKBIA,PIK3R5,SOCS1,SOCS3,TNFRSF1A,TNFRSF1B
Granulocyte Adhesion and Diapedesis	5.96	0.108	Not predicted	CCL19,CLDN4,CLDN7,CSF3,CXCL10,CXCL14,CXCL2,CXCL3,CXCR4,HSPB1,IL1R2,IL1RN,ITGB3,SDC4,SELP,TNFRSF1A,TNFRSF1B
Osteoarthritis Pathway	5.81	0.092	1	ADAMTS4,AGER,ANXA2,CEBPB,CREB5,DDIT4,ELF3,IHH,IL1R2,PRG4,PTHLH,S100A8,S100A9,SDC4,SOX9,SPHK1,SPP1,TNFRSF1A,TNFRSF1B
LXR/RXR Activation	5.71	0.126	0	AMBP,C4A/C4B,CD14,CLU,FGA,IL1R2,IL1RN,IL6,LCAT,LDLR,S100A8,TNFRSF1A,TNFRSF1B,UGT1A3
p38 MAPK Signaling	4.72	0.113	2.496	CREB5,DDIT3,DUSP1,DUSP10,HSPB1,HSPB7,IL1R2,IL1RN,MYC,PLA2G2A,TIFA,TNFRSF1A,TNFRSF1B
IL-10 Signaling	4.54	0.149	Not predicted	CD14,FCGR2A,FCGR2B,HMOX1,IL1R2,IL1RN,IL6,JUN,NFKBIA,SOCS3
IL-17A Signaling in Fibroblasts	3.94	0.212	Not predicted	CEBPB,CEBPD,IL6,JUN,LCN2,NFKBIA,NFKBIZ
Coagulation System	3.80	0.200	0.378	A2M,BDKRB2,FGA,FGB,FGG,PLAUR,SERPINE1
Hepatic Fibrosis / Hepatic Stellate Cell Activation	3.41	0.077	Not predicted	A2M,CCN2,CD14,COL7A1,CXCL3,EDN1,IL1R2,IL6,IL6R,KLF6,SERPINE1,TIMP1,TNFRSF1A,TNFRSF1B
VDR/RXR Activation	3.22	0.115	0.816	CD14,CDKN1A,CEBPB,CXCL10,GADD45A,IGFBP1,KLF4,SPP1,TRPV6

Agranulocyte Adhesion and Diapedesis	3.20	0.078	Not predicted	CCL19,CLDN4,CLDN7,CXCL10,CXCL14,CXCL2,CXCL3,CXCR4,Glycam1,IL1RN,SDC4,SELP,TNFRSF1A
Role of Tissue Factor in Cancer	3.02	0.087	Not predicted	CCN1,CCN2,F2RL1,FGA,FGB,FGG,HBEGF,ITGB3,PDXP,PIK3R5,PLAUR
Role of Macrophages, Fibroblasts and Endothelial Cells in Rheumatoid Arthritis	3.01	0.057	Not predicted	ADAMTS4,CEBPB,CEBPD,CREB5,F2RL1,IL1R2,IL1RN,IL6,IL6R,IL7,JUN,MYC,NFKBIA,PIK3R5,SOCS1,SOCS3,TNFRSF1A,TNFRSF1B
Atherosclerosis Signaling	2.65	0.085	Not predicted	ALOX15,CLU,CXCR4,IL1RN,IL6,LCAT,PLA2G2A,S100A8,SELP,TNFRSF12A
Role of JAK family kinases in IL-6-type Cytokine Signaling	2.64	0.200	Not predicted	IL6,IL6R,OSMR,SOCS1,SOCS3
Th1 and Th2 Activation Pathway	2.62	0.071	Not predicted	CXCR4,IL17RB,IL24,IL6,IL6R,IRF1,JUN,NFIL3,PIK3R5,RUNX3,SOCS1,SOCS3
Glucocorticoid Receptor Signaling	2.43	0.052	Not predicted	A2M,CDKN1A,CEBPB,CXCL3,DUSP1,FGG,FKBP5,HSPA1A/HSPA1B,IL1R2,IL1RN,IL6,JUN,KRT18,NFKBIA,PIK3R5,SERPINE1,SGK1
Hepatic Cholestasis	2.43	0.071	Not predicted	ADCY1,CD14,CYP8B1,IL1R2,IL1RN,IL6,JUN,LIF,NFKBIA,TNFRSF1A,TNFRSF1B
ERK5 Signaling	2.21	0.100	2.449	CREB5,FOSL1,LIF,MAP3K8,MYC,SGK1,SH2D2A
Role of IL-17A in Psoriasis	2.21	0.375	Not predicted	CXCL3,S100A8,S100A9
D-myo-inositol (1,4,5,6)-Tetrakisphosphate Biosynthesis	2.21	0.071	2.53	CA3,DUSP1,DUSP10,DUSP2,DUSP5,DUSP8,MINPP1,PDXP,Ppp2r3d,SOCS3

D-myo-inositol (3,4,5,6)-tetrakisphosphate Biosynthesis	2.21	0.071	2.53	CA3,DUSP1,DUSP10,DUSP2,DUSP5,DUSP8,MINPP1,PDXP,Ppp2r3d,SOCS3
GADD45 Signaling	2.19	0.211	Not predicted	CDKN1A,GADD45A,GADD45B,GADD45G
Role of Osteoblasts, Osteoclasts and Chondrocytes in Rheumatoid Arthritis	2.12	0.057	Not predicted	ADAMTS4,BIRC3,IL1R2,IL1RN,IL6,IL7,ITGB3,JUN,NFKBIA,PIK3R5,SPP1,TNFRSF1A,TNFRSF1B
Role of Cytokines in Mediating Communication between Immune Cells	1.98	0.132	Not predicted	CSF3,IL1RN,IL23A,IL24,IL6
3-phosphoinositide Degradation	1.98	0.065	2.53	CA3,DUSP1,DUSP10,DUSP2,DUSP5,DUSP8,MINPP1,PDXP,Ppp2r3d,SOCS3
Apelin Cardiac Fibroblast Signaling Pathway	1.98	0.182	-2	CCN2,IL6,SERPINE1,SPHK1
IL-12 Signaling and Production in Macrophages	1.97	0.069	Not predicted	ALOX15,CEBPB,CLU,IL23A,IRF1,JUN,MAP3K8,PIK3R5,S100A8
Production of Nitric Oxide and Reactive Oxygen Species in Macrophages	1.97	0.060	3.317	CLU,IRF1,JUN,MAP3K6,MAP3K8,NFKBIA,PIK3R5,RHOB,S100A8,TNFRSF1A,TNFRSF1B
Hematopoiesis from Pluripotent Stem Cells	1.97	0.128	Not predicted	CSF3,EPO,IL6,IL7,LIF
D-myo-inositol-5-phosphate Metabolism	1.97	0.063	2.53	CA3,DUSP1,DUSP10,DUSP2,DUSP5,DUSP8,MINPP1,PDXP,Ppp2r3d,SOCS3

GP6 Signaling Pathway	1.97	0.069	3	COL7A1,FGA,FGB,FGG,ITGB3,LAMA5,LAMB3,LAMC2,PIK3R5
p53 Signaling	1.96	0.075	0	BBC3,CDKN1A,GADD45A,GADD45B,GADD45G,JUN,PIK3R5,RPRM
Induction of Apoptosis by HIV1	1.96	0.098	0.816	BBC3,BIRC3,CXCR4,NFKBIA,TNFRSF1A,TNFRSF1B
HMGB1 Signaling	1.96	0.068	2.828	AGER,IL6,JUN,LIF,PIK3R5,RHOB,SERPINE1,TNFRSF1A,TNFRSF1B
Hematopoiesis from Multipotent Stem Cells	1.96	0.273	Not predicted	CSF3,EPO,IL7
IGF-1 Signaling	1.93	0.073	0	CCN1,CCN2,CCN3,IGFBP1,JUN,PIK3R5,SOCS1,SOCS3
Prolactin Signaling	1.86	0.080	0.816	CEBPB,IRF1,JUN,MYC,PIK3R5,SOCS1,SOCS3
iNOS Signaling	1.86	0.114	Not predicted	CD14,HMGA1,IRF1,JUN,NFKBIA
3-phosphoinositide Biosynthesis	1.86	0.056	2.714	CA3,DUSP1,DUSP10,DUSP2,DUSP5,DUSP8,MINPP1,PDXP,PIK3R5,Ppp2r3d,SOCS3
JAK/Stat Signaling	1.84	0.079	0.378	CDKN1A,CEBPB,IL6,JUN,PIK3R5,SOCS1,SOCS3
Superpathway of Inositol Phosphate Compounds	1.81	0.052	2.887	CA3,DUSP1,DUSP10,DUSP2,DUSP5,DUSP8,ITPKC,MINPP1,PDXP,PIK3R5,Ppp2r3d,SOCS3
IL-7 Signaling Pathway	1.81	0.077	0.816	BCL6,IL7,JUN,MYC,PIK3R5,SLC2A1,SOCS1
Germ Cell-Sertoli Cell Junction Signaling	1.81	0.058	Not predicted	A2M,MAP3K6,MAP3K8,PIK3R5,RHOB,TNFRSF1A,TUBA1C,TUBB2B,TUBB6,ZYX
Dendritic Cell Maturation	1.80	0.058	3	CREB5,FCGR2A,FCGR2B,IL1RN,IL23A,IL6,NFKBIA,PIK3R5,TNFRSF1A,TNFRSF1B
ATM Signaling	1.72	0.073	Not predicted	CDKN1A,CREB5,GADD45A,GADD45B,GADD45G,JUN,NFKBIA

TNFR2 Signaling	1.72	0.133	1	BIRC3,JUN,NFKBIA,TNFRSF1B
Sertoli Cell-Sertoli Cell Junction Signaling	1.72	0.056	Not predicted	A2M,CLDN4,CLDN7,JUN,MAP3K6,MAP3K8,TNFRSF1A,TUBA1C,TUBB2B,TUBB6
Th1 Pathway	1.70	0.065	0.707	IL6,IL6R,IRF1,NFIL3,PIK3R5,RUNX3,SOCS1,SOCS3
Glioma Invasiveness Signaling	1.64	0.080	1.633	CD44,ITGB3,PIK3R5,PLAUR,RHOB,TIMP1
Role of JAK2 in Hormone-like Cytokine Signaling	1.64	0.125	Not predicted	EPO,SH2B2,SOCS1,SOCS3
Extrinsic Prothrombin Activation Pathway	1.63	0.188	Not predicted	FGA,FGB,FGG
Adipogenesis pathway	1.58	0.061	Not predicted	ARNTL,CEBPB,CEBPD,DDIT3,EGR2,KLF5,SOX9,TNFRSF1A
Neuroinflammation Signaling Pathway	1.54	0.045	2.887	AGER,BIRC3,CREB5,CXCL10,HMOX1,IL6,IL6R,JUN,PIK3R5,PLA2G2A,S100B,SNCA,TNFRSF1A
NRF2-mediated Oxidative Stress Response	1.53	0.051	1.89	ENC1,FKBP5,FOSL1,GPX2,HMOX1,JUN,JUNB,JUND,MAFF,PIK3R5
Complement System	1.53	0.114	1	C1QB,C4A/C4B,CFD,CFI

Comparison of the gene expression profile of CHF+Vehicle and CHF+RTX rats revealed an entirely different profile, with the majority of the differentially expressed genes down-regulated in CHF+RTX rats (**Table 9**). A total of 124 genes were differentially expressed between CHF+Vehicle and CHF+RTX rats, and 96 genes were downregulated in CHF+RTX (**Figure 9**). KIM-1 (Havcr1) expression was only increased by ~ approximately 5-fold in CHF rats treated with RTX compared to sham rats (**Figure 10 C**). However, Ngal was similarly elevated in both CHF+Vehicle and CHF+RTX rats. Gene expression for Il24, Nov, and Ptprzl1 were reduced compared to that in CHF+Vehicle rats, suggesting that cardiac afferent ablation by RTX may prevent the development of renal dysfunction by rescuing dying kidney cells and ameliorating a potentially hypoxic environment in the setting of CHF. Enriched GO categories showed that pathways that regulate the IL-1β secretion was enhanced after RTX treatment (**Figure 11**). Surprisingly, pathways that can negatively regulate blood vessel diameter were also enhanced, implying that RTX may improve renal perfusion through ameliorating intra-renal vasoconstriction. IPA analysis identified several pathways that are involved in interleukin 12 (IL-12) signaling and production in macrophages, LXR/RXR activation, and wnt/-catenin signaling were enriched (**Table 10**).

Table 9. Differentially expressed genes between CHF+Veh and CHF+RTX

Gene	log2 Fold Change	P value	P adj	Direction
Cyp2c11l	3.5	2.05E-12	3.17E-09	up
Serpinb12	3.5	0.003295	0.041408	up
Mchr1	3.0	5.88E-05	0.002798	up
Scd1	2.6	0.000462	0.011572	up
Ptprq	2.5	5.17E-05	0.002546	up
Sds	2.4	0.000342	0.009537	up
Ros1	2.3	3.03E-05	0.001779	up
Armc3	2.2	0.001841	0.029318	up
Fzd5	2.0	1.47E-14	5.30E-11	up
Anxa13	2.0	7.66E-05	0.003341	up
Arl5b	1.9	1.99E-12	3.17E-09	up
Cabp7	1.8	0.002721	0.036872	up
Slco1a1	1.8	6.12E-07	8.95E-05	up
Coq10b	1.7	5.80E-08	1.21E-05	up
Ccdc114	1.7	0.000291	0.008695	up
Fbxo32	1.7	1.73E-08	4.56E-06	up
Phf21b	1.7	0.003203	0.0407	up
Yod1	1.7	2.98E-10	1.50E-07	up
Gramd1b	1.6	2.14E-08	5.53E-06	up
Upp2	1.6	1.14E-08	3.26E-06	up
Pou3f1	1.6	0.000628	0.014497	up
Spata22	1.6	4.07E-05	0.002182	up
Slc1a4	1.6	2.33E-06	0.000247	up
Gnat1	1.5	0.000286	0.008619	up
Irf4	1.5	0.000589	0.013837	up
Egfr	1.5	2.81E-05	0.001683	up
Ddx25	1.5	0.000346	0.009554	up
Prdm1	1.5	0.000138	0.005216	up
Rcsd1	-1.5	0.002543	0.035443	down
Gja5	-1.5	4.86E-05	0.00247	down
Apoc2	-1.5	0.002882	0.037973	down
Sash3	-1.5	0.002665	0.036524	down
Tgfb2	-1.5	0.000206	0.006874	down
Tlr4	-1.5	0.002468	0.034622	down
Ccnb2	-1.5	0.001014	0.019749	down
Prtfdc1	-1.5	0.002189	0.032779	down
Marcks	-1.5	7.91E-09	2.48E-06	down
Olfml3	-1.5	0.000123	0.004795	down

Dlgap5	-1.5	0.000768	0.016206	down
Cmtm3	-1.5	6.43E-05	0.002988	down
Lyz2	-1.5	1.14E-18	1.23E-14	down
Chst12	-1.5	0.000301	0.008841	down
Dcn	-1.5	3.04E-10	1.50E-07	down
Cyp26b1	-1.5	0.002755	0.037097	down
Selplg	-1.6	0.00171	0.027848	down
Traf1	-1.6	0.004325	0.049664	down
Bst1	-1.6	0.000279	0.008442	down
Cd44	-1.6	1.93E-05	0.001268	down
Ect2	-1.6	0.000202	0.006771	down
Tnfsf10	-1.6	5.35E-05	0.002608	down
Top2a	-1.6	9.25E-06	0.000715	down
Spi1	-1.6	2.27E-05	0.001436	down
Baat	-1.6	0.000861	0.017685	down
Cd200	-1.6	0.000183	0.006252	down
Znrd1as1	-1.6	5.89E-05	0.002798	down
Pou2af1	-1.6	0.004064	0.047842	down
Tbxas1	-1.6	2.71E-06	0.000277	down
Gngt2	-1.6	6.99E-06	0.000582	down
Dkk3	-1.6	0.000349	0.009582	down
Fcrl2	-1.6	0.002425	0.034371	down
Ccl21	-1.6	3.74E-05	0.002054	down
Adamts2	-1.7	0.003405	0.042241	down
Axl	-1.7	1.66E-05	0.001119	down
Hfe2	-1.7	0.002622	0.036169	down
Adgre1	-1.7	4.74E-05	0.002434	down
Hmx2	-1.7	0.000227	0.007292	down
Plek	-1.7	1.01E-07	1.88E-05	down
C6	-1.7	0.002006	0.030787	down
Nov	-1.8	0.003287	0.041408	down
Pycard	-1.8	7.21E-06	0.000596	down
Mki67	-1.8	1.00E-09	4.01E-07	down
Egflam	-1.8	0.000492	0.01213	down
Hacd4	-1.8	0.002376	0.034123	down
Lgals1	-1.8	8.83E-11	7.63E-08	down
Alox15	-1.8	3.19E-05	0.001827	down
Pnma2	-1.8	0.002867	0.037811	down
Emp3	-1.8	3.17E-06	0.00031	down
Scara3	-1.8	5.01E-05	0.002514	down
Rab3il1	-1.8	0.000589	0.013837	down

Srpx2	-1.8	0.000149	0.005519	down
Lck	-1.8	3.50E-05	0.001955	down
Rem1	-1.8	6.25E-05	0.002918	down
B3galt2	-1.9	0.000623	0.014459	down
Sox18	-1.9	0.002398	0.034178	down
Igsf6	-1.9	2.55E-05	0.001578	down
Tlr8	-2.0	0.000411	0.010648	down
Clec12a	-2.0	2.57E-06	0.00027	down
Loxl1	-2.0	1.90E-10	1.21E-07	down
Clec4a1	-2.0	5.46E-05	0.002651	down
Cfi	-2.0	5.68E-08	1.21E-05	down
Evi2a	-2.0	0.001651	0.027098	down
Ccl19	-2.1	9.16E-06	0.000715	down
Tril	-2.1	0.000656	0.014837	down
Arl11	-2.1	1.06E-06	0.000133	down
Trpc6	-2.1	0.000898	0.01824	down
Eln	-2.1	8.01E-05	0.003457	down
Agtr1b	-2.2	0.000192	0.006495	down
Srms	-2.2	0.004184	0.048829	down
Gpr34	-2.2	0.001115	0.020892	down
Ptprz1	-2.2	0.000425	0.0109	down
Upk3bl	-2.2	7.83E-05	0.003391	down
Lum	-2.2	0.001497	0.025329	down
Cenpf	-2.2	6.03E-07	8.95E-05	down
C5ar1	-2.2	0.000222	0.007188	down
LOC100365008	-2.2	0.001527	0.025604	down
Hsd17b2	-2.3	0.000301	0.008841	down
Adra1d	-2.3	0.001019	0.019797	down
Folr2	-2.3	0.000333	0.009366	down
Fibin	-2.4	4.02E-05	0.002173	down
Col1a1	-2.4	8.03E-09	2.48E-06	down
C4b	-2.4	9.30E-13	2.01E-09	down
Clec4a3	-2.4	1.16E-09	4.50E-07	down
Il20ra	-2.5	0.004253	0.049339	down
Lilra5	-2.5	0.002745	0.037061	down
Gpnmb	-2.7	2.62E-06	0.000273	down
Kng1l1	-2.7	0.000173	0.006028	down
Fam180a	-2.9	4.76E-06	0.000426	down
Cxcl13	-3.1	0.000158	0.005806	down
Scara5	-3.1	0.000212	0.006989	down
Cyp3a9	-3.2	0.000856	0.017649	down

Havcr1	-4.4	4.60E-06	0.000419	down
Ubd	-4.5	0.000214	0.007027	down
Il24	-6.0	0.000278	0.008427	down
Fam111a	-7.7	2.15E-05	0.001369	down

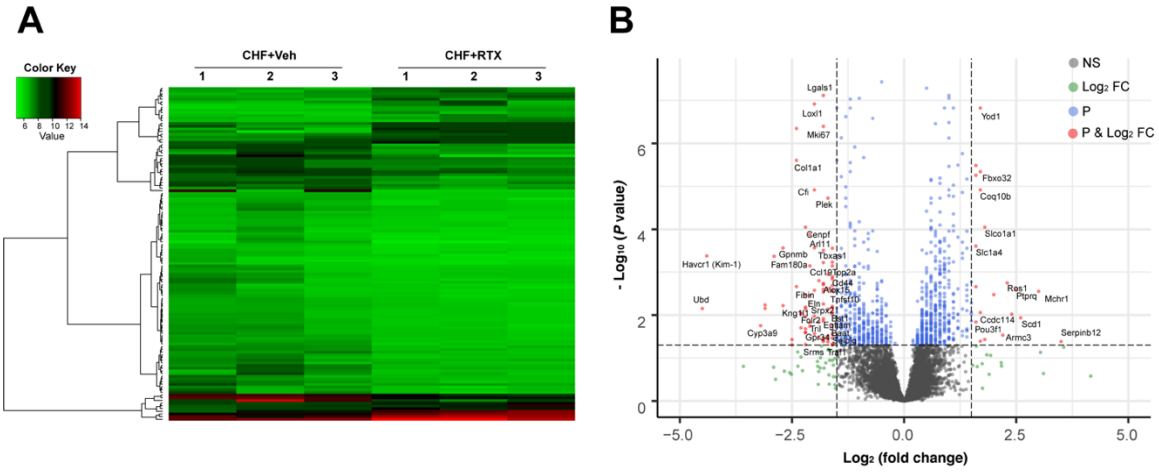

Figure 9. A. Heatmap of differentially expressed genes extracted from kidneys of CHF+Vehicle rats when compared to CHF+RTX. Genes were clustered according to their expression profile. Red representing higher level of expression and blue representing lower expression. Gene expression values were converted to z-scores to facilitate comparison, and for visual clarity. B. The volcano plot of differentially expressed genes between CHF+Vehicle and CHF-RTX rat kidneys. The red dots represent differentially expressed genes with at least 1 $\log_2$ fold-change between CHF when compared to CHF+RTX and BH adjusted P-value <0.05; green and blue dots indicate genes with $\log_2$ fold change ≥1 or Benjamini-Hochberg (BH) adjusted P-value ≤ 0.05 respectively. Grey dots indicate genes that had did not meet the cutoff for fold change or P-value. CHF+Veh group, n=3; CHF+RTX group, n=3.

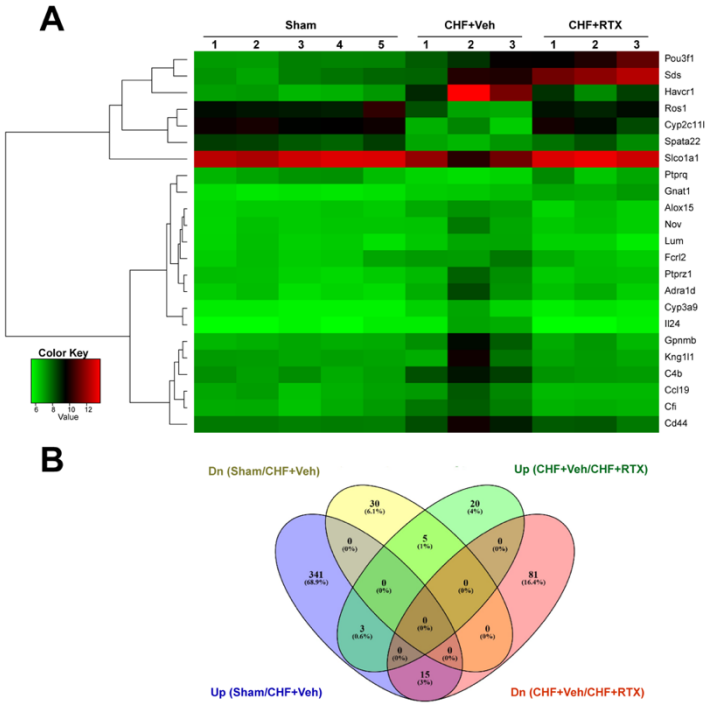

C

15 common elements in "Up(Sham/CHF+Veh)" and "Dn(CHF+Veh/CHF+RTX)"		
Genes	Fold (CHF+Veh vs Sham)	Fold (CHF+RTX vs Sham)
Havcr1 (Kim1)	104.19	4.88
Il24	55.28	0.85
Cyp3a9	16.69	1.82
Adra1d	9.89	1.97
Gpnmb	7.32	1.16
Kng1l1	5.98	0.95
Ptprz1	5.68	1.26
C4b	5.54	1.03
Cd44	4.54	1.54
Alox15	3.76	1.08
Nov	3.61	1.07
Cfi	3.48	0.87
Fcrl2	3.38	1.09
Ccl19	2.77	0.67
Lum	2.75	0.6
5 common elements in "Dn(Sham/CHF+Veh)" and "Up(CHF+Veh/CHF+RTX)"		
Genes	Fold (CHF+Veh vs Sham)	Fold (CHF+RTX vs Sham)
Slco1a1	0.35	1.23
Spata22	0.19	0.59
Ptprq	0.18	1
Ros1	0.16	0.79
Cyp2c11l	0.07	0.75
3 common elements in "Up(sham/CHF)" and "Up(CHF/CHF-RTX)"		
Genes	Fold (CHF+Veh vs Sham)	Fold (CHF+RTX vs Sham)
Sds	7.03	37.22
Pou3f1	4.9	15
Gnat1	4	11.28

Figure 10. RNA sequencing results. A. Heat map of RNA sequencing data showing the altered gene profiles in whole-kidney tissues from CHF rats with and without RTX treatment along with sham. Notice that Kim1(a specific proximal tubular damage marker) was increased in whole-kidney tissues of CHF rats, which was largely prevented by RTX. B. Venn diagram highlighting the number of genes differentially expressed between CHF/Sham and CHF/CHF-RTX. C. Table shows the common genes changed between different comparisons and the fold change. Sham group, n=5; CHF+Veh group, n=3; CHF+RTX group, n=3. Kim1, kidney injury molecule-1.

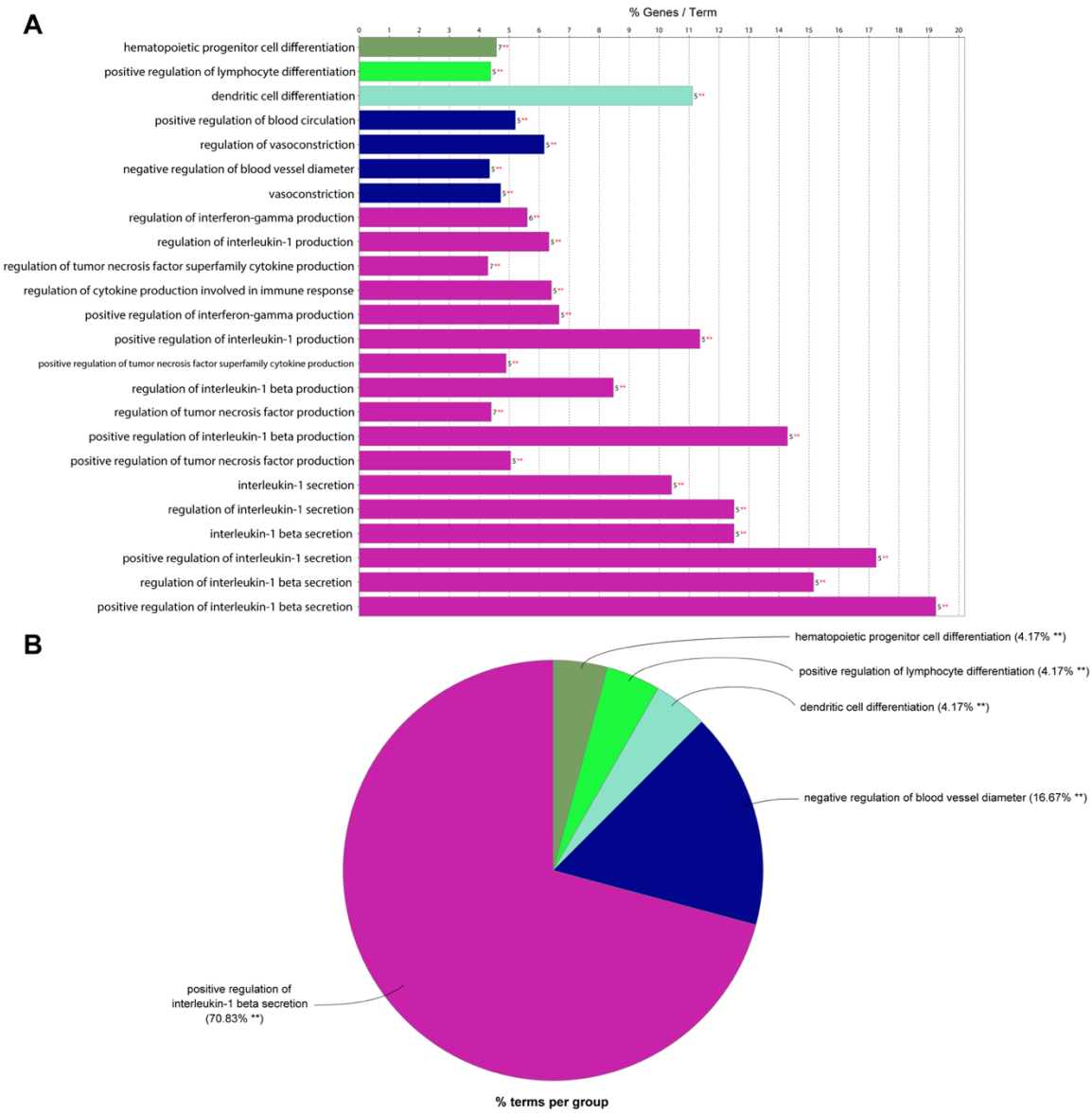

Figure 11. Gene Ontology (GO) analysis of differentially expressed genes in CHF+Vehicle when compared to CHF+RTX performed using the Cytoscape plugin ClueGO. GO terms represented includes major functional category groupings for biological process and molecular function along with KEGG pathways. A. GO/pathway terms specific for the differentially expressed genes. The bars represent the number of highly expressed genes associated with the terms. B. An overview chart showing the percentage contribution of each enriched functional group, including specific terms for the differentially expressed genes in CHF+Vehicle when compared to RTX. CHF+Veh group, n=3; CHF+RTX group, n=3.

Table 10. IPA Enriched Canonical pathways between CHF+ vehicle and CHF+ RTX

The significance values (p-value of overlap) for the canonical pathways are calculated by the right-tailed Fisher's Exact Test. The ratio is the number of molecules in a given pathway divided by the total number of molecules that make up that pathway and that are in the reference set. Z-scores indicate activity of a pathway. Positive Z-scores indicate activation, and negative z-score predicts overall decrease in activity.

Ingenuity Canonical Pathways	-log(p-value)	Ratio	z-score	Molecules
IL-12 Signaling and Production in Macrophages	3.85	0.046	Not predicted	ALOX15,APOC2,LYZ,SPI1,TGFB2,TLR4
LXR/RXR Activation	3.24	0.045	0	APOC2,C4A/C4B,LYZ,SCD,TLR4
Wnt/β-catenin Signaling	3.24	0.036	1.342	CD44,DKK3,FZD5,SOX18,TGFB2,UBD
Atherosclerosis Signaling	3.12	0.042	Not predicted	ALOX15,APOC2,COL1A1,LYZ,SELPLG
Hepatic Fibrosis / Hepatic Stellate Cell Activation	3.08	0.033	Not predicted	Agtr1b,CCL21,COL1A1,EGFR,TGFB2,TLR4
Phagosome Formation	3.02	0.040	Not predicted	C5AR1,Fcrls,SCARA3,TLR4,TLR8
Toll-like Receptor Signaling	2.97	0.054	Not predicted	TLR4,TLR8,TRAF1,UBD
Complement System	2.91	0.086	Not predicted	C4A/C4B,C5AR1,CFI
Altered T Cell and B Cell Signaling in Rheumatoid Arthritis	2.75	0.047	Not predicted	CCL21,CXCL13,TLR4,TLR8
Granulocyte Adhesion and Diapedesis	2.57	0.032	Not predicted	C5AR1,CCL19,CCL21,CXCL13,SELPLG
Agranulocyte Adhesion and Diapedesis	2.45	0.030	Not predicted	C5AR1,CCL19,CCL21,CXCL13,SELPLG
Inflammasome pathway	2.24	0.105	Not predicted	PYCARD,TLR4
Role of Pattern Recognition Receptors in Recognition of Bacteria and Viruses	2.09	0.031	Not predicted	C5AR1,TGFB2,TLR4,TLR8
Role of Macrophages, Fibroblasts and Endothelial Cells in Rheumatoid Arthritis	1.91	0.019	Not predicted	C5AR1,DKK3,FZD5,TLR4,TLR8,TRAF1
L-serine Degradation	1.74	0.333	Not predicted	SDS
Colorectal Cancer Metastasis Signaling	1.74	0.020	0	EGFR,FZD5,TGFB2,TLR4,TLR8
Tec Kinase Signaling	1.73	0.024	Not predicted	GNAT1,LCK,TLR4,TNFSF10

Estrogen Biosynthesis	1.61	0.050	Not predicted	CYP3A7,HSD17B2
NF-κB Signaling	1.60	0.022	-1	EGFR,LCK,TLR4,TLR8
Production of Nitric Oxide and Reactive Oxygen Species in Macrophages	1.58	0.022	Not predicted	APOC2,LYZ,SPI1,TLR4
Neuroinflammation Signaling Pathway	1.49	0.017	-1.342	CD200,PYCARD,TGFB2,TLR4,TLR8
FXR/RXR Activation	1.46	0.026	Not predicted	APOC2,BAAT,C4A/C4B
Cell Cycle: G2/M DNA Damage Checkpoint Regulation	1.43	0.040	Not predicted	CCNB2,TOP2A
Phototransduction Pathway	1.43	0.040	Not predicted	GNAT1,GNGT2
LPS/IL-1 Mediated Inhibition of RXR Function	1.40	0.019	Not predicted	APOC2,CHST12,CYP3A7,TLR4

Subsequently, we analyzed genes that were common between the two comparisons, (i.e., sham vs CHF+Vehicle, and CHF+Vehicle vs CHF+RTX). We found 23 genes that were common among these comparisons (**Figure 10**). The majority of these 23 genes showed a reversal in gene expression in CHF+RTX rats. For example, the kidney damage marker gene, Kim-1 (Havcr1) was upregulated in CHF+Vehicle rats compared to sham but downregulated in CHF-RTX rats when compared to CHF+Vehicle rats (**Table 7**). Cellular death-associated genes, such as Il24 and Nov showed the same trend. Interestingly, Ptprz1, which has been found to be expressed in human embryonic kidney cells under hypoxic conditions, was upregulated in CHF+Vehicle rats was also attenuated by RTX. In addition, alpha-1d adrenergic receptor (Adra1d) was upregulated in CHF+Vehicle rats and was attenuated by RTX.

Pathways enrichment analysis

Based on the findings that genes associated with apoptosis, hypoxia, inflammation, and renal damage were upregulated in rats with CHF, we investigated the mechanisms underlying the renal dysfunction in CRS type 2 by examining the pathways for apoptosis, hypoxia, inflammation, and renal damage. Among the differentially expressed genes between sham and CHF+Vehicle rats, the apoptotic pathway was the most affected. Of the 96 differentially expressed genes associated with apoptosis, the majority were upregulated in CHF+Vehicle rats when compared to sham rats (**Figure 12**). Eleven genes were differentially regulated in the hypoxia pathway. All of the genes associated with hypoxia were upregulated in CHF+Vehicle rats (**Figure 13**). Differentially expressed genes associated with inflammation also followed the same trend, with the majority upregulated in CHF+Vehicle rats (**Figure 14**). All of the differentially expressed genes between sham and CHF+Vehicle rats that are associated with kidney damage were upregulated in CHF+Vehicle rats, indicating the development of renal dysfunction at 18 weeks post-MI (**Figure 15**).

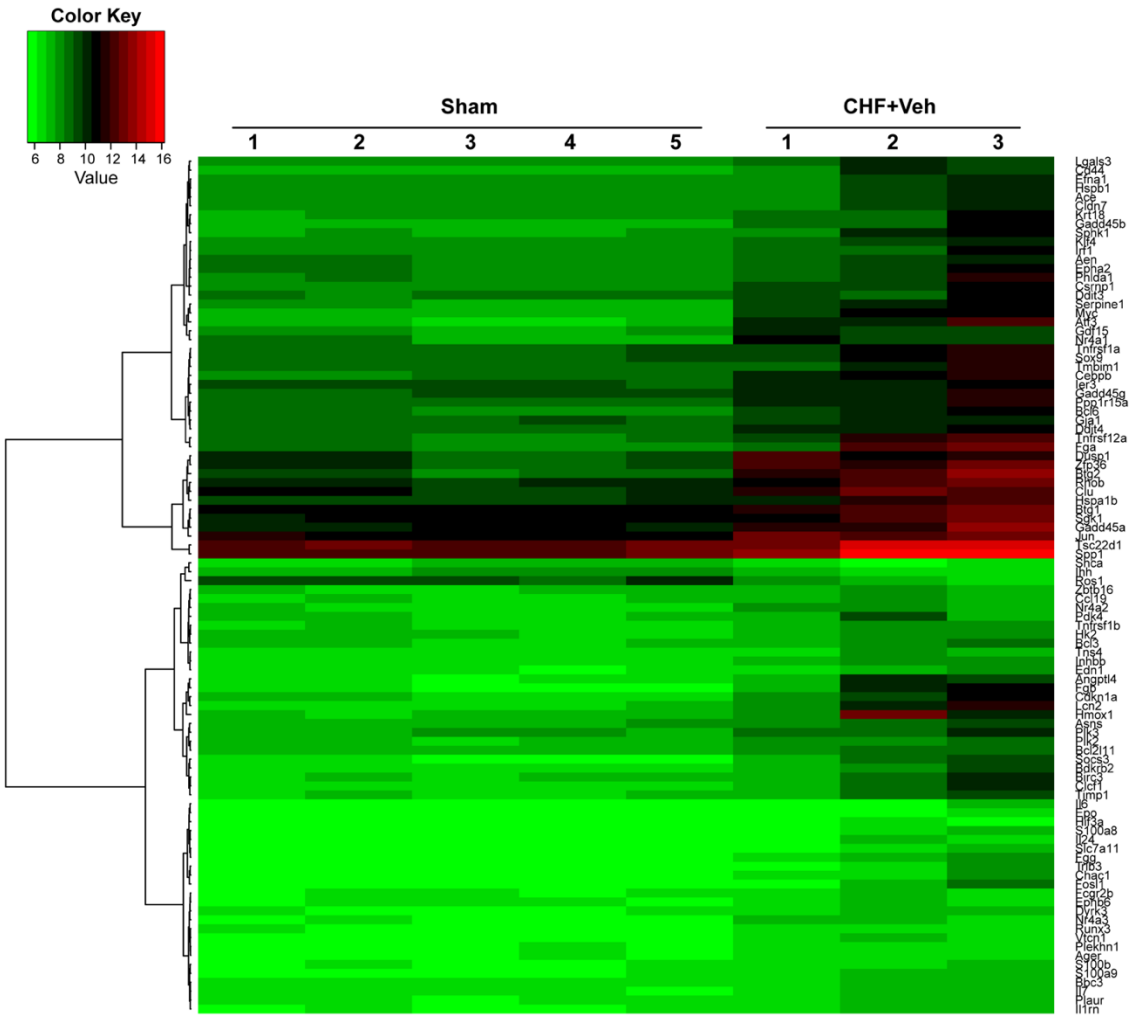

Figure 12. Heatmap of differentially expressed genes in apoptosis related pathways in kidneys of CHF+Vehicle rats when compared to sham. Genes were clustered according to their expression profile. Red representing higher level of expression and blue representing lower expression. Gene expression values were converted to z-scores to facilitate comparison, and for visual clarity. Sham group, n=5; CHF+Veh group, n=3.

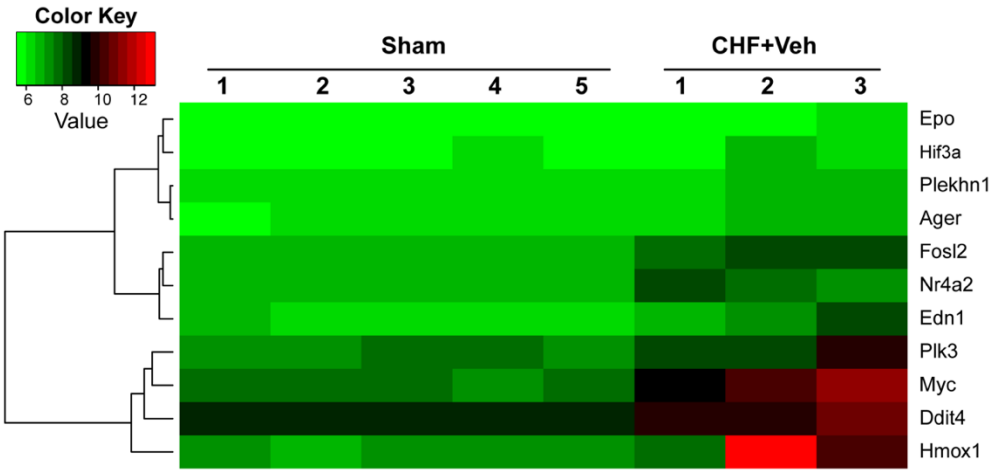

Figure 13. Heatmap of differentially expressed genes in hypoxia related pathways extracted in kidneys of CHF+Vehicle rats when compared to sham. Genes were clustered according to their expression profile. Red representing higher level of expression and blue representing lower expression. Gene expression values were converted to z-scores to facilitate comparison, and for visual clarity. Sham group, n=5; CHF+Veh group, n=3.

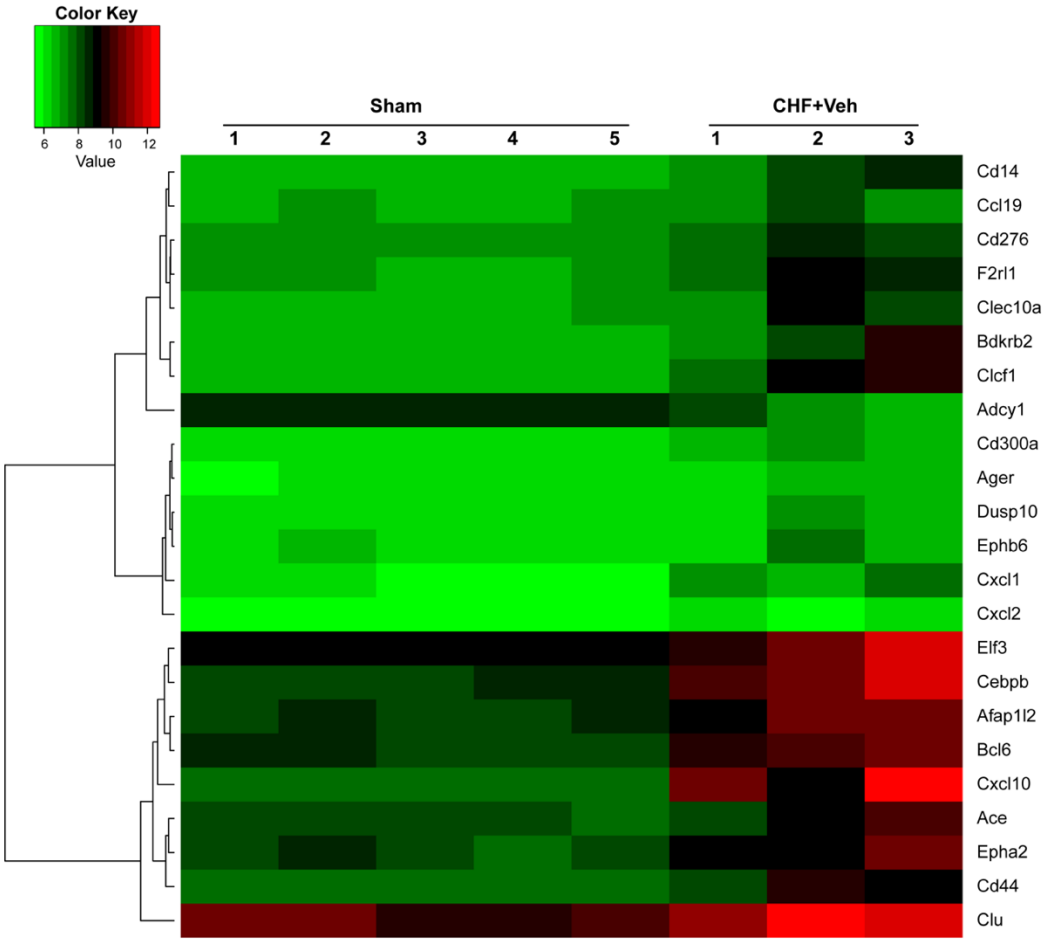

Figure 14. Heatmap of differentially expressed genes in inflammation pathways in kidneys of CHF+Vehicle rats when compared to sham. Genes were clustered according to their expression profile. Red representing higher level of expression and blue representing lower expression. Gene expression values were converted to z-scores to facilitate comparison, and for visual clarity. Sham group, n=5; CHF+Veh group, n=3.

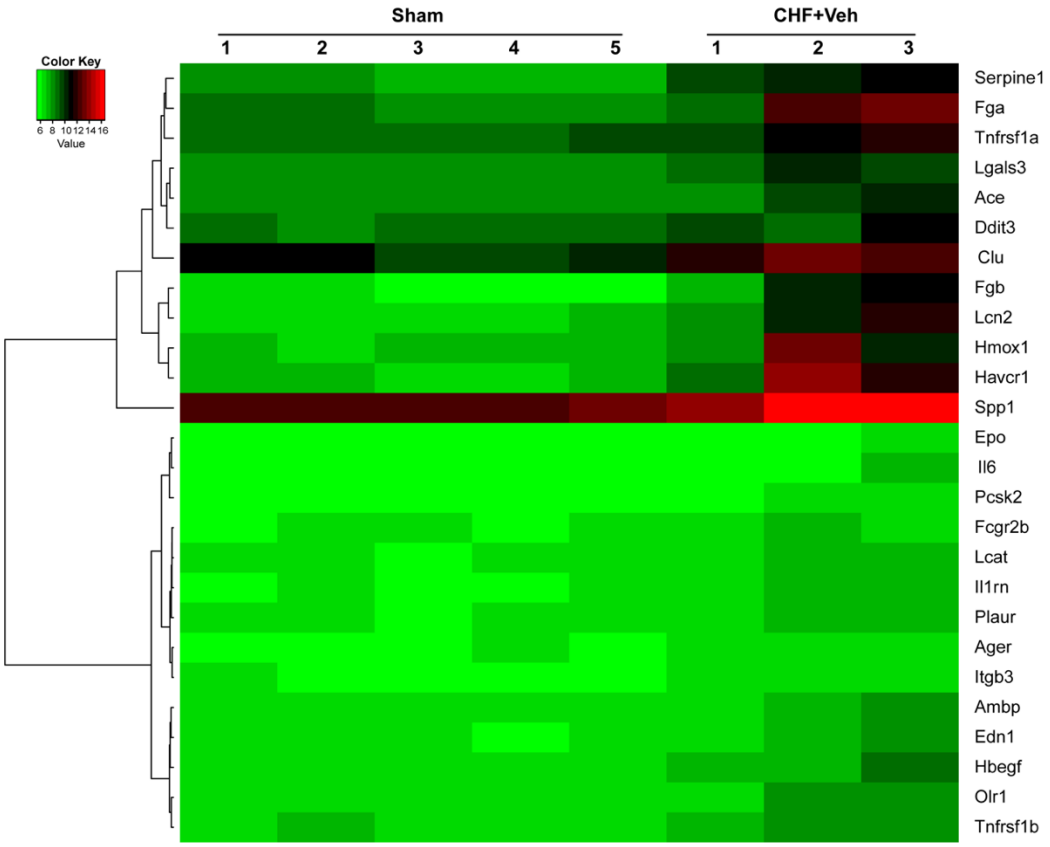

Figure 15. Heatmap of differentially expressed genes in kidney damage pathways in kidneys of CHF+Vehicle rats when compared to sham. Genes were clustered according to their expression profile. Red representing higher level of expression and blue representing lower expression. Gene expression values were converted to z-scores to facilitate comparison, and for visual clarity. Sham group, n=5; CHF+Veh group, n=3.

To identify the effect of cardiac afferent ablation on the pathways for apoptosis, hypoxia, inflammation, and renal damage, we analyzed differentially expressed genes associated with these pathways by comparing CHF+Vehicle rats with CHF+RTX rats. We did not find any change in the genes associated with hypoxia after RTX treatment. Among these four pathways, the maximum number of differentially expressed genes were associated with apoptosis. Interestingly, the majority of the differentially expressed genes associated with apoptosis were downregulated in CHF+RTX rats (**Figure 16).** This trend was also noted for genes associated with inflammation (**Figure 17**) and kidney damage (**Figure 18**).

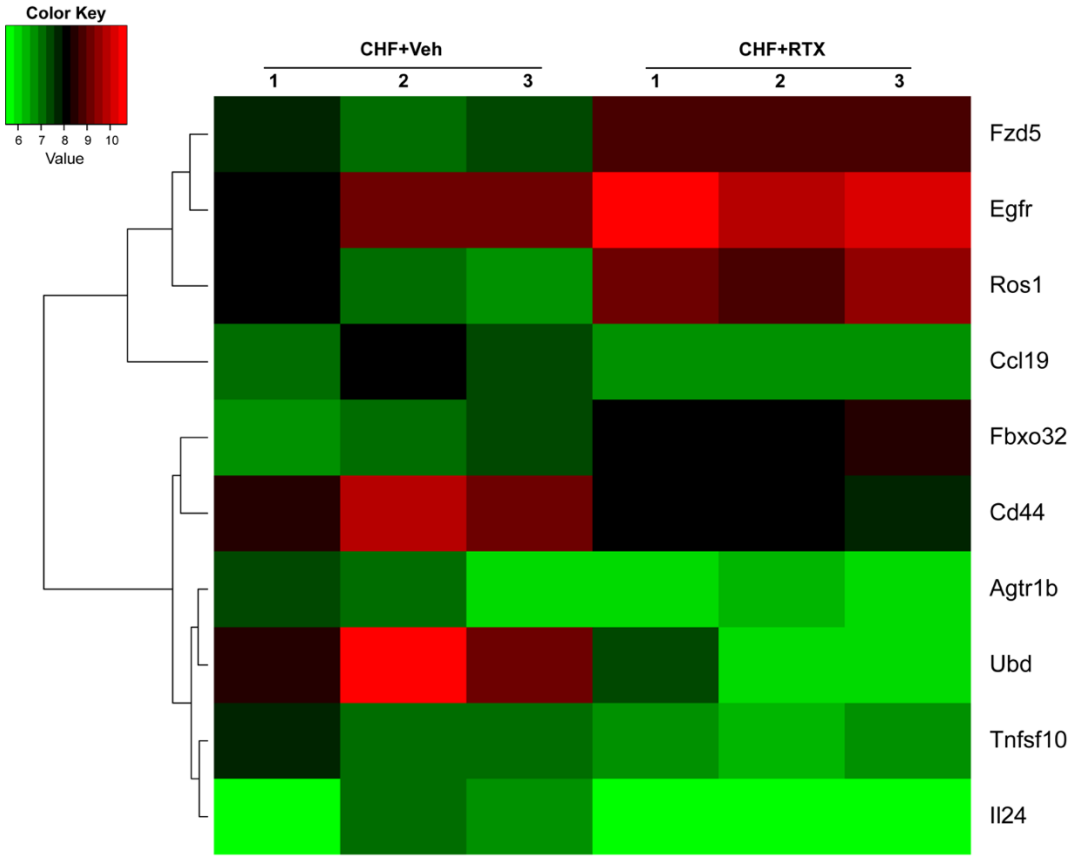

Figure 16. Heatmap of differentially expressed genes in apoptosis pathways in kidneys of CHF+RTX rats when compared to CHF+Vehicle treated rats. Genes were clustered according to their expression profile. Red representing higher level of expression and blue representing lower expression. Gene expression values were converted to z-scores to facilitate comparison, and for visual clarity. CHF+Veh group, n=3; CHF+RTX group, n=3.

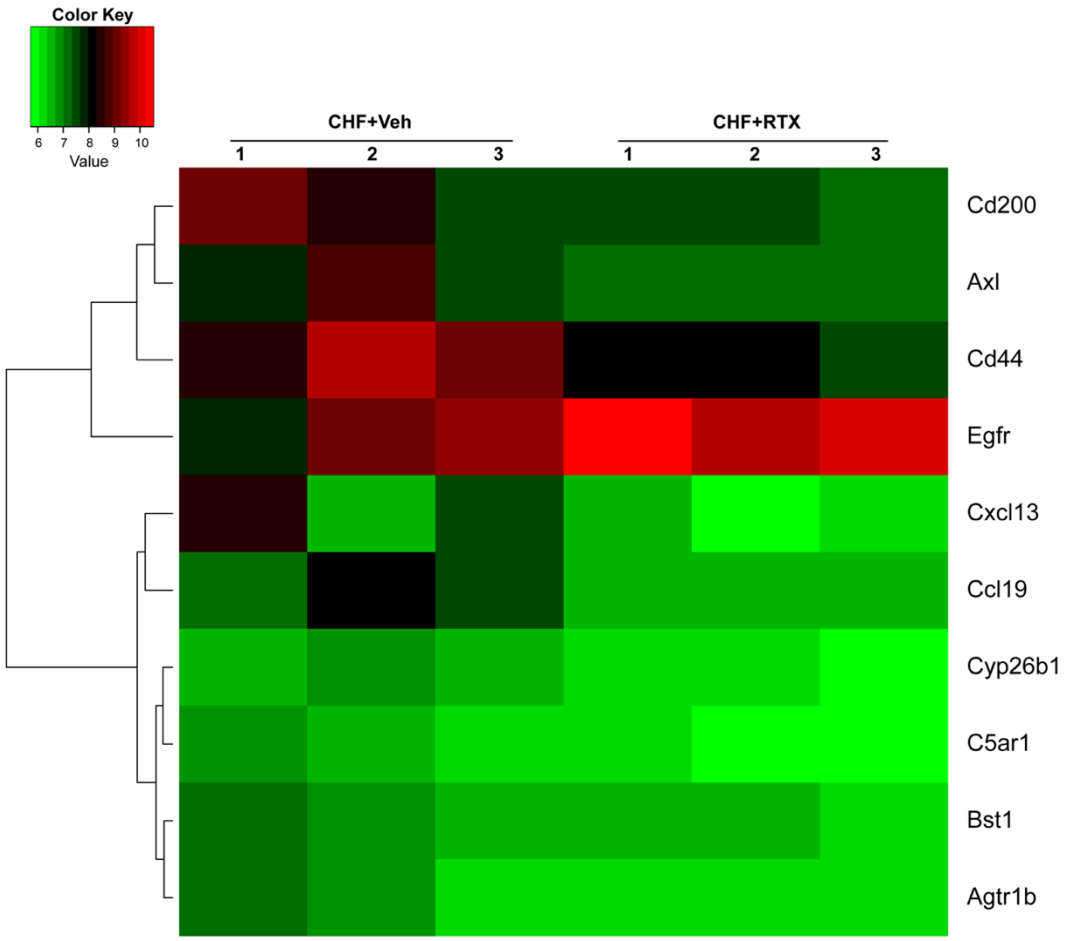

Figure 17. Heatmap of differentially expressed genes in inflammation pathways in kidneys of CHF+RTX rats when compared to CHF+Vehicle treated rats. Genes were clustered according to their expression profile. Red representing higher level of expression and blue representing lower expression. Gene expression values were converted to z-scores to facilitate comparison, and for visual clarity. CHF+Veh group, n=3; CHF+RTX group, n=3.

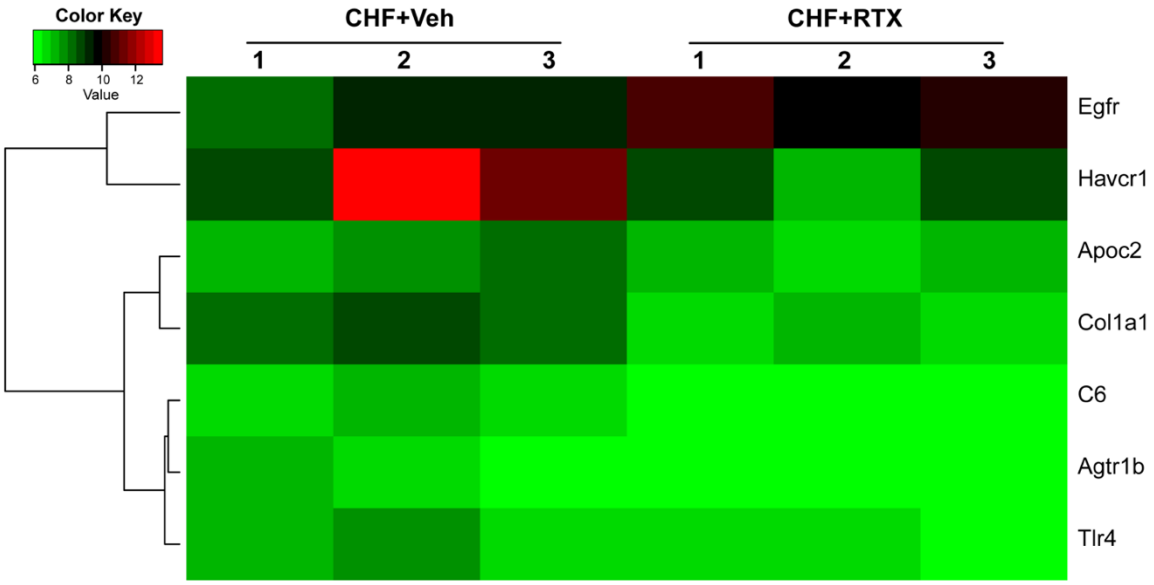

Figure 18. Heatmap of differentially expressed genes in kidney damage pathways in kidneys of CHF+RTX rats when compared to CHF+Vehicle treated rats. Genes were clustered according to their expression profile. Red representing higher level of expression and blue representing lower expression. Gene expression values were converted to z-scores to facilitate comparison, and for visual clarity. CHF+Veh group, n=3; CHF+RTX group, n=3.

To validate the effects of RTX on mRNA expression of Kim-1, subsequent real-time PCR experiments were performed. In the renal cortex of CHF+Vehicle rats Kim-1 mRNA level was increased by ~300 fold, which was largely prevented in CHF+RTX rats (only 4-fold increase). A similar trend was observed in the renal medulla. However, the mRNA expression of Ngal were comparable in the renal cortex and medulla of CHF+Vehicle rats and CHF+RTX rats in comparison to sham rats (**Figure 19 A-D**).

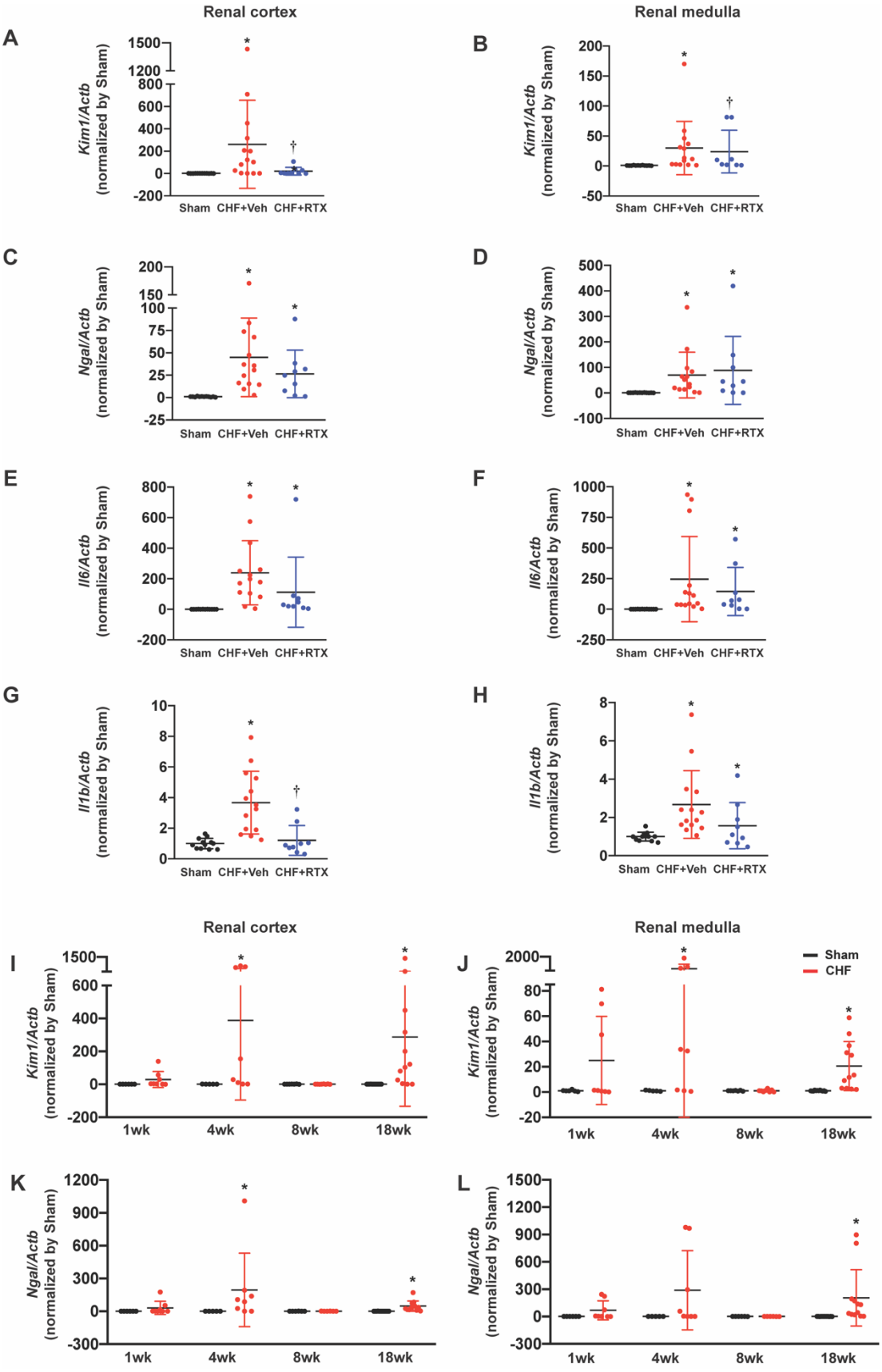
Renal cortex
Renal medulla
A
B
C
D
E
F
G
H
Kim1/Actb (normalized by Sham)
Ngal/Actb (normalized by Sham)
Il6/Actb (normalized by Sham)
Il1b/Actb (normalized by Sham)
Sham
CHF+Veh
CHF+RTX
I
J
K
L
Sham
CHF
1wk
4wk
8wk
18wk

Figure 19. Real-time PCR data showing *Kim1*(**A, B**), *Ngal* (**C, D**), *Il6* (**E, F**), and *Il1b* (**G, H**) mRNA expressions in the renal cortex and medulla from sham, CHF, and CHF+RTX rats. Sham group, n=12 for A-H; CHF+Veh group, n=14 for A-H; CHF+RTX group, n=9 for A, C-H, n=8 for B. Real-time PCR data showing the time-course for alterations in *KIM-1* (**I, J**) and *Ngal* (**K, L**) mRNA expressions in renal cortex and medulla from sham and CHF rats. **I**, **J**. For 1 week, 4 weeks, 8 weeks and 18weeks post-surgery, Sham group, n=6, 5, 7, and 12 respectively; CHF group, n=8, 8, 8, and 12 respectively. **K, L.** For 1 week, 4 weeks, 8 weeks and 18weeks post-surgery, Sham group, n=6, 5, 6, and 12 respectively; CHF group, n=8, 8, 6, and 12 respectively. *Kim1*, kidney injury molecule-1; *Ngal*, neutrophil gelatinase-associated lipocalin; *Il6*, interleukin 6; *Il1b*, interleukin 1 beta; *Actb*, actin beta. **P*<0.05 vs. Sham. †, *P*<0.05 vs. CHF+Vehicle.

PCR data of kidney damage, and inflammation markers

In addition, RNA-Seq demonstrated that inflammatory gene expression was significantly upregulated by 30-100 fold in 18-week post-MI rats. mRNA expressions of Il6 in the renal cortex and medulla were increased in CHF rats regardless of treatment. However, mRNA expression of Il1b in the renal cortex was increased by ~4 fold in CHF+Vehicle rats, which was attenuated by RTX treatment. In the renal medulla, RTX did not alter mRNA expression of Il1b in the CHF+Vehicle rats (**Figure 19 E-H**).

Time-course changes of kidney damage markers after myocardial infarction

To determine the time-course of renal damage markers, mRNA expression of Kim-1 and Ngal were measured in the renal cortex and medulla (**Figure 19 I-L**). We found that both Kim-1 and Ngal levels were increased at 4 weeks post-MI, suggesting the occurrence of acute kidney injury in the early stages post-MI. Surprisingly, 8 weeks after MI Kim-1 and Ngal expression was undetectable. Eighteen weeks post-MI, Kim-1, and Ngal expression increased again. Changes in blood chemistry that indicate renal dysfunction were detected around the same time window (16-18 weeks post-MI) in CHF+Vehicle rats (**Table 5**). Therefore, in our rat model of CHF, we considered 16-18 weeks post-MI as the experimental window to study the CRS type 2.

RNA-Seq data suggest that several genes related to inflammation, apoptosis, and hypoxia were also involved in the development of renal dysfunction. Therefore, the time-course changes of the expression of those genes were also evaluated. Gene expression of inflammatory cytokines including Il1b, Il6, and inducible nitric oxide synthase (iNos) was increased during the early stage (1week and/or 4 weeks) post-MI. The expression in rats with 8 weeks post-MI was comparable with that in sham rats, whereas the expression increased again at 4 months post-MI (**Figure 20 A-D, G, H**). However, the expression of tumor necrosis factor alpha (Tnfa) only increased at 4 weeks post-MI (**Figure 20 E, F**).

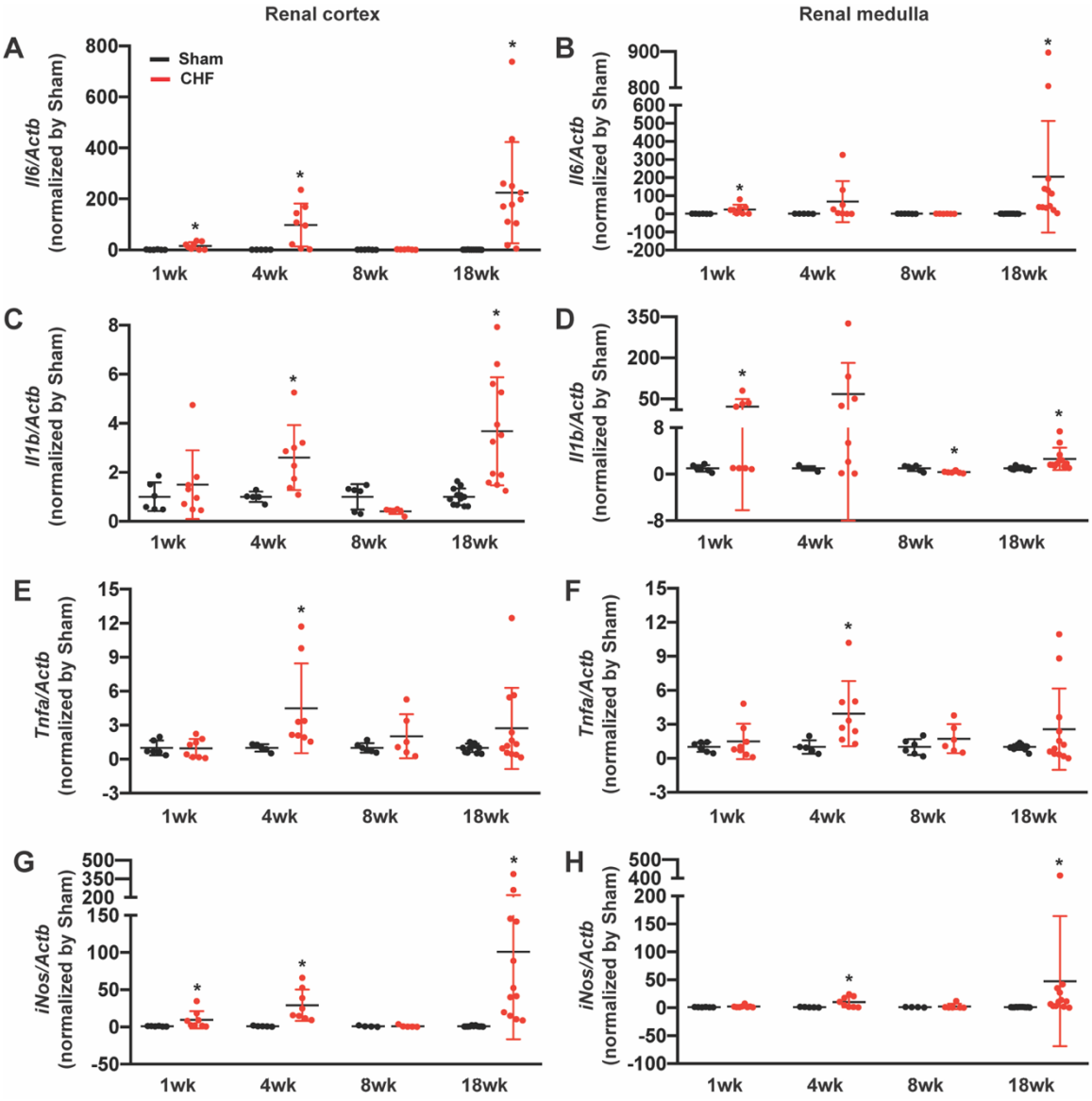

Figure 20. Real-time PCR data showing the time-course alteration in the *Il6* (A, B), *Il1b* (C, D), *Tnfa* (E, F) and *iNos* (G, H) mRNA expressions in both renal cortex and medulla from sham and CHF rats. *Il6*, interleukin 6; *Il1b*, interleukin 1 beta; *Tnfa*, tumor necrosis factor alpha; *iNos*, inducible nitric oxide synthases; *Actb*, actin beta. A-F. For 1 week, 4 weeks, 8 weeks and 18weeks post-surgery, Sham group, n=6, 5, 6, and 12 respectively; CHF group, n=8, 8, 6, and 12 respectively. G. For 1 week, 4 weeks, 8 weeks and 18weeks post-surgery, Sham group, n=6, 5, 4, and 11 respectively; CHF group, n=8, 8, 5, and 12 respectively. H. For 1 week, 4 weeks, 8 weeks and 18weeks post-surgery, Sham group, n=6, 5, 4, and 12 respectively; CHF group, n=8, 8, 6, and 12 respectively. *P<0.01 vs. Sham.

Gene expression of hypoxia-inducible factor 1 alpha (Hif1a) and Hif3a was increased at 1 month post-MI (**Figure 21 C-F**). However, gene expression of erythropoietin (Epo), which is regulated by the HIF-1 signaling pathway and is also an indicator of severe renal failure, was increased at the late stage post-MI, consistent with the development of renal dysfunction at 4 months post-MI (**Figure 21 A, B**).

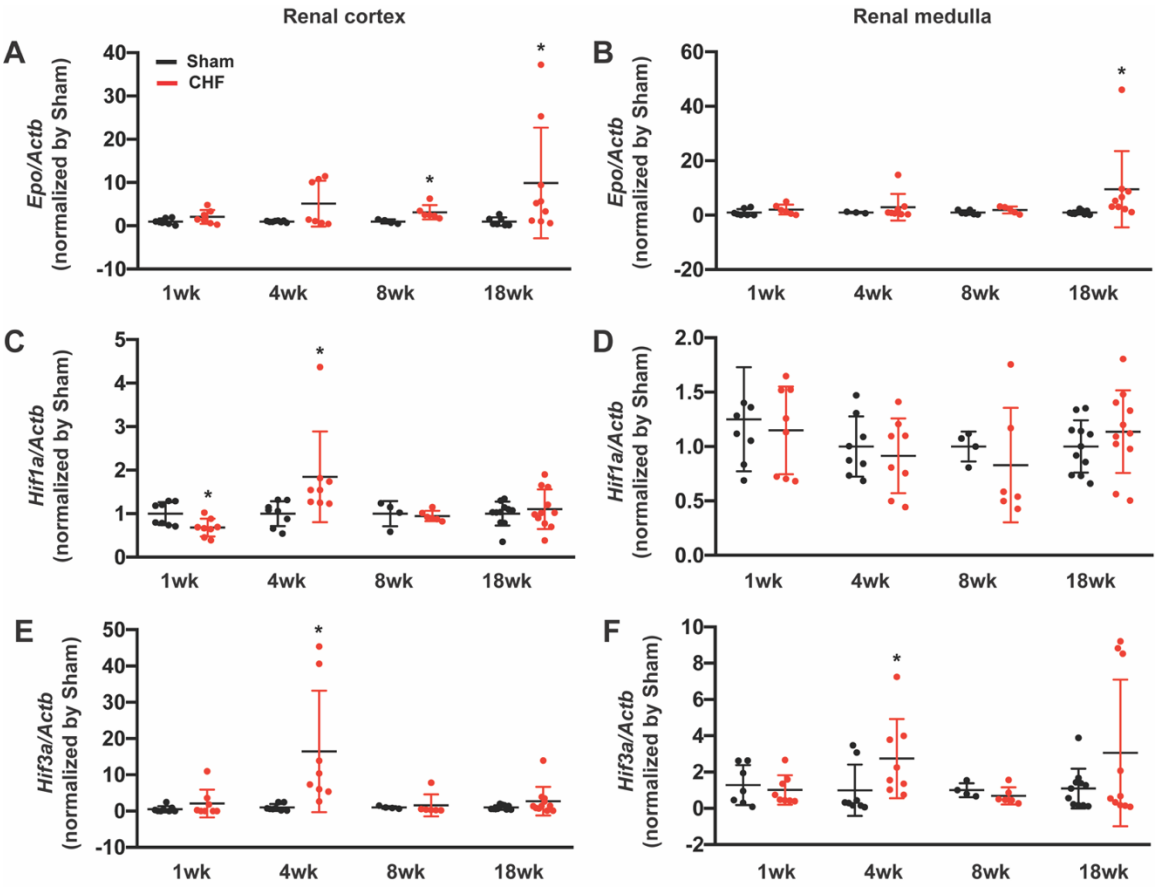

Figure 21. Real-time PCR data showing the time-course alteration in the *Epo* (A, B), *Hif1a* (C, D), and *Hif3a* (E, F) mRNA expressions in both renal cortex and medulla from sham and CHF rats. *Epo*, erythropoietin; *Hif1a*, hypoxia-inducible factor 1 alpha; *Hif3a*, hypoxia-inducible factor 3 alpha; *Actb*, actin beta. A. For 1 week, 4 weeks, 8 weeks and 18weeks post-surgery, Sham group, n=7, 8, 4, and 7 respectively; CHF group, n=7, 7, 6, and 9 respectively. B. For 1 week, 4 weeks, 8 weeks and 18weeks post-surgery, Sham group, n=7, 3, 6, and 9 respectively; CHF group, n=6, 8, 5, and 9 respectively. C, D. For 1 week, 4 weeks, 8 weeks and 18weeks post-surgery, Sham group, n=8, 8, 4, and 11 respectively; CHF group, n=8, 8, 6, and 11 respectively. E. For 1 week, 4 weeks, 8 weeks and 18weeks post-surgery, Sham group, n=8, 8, 4, and 10 respectively; CHF group, n=8, 8, 6, and 11 respectively. F. For 1 week, 4 weeks, 8 weeks and 18weeks post-surgery, Sham group, n=7, 8, 4, and 11 respectively; CHF group, n=8, 8, 6, and 10 respectively. *P<0.01 vs. Sham.

Activating transcription factor 3 (ATF3) is induced upon physiological stress in various tissues and is involved in the apoptotic process. Gene expression of Atf3 was immediately increased after myocardial infarction (1 week post-MI) and at the late stage (4 months post-MI). Interestingly, gene expression of Atf3 between 1 week and 4 months post-MI was normal (**Figure 22 A, B**).

Heme oxygenase 1 (HMOX1) participates in anti-inflammatory processes as well as apoptotic processes by upregulating interleukin 10 (Il10) and interleukin 1 receptor antagonist (Il1ra) expression. Gene expression of Hmox1 was increased at 4 weeks post-MI. Similarly, 8 weeks post-MI, the expression of Hmox1 was comparable with that in sham rats. However, the expression increased again at 4 months post-MI (**Figure 22 C, D**). In addition, gene expression for arginine vasopressin receptor 2 (Avpr2) was decreased at 4 months post-MI in CHF+Vehicle rats (**Figure 22 E, F**).

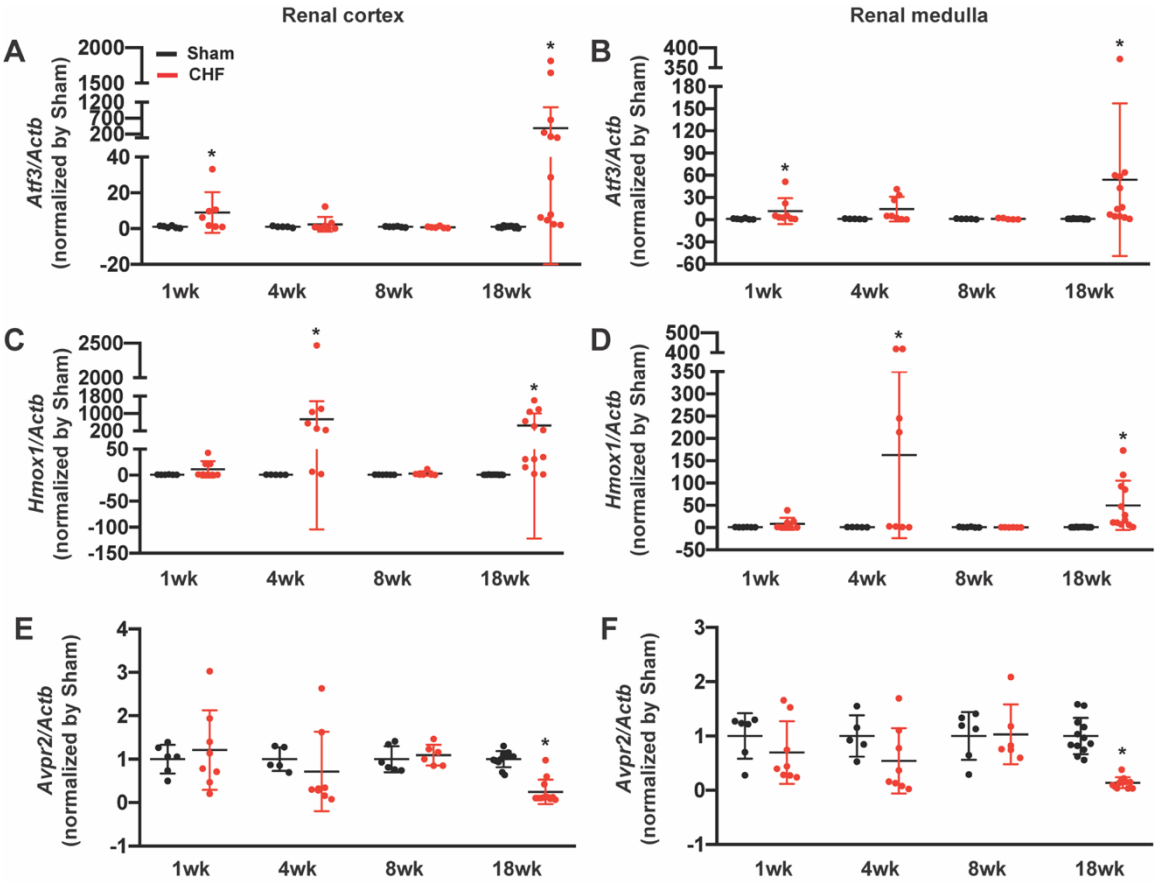

Figure 22. Real-time PCR data showing the time-course alteration in the Atf3 (A, B), Hmox1 (C, D), and Avpr2 (E, F) mRNA expressions in both renal cortex and medulla from sham and CHF rats. Atf3, activating transcription factor 3; Hmox1, heme oxygenase 1; Avpr2, arginine vasopressin receptor 2; Actb, actin beta. A. For 1 week, 4 weeks, 8 weeks and 18weeks post-surgery, Sham group, n=6, 5, 6, and 12 respectively; CHF group, n=7, 8, 6, and 12 respectively. B. For 1 week, 4 weeks, 8 weeks and 18weeks post-surgery, Sham group, n=6, 5, 5, and 12 respectively; CHF group, n=8, 8, 5, and 12 respectively. C-F. For 1 week, 4 weeks, 8 weeks and 18weeks post-surgery, Sham group, n=6, 5, 6, and 12 respectively; CHF group, n=8, 8, 6, and 12 respectively. *P<0.01 vs. Sham.

Acute and chronic hemodynamic data

To further investigate the mechanism underlying the observed beneficial effects of RTX in CHF, renal hemodynamics was examined in the sham, CHF+Vehicle, and CHF+RTX groups 4 months after MI. As shown in **Figure 23 A-E**, acute CSAR activation by BK slightly increased MAP, HR, RVR, and decreased RBF in sham rats. However, compared to sham, CHF+Vehicle rats exhibited exaggerated renal sympathetic nerve activity and an increase in the MAP, HR, RVR, along with a marked reduction in renal perfusion. The RVR was significantly increased in the CHF+Vehicle rats while the renal perfusion was significantly decreased in comparison to sham rats (**Figure 23 F, G**). Epicardial RTX application partially restored the abnormal RBF and RVR seen in CHF+Vehicle rats, which supports the concept that neural crosstalk between the heart and the kidneys in CHF aggravates renal ischemia through CSAR control of renal sympatho-excitation.

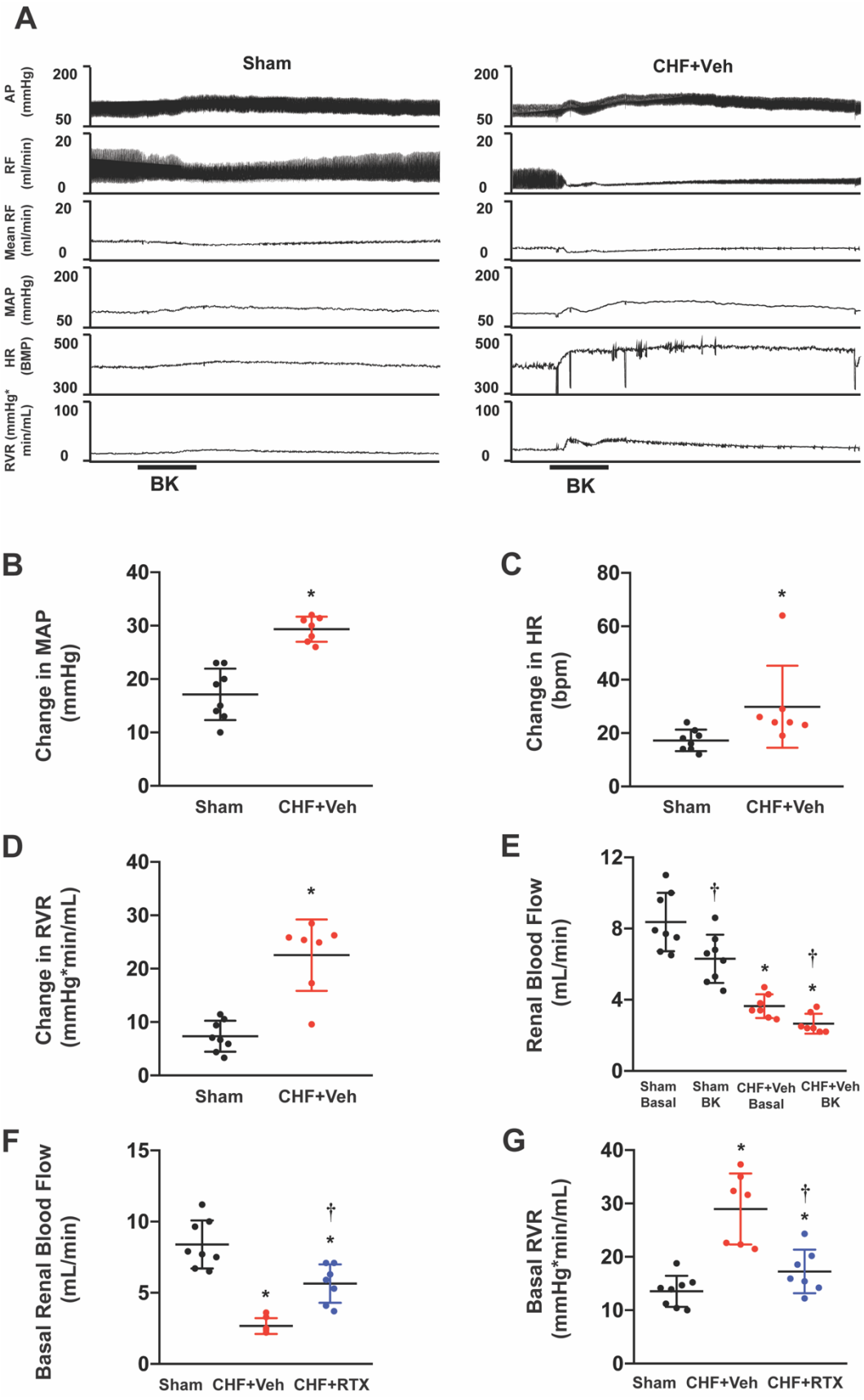
A
Sham
CHF+Veh
AP (mmHg)
RF (ml/min)
Mean RF (ml/min)
MAP (mmHg)
HR (BMP)
RVR (mmHg* min/mL)
BK
B
Change in MAP (mmHg)
C
Change in HR (bpm)
D
Change in RVR (mmHg*min/mL)
E
Renal Blood Flow (mL/min)
Sham Basal
Sham BK
CHF+Veh Basal
CHF+Veh BK
F
Basal Renal Blood Flow (mL/min)
CHF+RTX
G
Basal RVR (mmHg*min/mL)

Figure 23. Hemodynamic measurements after acute cardiac afferent activation and chronic cardiac afferent ablation in response to epicardial application of bradykinin. **A-E.** Cardiac afferent activation caused an exaggerated renal vasoconstriction in the post-MI rats. **F, G.** CSAR ablation by RTX partially restored the decreased renal blood flow and reduce renal vascular resistance (RVR) in CHF rats. Sham group, n=8; CHF+Veh group, n=7; CHF+RTX group, n=7. **P*<0.05 vs. Sham. †*P*<0.05 vs. CHF+Vehicle.

Central venous pressure data

Figure 24 shows original recording (**panels A and B**) and group data of CVP in Sham, CHF+Veh, and CHF treated with RTX. The Sham rat displayed a typical CVP (green tracing), from which we can see a rise in pressure (a wave) caused by right atrial systole, a decrease in pressure (x descent) due to right atrial relaxation, a 2nd small peak pressure (v wave) by a rapid filling of right atrium, and a 2nd mild decrease of pressure (y descent) due to the atrial emptying. In comparison to sham rats, the average CVP levels increased in the setting of chronic heart failure, which were ameliorated by CSAR ablation with RTX (**Panel C, Figure 24**).

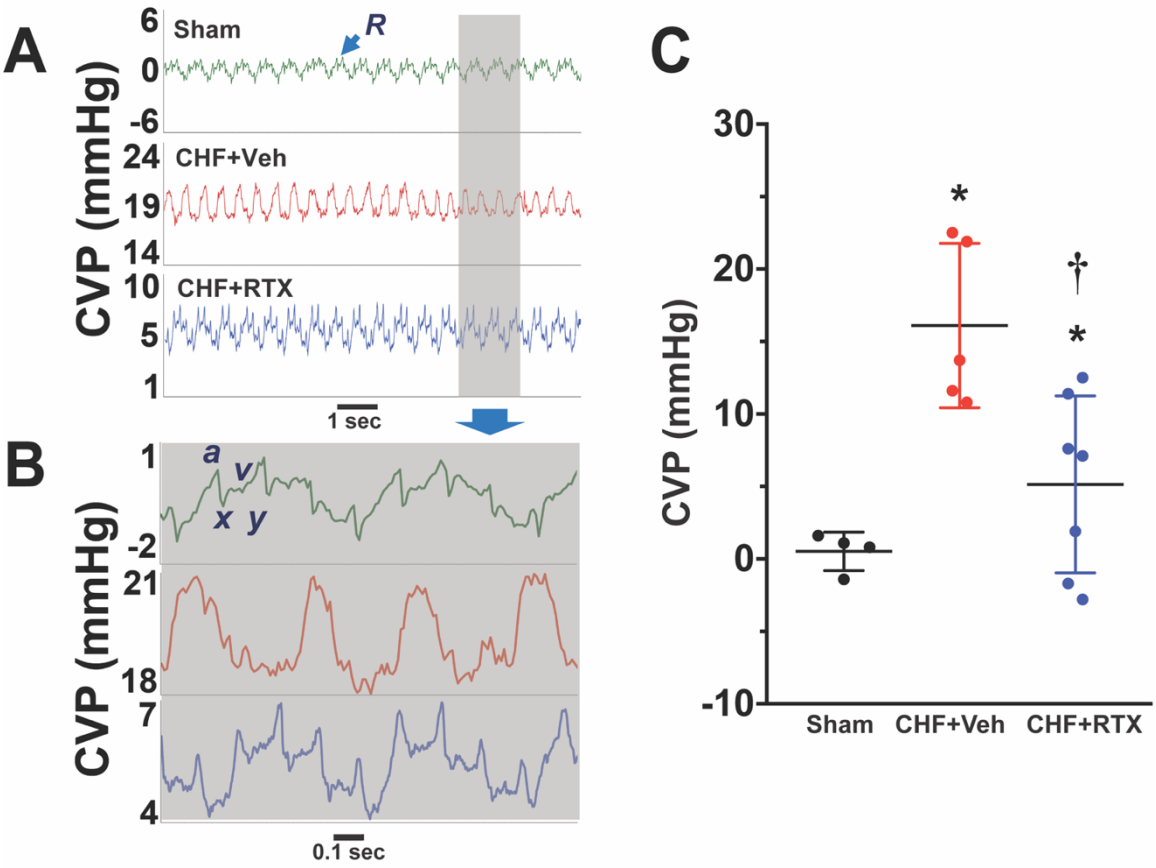

Figure 24. Original recording (A and B) and summary data (C) showing that cardiac spinal afferent ablation by RTX reduced the increased central venous pressure (CVP) in CHF rats. R: respiratory wave; a wave: atrial contraction; x descent: atrial relaxation; v wave: systolic filling of atrium; y descent: early ventricular filling. Sham group, n=4; CHF+Veh group, n=5; CHF+RTX group, n=7. *P<0.05 vs. Sham. †, P<0.05 vs. CHF+Vehicle.

Long-term survival data

A subgroup of rats with CHF that were treated with vehicle or RTX were followed for six months so that survival could be assessed (**Figure 25**). During the early stage post-MI, the survival between CHF and CHF+RTX was comparable. However, after 3-4 months post-MI when renal impairment has developed in CHF rats, there was a dramatic drop in survival in CHF+Vehicle rats. On the other hand, a significant improvement in long-term survival in the RTX-treated CHF group was observed ($p < 0.05$), indicating that improvement of renal function by interruption of this neural pathway may improve prognosis CHF.

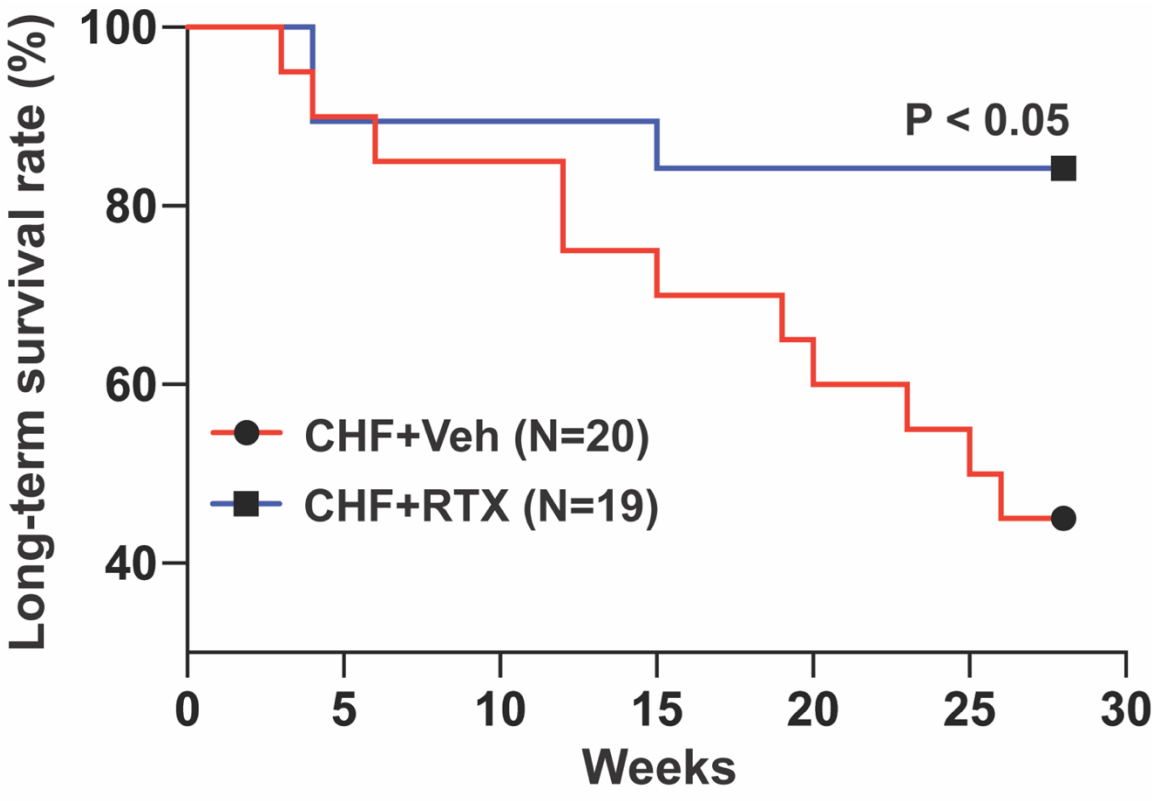

Figure 25. Kaplan-Meier survival rates between CHF rats treated with epicardial application of RTX (n=19) or vehicle (n=20) at the time of MI.

Effects of intra-stellate injection of RTX in rats with cardio-renal syndrome type 2

Validation of SG injection of RTX

To validate the effect of SG injection of RTX, epicardial application of BK (10 μg/mL) was performed to stimulate cardiac spinal afferent in anesthetized, bilaterally vagotomized rats. CSAR activation in the rats that received intra-stellate injection of vehicle (SG Veh group) evoked a sympatho-excitatory response as evidenced by increased MAP, increased HR and increased RSNA, which were reduced in the rats that received intra-stellate injection of RTX (SG RTX group), indicating that local application of RTX into stellate ganglia effectively reduced the CSAR.

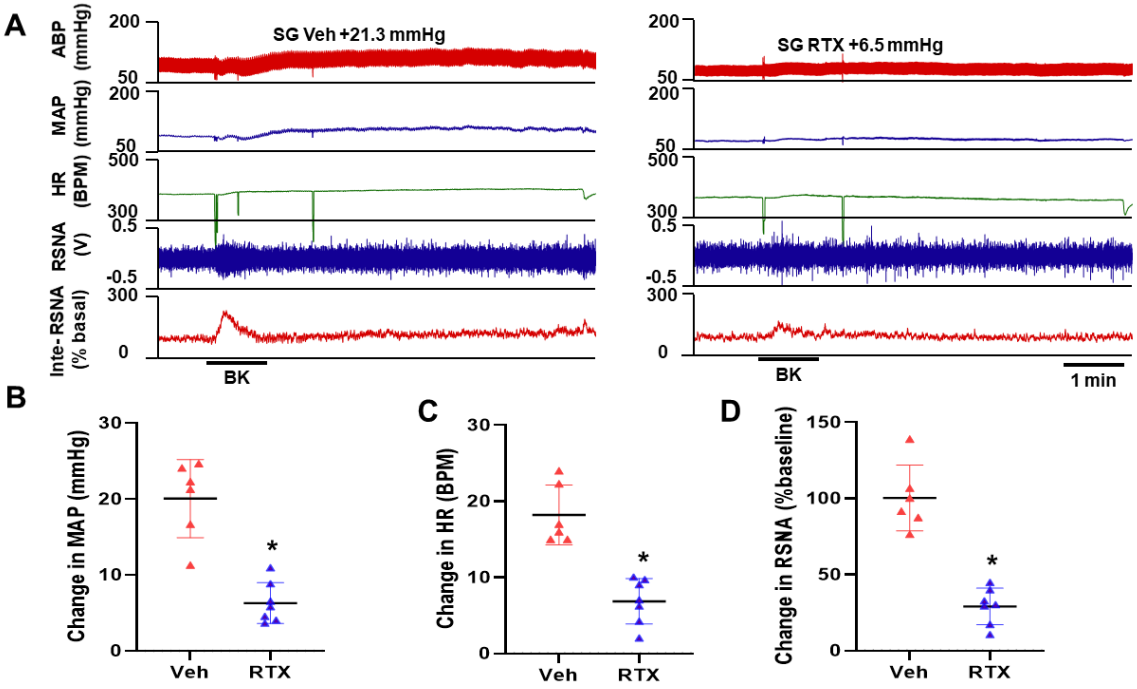

Figure 26. (A) Representative recording showing the response to epicardial application of BK (10 µg/mL) in an anesthetized and vagotomized rat. Cardiac spinal afferent reflex (CSAR), arterial blood pressure (ABP), mean arterial blood pressure (MAP), heart rate (HR), renal sympathetic nerve activity (RSNA), integrated RSNA (iRSNA) as a % of baseline. (B) The change in MAP, HR and RSNA from baseline. Data presented as mean ± SD. N=6 for each group. $^{*}P<0.05$ vs. SG Veh.

Morphological data and echocardiographic data

There was no difference in infarct sizes between CHF+SG Veh rats and CHF+SG RTX rats (39.8±8.4% in CHF+SG Veh group and 36.8±9.6% in CHF+SG RTX group; **Figure 27**). To evaluate the effects of the application of RTX on the stellate ganglia on cardiac remodeling of CHF rats, LV dimensions and volumes at different time points post-MI were performed. LV dimensions and volumes were comparable between CHF+SG Veh and CHF+SG RTX (**Figure 28**, **Figure 29**).

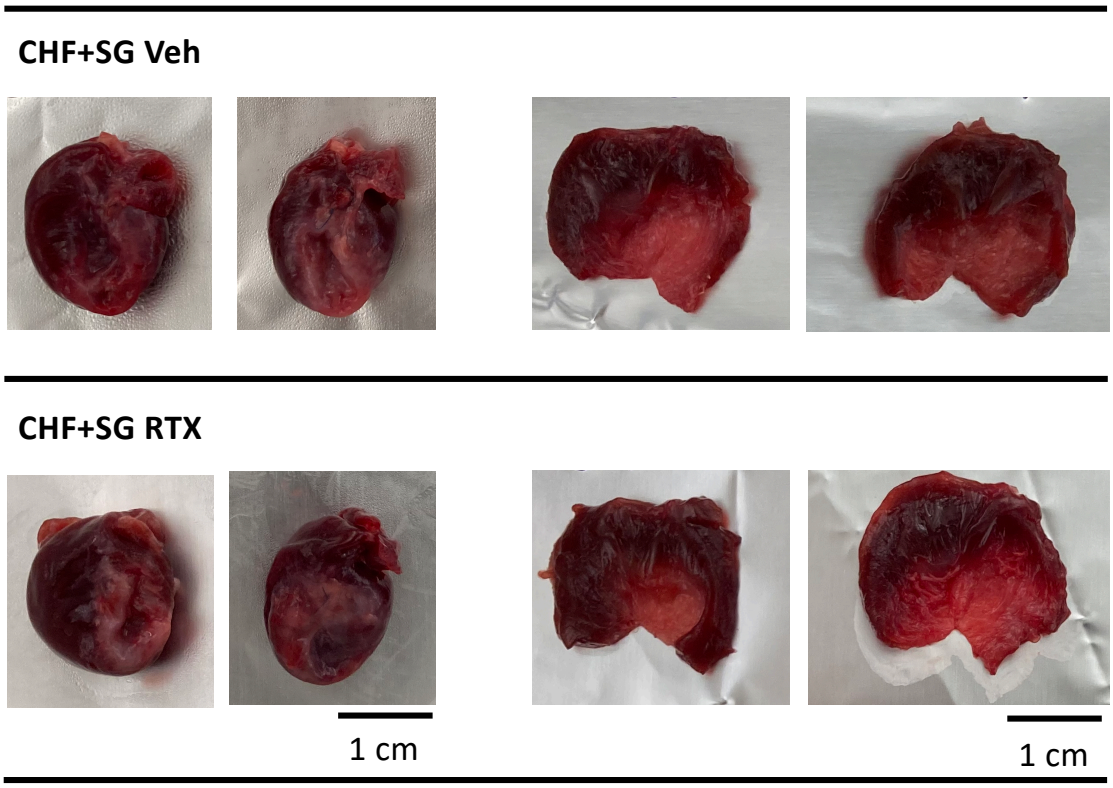

Figure 27 Gross morphology of infract hearts and infarct sizes of CHF rats treated with intra-stellate injection of vehicle or RTX.

CHF+SG Veh

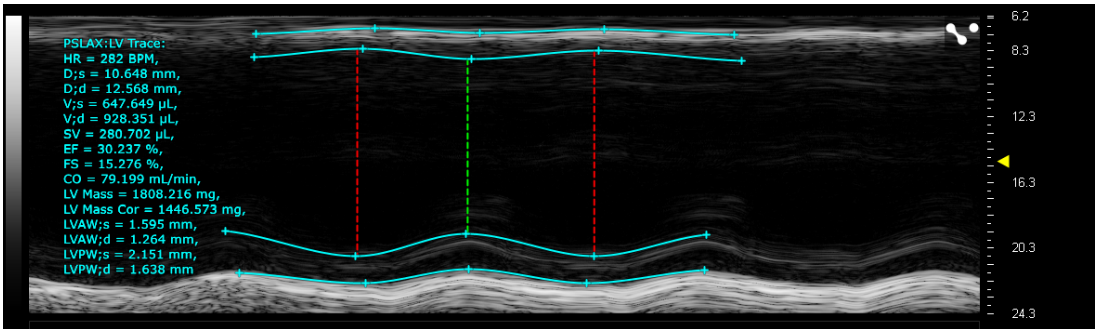

CHF+SG RTX

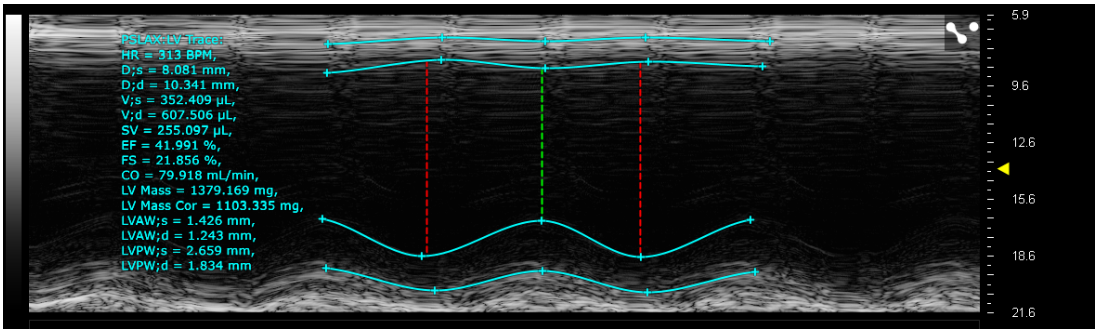

Figure 28 Representative M-mode, long-axis, and two-dimensional echocardiography images of the LV from CHF rats treated with intra-stellate injection of vehicle or RTX at 18 weeks post-MI.

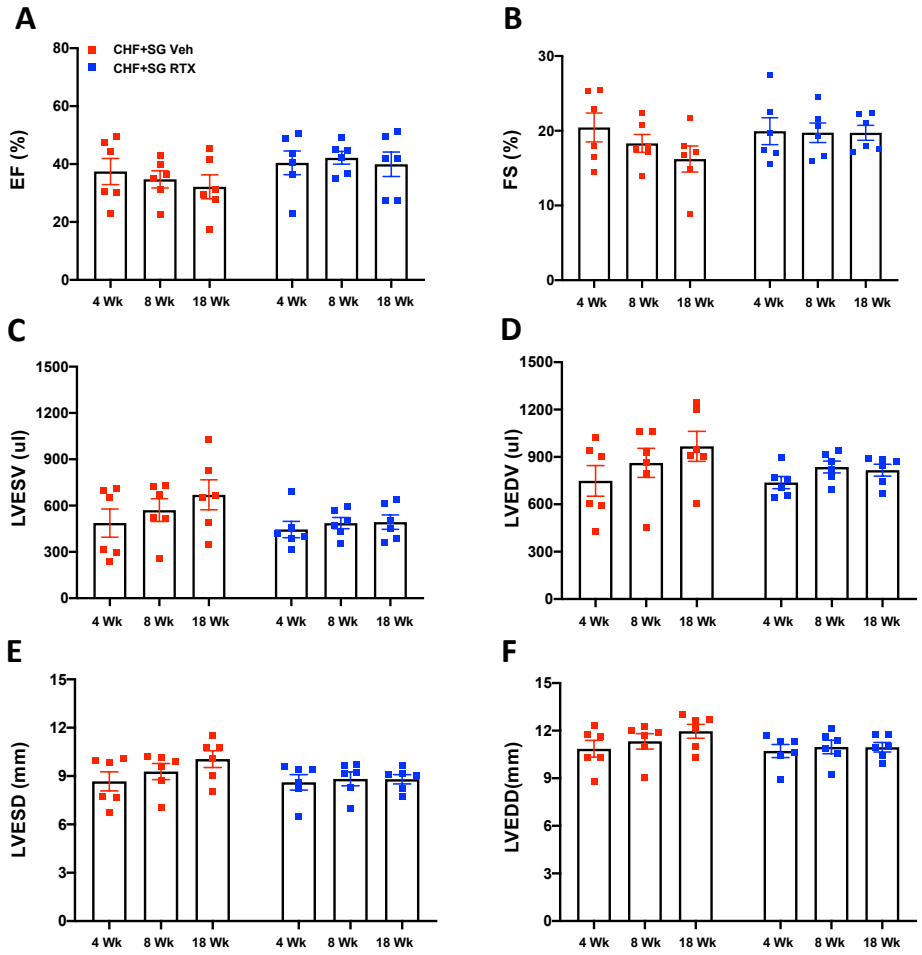

Figure 29. Echocardiographic measurements including EF (**A**), FS (**B**), LVESV (**C**), LVEDV (**D**), LVESD (**E**), and LVEDD (**F**) in CHF+SG Veh and CHF+SG RTX rats. EF, ejection fraction; FS, fractional shortening; LVESV, left ventricular end-systolic volume; LVEDV, left ventricular end-diastolic volume; LVESD, left ventricular end-systolic diameter; LVEDD, left ventricular end-diastolic diameter.

Blood analysis data

We investigated the renal functions at the time point of 16 weeks post-MI. Blood analysis of creatinine, BUN, and electrocytes are summarized in **Table 11**. Compared with CHF+SG Veh, SG injection of RTX reduced the BUN levels and tended to decrease the potassium levels, implying that SG injection of RTX improved renal function in the setting of CHF.

Table 11. Blood analysis in CHF+Sham, and CHF+SG RTX rats

Parameters	CHF+SG Veh (n=6)	CHF+SG RTX (n=6)
Na, mM	140.2±0.8	140.5±1.4
K, mM	5.17±1.15	4.50±0.62
Cl, mM	101.3±1.2	101.5±1.5
iCa, mM	1.35±0.09	1.35±0.04
TCO_2, mM	29.7±3.3	30.3±2.6
BUN, mg/dL	30.5±5.9	23.2±1.7 *
Crea, mg/dL	0.62±0.19	0.43±0.15
HCt, %PCV	51.2±4.9	46.2±1.8
Hb, g/dL	17.5±1.7	15.7±0.6 *
AnGap	15.2±2.4	14.2±1.6

Values are mean ± SD. Na, sodium; K, potassium; Cl, chloride; iCa, ionized calcium; TCO2, total carbon dioxide; BUN, blood urea nitrogen; Crea, creatinine; HCt, hematocrit; Hb, hemoglobin; AnGap, anion gap. *P<0.05 vs. CHF+Veh.

PCR data of kidney damage, and inflammation markers

To evaluate the renal dysfunction developed during the progression of CHF, the mRNA expression of *Kim1* and *Ngal* were measured. The mRNA levels of *Kim1* and *Ngal* in the renal cortex were increased in the CHF+SG Veh rats compared with sham rats (**Figure 30 A-D**). Similar trends were observed in the medulla (**Figure 30 A-D**). The mRNA expression of *Il1b* and *Il6* in the kidneys were examined to investigate the effects of SG injection of RTX on inflammation. Similarly, the mRNA expression of *Il6* tended to increase in the kidneys of CHF+SG Veh and CHF+SG RTX rats, however, compared with sham rats, the changes of mRNA expressions of *Il1b* in the CHF+SG Veh and CHF+SG RTX did not reach significance (**Figure 30 E-H**).

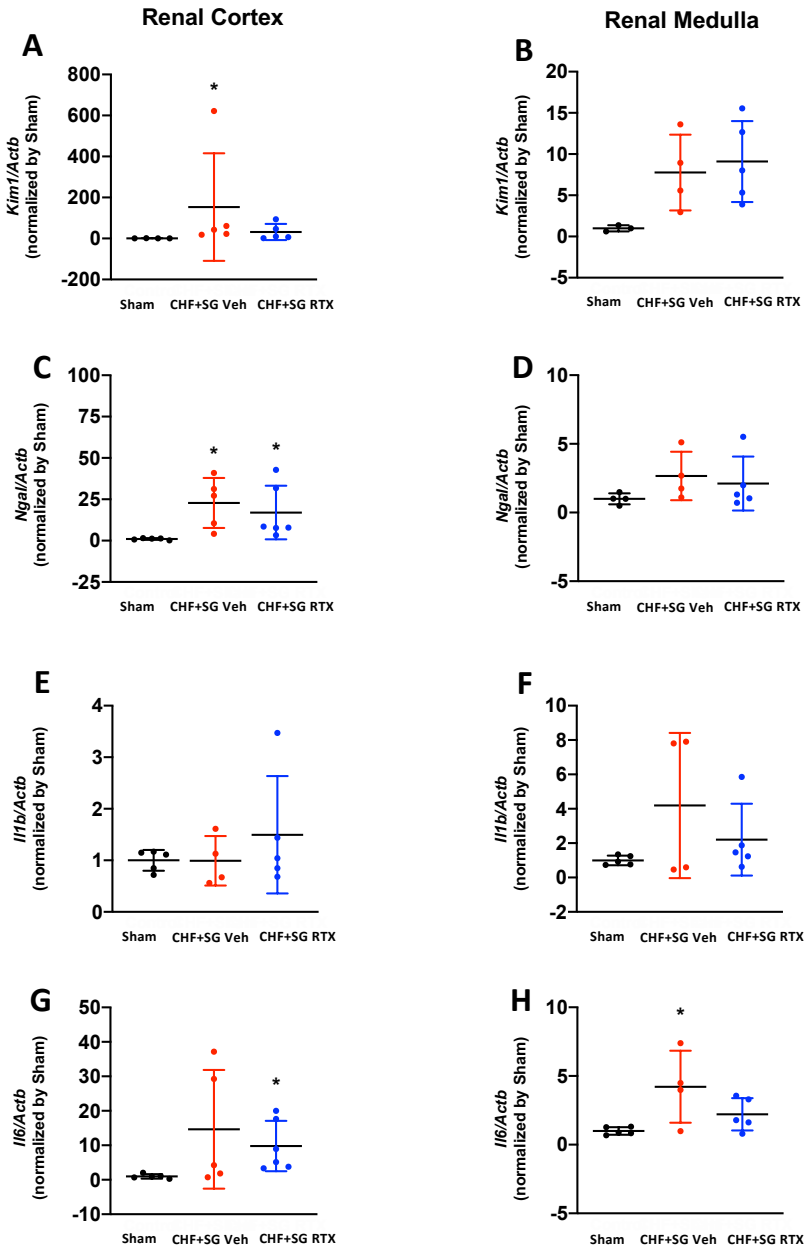

Figure 30. Real-time PCR data showing *Kim1*(**A, B**), *Ngal* (**C, D**), *Il1b* (**E, F**), and *Il6* (**G, H**) mRNA expressions in the renal cortex and medulla from sham, CHF+SG Veh, and CHF+SG RTX rats. Sham group, n=3-5 for A-H; CHF+ SG Veh group, n=4-5 for A-H; CHF+SG RTX group, n=5-6 for A-H. *Kim1*, kidney injury molecule-1; *Ngal*, neutrophil gelatinase-associated lipocalin; *Il6*, interleukin 6; *Il1b*, interleukin 1 beta; *Actb*, actin beta. *, $P<0.05$ vs. Sham.

Discussion

In this study we hypothesized that ablation of cardiac spinal afferents using the selective afferent neurotoxin, RTX ameliorates renal dysfunction in the late stages of CHF, thus reducing the pathogenesis of the CRS Type 2. The primary findings of this study include: 1) in this rat model of MI-induced CHF, renal injury temporarily occurred at an early stage post-MI (i.e. within the first month) and chronically developed into renal dysfunction at 4 months post-MI; 2) CSAR ablation by epicardial application of RTX at the time of MI prevented renal dysfunction, especially renal proximal tubular damage as evidenced by preventing increased levels of BUN, creatinine, potassium, microalbuminuria, renal fibrosis, and tubular injury, and by attenuation of both enhanced KIM-1 gene expression and increased urinary KIM-1 concentration and; 3) by reduction in renal proximal tubular damage and mortality of CHF rats; 4) CSAR ablation by intra-stellate injection of RTX at 4 weeks post MI had similar protective effect on renal function in CHF rats. These effects were accompanied by partial restoration of cortical blood flow and reduced renal venous congestion. This study suggests that CSAR ablation may be a promising therapeutic target in the treatment of the CRS type 2.

Heart failure is a major healthcare concern worldwide. Chronic kidney disease, which is defined as estimated glomerular filtration rate (eGFR) < 60 mL/min/1.73 m^2, is one of the most prevalent comorbidities in patients with CHF and is independently associated with adverse clinical outcomes.[5] Approximately 41% of all-cause mortality in CHF patients is attributed to co-existing renal failure.[104] CRS type 2, the most common subtype, is used to describe renal dysfunction caused by CHF. However, the mechanism underlying the development of CRS type 2 remains unclear due to a lack of an appropriate animal model to mimic this pathological process. The natural clinical development of the CRS is complicated by other co-morbidities, including other cardiovascular diseases, metabolic disorders, drugs, and aging. An appropriate animal model of the clinical scenario for CRS type 2 with time-course renal damage is crucial in order to uncover the

mechanisms and potential therapies. Previously, Lekawanvijit et al.[105] evaluated renal function over time in the rat MI model. They found that renal cortical fibrosis and 24-hour urinary albumin increased and were both maximal at 16 weeks post-MI. In addition, they found that KIM-1 positive staining in the tubules was higher in MI rats compared with sham at 1, 4, 12 and 16 weeks post-MI. However, at 8 weeks post-MI, KIM-1 levels of MI animals were comparable to that of sham, suggesting that there may be a compensatory stage between temporary kidney damage and chronic kidney disease after MI. However, in their study, there was no increase in mRNA expression of Ngal in the kidneys of MI rats at all time points, although renal impairment was detected in the late stages of CHF in their animal model. In the present study, we confirmed that for a rat model of MI-induced CHF, at least 16-18 weeks is required for the development of chronic kidney damage after MI. Here we provide additional time course information, including a survival analysis from initial MI to six months post-MI. The advantage of this model is that it resembles the chronic pathological progression of renal dysfunction in the setting of heart failure observed clinically. Four months post-MI, CHF rats exhibited increased levels of nitrogen metabolites, presented electrolyte disturbances, and microalbuminuria, indicating damage to the glomerular barrier and decreased proximal reabsorptive capacity for protein transport. Taken together, CHF rats demonstrated early kidney injury at the early stage of MI (i.e., within 1month post-MI), and then underwent a compensatory period when renal function seemed normal at 8 weeks post-MI. At 4 months, post-MI rats developed chronic renal impairment, which eventually accelerated to death of CHF rats as shown in our survival analysis.

Hemodynamic changes due to decreased cardiac output in CHF and dysregulation of the neuro-humoral regulation contribute to the pathophysiology of CRS type 2. Other factors such as inflammation, oxidative stress, and metabolic and nutritional changes also contribute to the pathological development of renal dysfunction in heart failure.[90] However, the upstream factors that drive these changes are still unclear. In the setting of CHF, one of the most common and

significant problems is excessive sympatho-excitation. Patients with high plasma norepinephrine have a poor survival prognosis.[9] There are several cardiovascular reflexes contributing to sympathetic excitation including an increased chemoreflex, the blunted arterial baroreflex and the enhanced CSAR.[106] The CSAR, a pathological sympatho-excitatory reflex, is silent in the normal state but becomes tonically activated in CHF, and contributes to global sympatho-excitation to the heart and the kidneys[33, 42]. Our previous studies demonstrated that in the setting of CHF, the CSAR is sensitized centrally and peripherally.[33, 35, 107] We previously provided evidence[35] showing that chronic and selective cardiac spinal afferent denervation by epicardial application of RTX at the time of MI prevented the exaggerated renal and cardiac sympatho-excitation in rats with MI-induced CHF. These data strongly suggest that selective CSAR ablation may be clinically beneficial to the heart in the setting of CHF. The current study demonstrates that cardiac afferent denervation by epicardial application of RTX at the time of MI also benefits the kidneys in CHF as evidenced by improvement in the GFR, blood creatinine, BUN and potassium, and prevention of microalbuminuria by RTX. At the molecular level, we show that cardiac afferent denervation by epicardial application of RTX at the time of MI has a selective protective effect on the renal cortex, especially on proximal tubular dysfunction supported by the reduced mRNA expression of KIM-1 and reduced urinary KIM-1 levels in CHF after RTX application. We also provided additional evidence that cardiac afferent denervation by intra-stellate injection of RTX at 4 weeks post MI had a similar renal protective effect on renal function, suggesting that cardiac afferent denervation following heart failure still has the beneficial effect on the kidneys. Furthermore, this new intra-stellate RTX injection approach might have more translational therapeutic potential than the epicardial application approach. In the clinic, although epicardial application of RTX is applicable, the MI-induced scar formation and cardiac interstitial fibrosis could largely affect the efficiency of RTX in cardiac afferent denervation via the epicardial delivery route. Compared to the epicardial delivery, injection of RTX into the stellate ganglia at the post-MI stage could be a better approach to perform cardiac afferent denervation. In anatomy, the stellates not only contain soma for

sympathetic efferent fibers but also fibers of passage for thoracic afferents as they course through DRGs and enter the spinal cord. It should be noted that in humans the stellate ganglia can be easily identified, and that this type of transcutaneous procedure can be performed with fluoroscopic or ultrasound guidance (intra-ganglionic or nerve 'block' approach). Compared to epicardial delivery that requires relatively larger injection volume (80-100 μl/per rat), intra-stellate injection requires a much smaller volume (10 μl for bilateral injection), which minimizes the risk of systemic absorption of RTX.

Considering the fact that renal proximal tubules are located in the renal cortex where the majority of RBF is distributed, it is likely that chronic CSAR ablation improves renal proximal tubular damage by partially restoring renal blood flow in CHF. We confirmed that in the setting of CHF, the overactive CSAR modulates renal function through further exacerbation of renal ischemia. Cardiac afferent denervation ameliorated the renal vasoconstriction and partially restored RBF, suggesting a protective effect of RTX on renal perfusion.

In our study, we observed that an increase in CVP in the rats with CHF may contribute to renal venous hypertension and loss of renal function, which could be attenuated by RTX. Tonic activation of the CSAR in CHF provides a continuous sympathetically-mediated vasoconstrictor tone to visceral vascular beds including the kidneys, resulting in both chronic renal ischemia and potent peripheral vasoconstriction. The latter, in combination with the decreased intrinsic myocardial contractility causes a volume shift from the peripheral circulation to the thorax, thus increasing CVP and contributing to renal venous congestion. Based on our hemodynamic data we propose that both CSAR-induced renal ischemia and venous congestion contribute to chronic kidney dysfunction, which were attenuated by chronic ablation of the CSAR by epicardial RTX.

Our time-course study showed that gene expression of KIM-1 is elevated in the early and late stages post-MI, while in the middle stage, KIM-1 expression is comparable with that in sham animals. Tubular expression of KIM-1 is strongly related to interstitial fibrosis and inflammation,

while it is negatively associated with renal function.[108] More studies are required to discover how KIM-1 participates in the pathological changes in the renal repair. Furthermore, the pathways mediating the regulation of KIM-1 are unknown. Ajay et al. identified that Checkpoint Kinase 1 (Chk1) and Signal Transducer and Activator of Transcription-3 (STAT3) are critical upstream regulators of KIM-1 expression after ischemic or oxidant stress to the kidney using a bioinformatics approach.[109]

Pro-inflammatory cytokines play a central role in cell damage and dysfunction contributing significantly to the development of CHF. Our RNA-Seq analysis and PCR results show that pro-inflammatory gene expression and inflammatory pathways were upregulated in the kidneys of CHF rats which were attenuated by CSAR ablation, indicating the involvement of inflammation in the development of renal impairment in CHF. The enhanced sympathetic tone and the activation of the renin-angiotensin-aldosterone system (RAAS) in CHF, which leads to the renal vasoconstriction, is considered as a major cause of local inflammation.[110] In addition, biomechanical stress due to volume overload and venous congestion in CHF promotes the release of pro-inflammatory mediators from activated vascular endothelium that in turn may further impair renal function.[111, 112] Venous congestion causes a significant increase in plasma IL-6, and TNF-α as well as norepinephrine (NE) in a dog model of CHF.[113] The current study shows that in the renal cortex, the increased gene expression of Il1b was attenuated by RTX, which may explain the beneficial effect of cardiac afferent denervation. However, these preferential effects of RTX on IL-1β rather than other cytokines in the renal cortex need further study. Overall, chronic ablation of cardiac afferents attenuates renal dysfunction by reducing renal ischemia and renal congestion, which may reduce renal inflammation. Moreover, apoptosis also contributes to tubular damage and interstitial fibrosis during the progression of chronic kidney damage.[114] Glomerular and tubular atrophy in CHF may be due to caspase-mediated apoptosis has also been observed in a rat model of infrarenal aortocaval fistula.[115] In the current study, several genes and pathways that are related to apoptosis

are upregulated in the setting of CHF, indicating apoptosis is involved in the pathological process mediating renal damage.

Reduction in renal oxygen impairs energy generation as well as induces several genes that may mediate the progression of renal injury.[116] Recently Veach et al. showed that human proximal tubule cells (HK-2) responded to various stimuli, including hypoxia (1% O_2) indicative of the upregulation of KIM-1 expression.[117] Renal ischemia plus the reduction in capillary density due to endothelial cell apoptosis after the initial insult may cause renal hypoxia.[118] Our RNA-Seq data show that hypoxia pathways and several hypoxia-related genes, including Hif1, Epo, and Ptprz1 were upregulated in the CHF, suggesting the existence of and the involvement of renal hypoxia in CHF. CSAR ablation attenuated the increased expression of Ptprz1, suggesting that the effects of cardiac afferent ablation may reduce hypoxia in CHF.

Other mechanisms contributing to the beneficial effects of RTX cannot be excluded, such as the effect of RTX on enhanced vasopressin in CHF. Inappropriately high levels of plasma vasopressin in patients with heart failure contribute the exacerbation of CHF.[119] The direct projection of cardiac sympathetic afferents to the paraventricular nucleus of the hypothalamus has been documented.[120] We found that gene expression of the Avpr2 was decreased at the late stages of CHF, implying that there was an increase in vasopressin which downregulates the expression of Avpr2. Therefore, we believe that the CSAR may also modulate the expression of vasopressin, leading to changes in blood volume.

CHAPTER 2: RENAL DENERVATION ATTENUATES PROXIMAL TUBULAR DAMAGE IN RATS WITH CARDIO-RENAL SYNDROME TYPE 2

Introduction

Excessive activation of the sympathetic nervous system (SNS) plays a prominent role in the development and progression of CHF. Therefore, attenuation of overactive sympathetic signaling pathway is considered as a potential therapeutic strategy for CHF. In Chapter 1, our study demonstrated that downregulation of sympathetic tone through CSAR ablation in a rat model of MI-induced CHF prevented renal dysfunction and improved the mortality, possibly through partial restoration of cortical blood flow and reduced renal venous congestion. In this study, we examined whether RDN mimics the beneficial effects of CSAR ablation on renal perfusion and renal function in CHF rats**.** We propose that tonic CSAR activation in CHF increases renal sympathetic outflow contributing to renal vasoconstriction and disease progression. If so, RDN should, at least in part, mimic the beneficial effects of CSAR ablation on renal function in CHF rats. Here, we tested the hypothesis that unilateral renal denervation performed one month post myocardial infarction, would producing long-term improvements in renal function and cardiac function in a rat model of heart failure. More importantly, we aimed to examine the effect of renal denervation on changes in kidney damage and inflammation in CHF rats. Unilateral renal denervation was performed on the left kidneys one-month post-MI. The contralateral (non-denervated) kidneys were used as the control in order to preclude the influence of other systemic factors on renal tissue damage.

Methods

Experiments were performed on adult, male, 400-500g Sprague-Dawley rats purchased from the Charles River Laboratories. The overall experimental protocol is outlined in **Figure 31**.

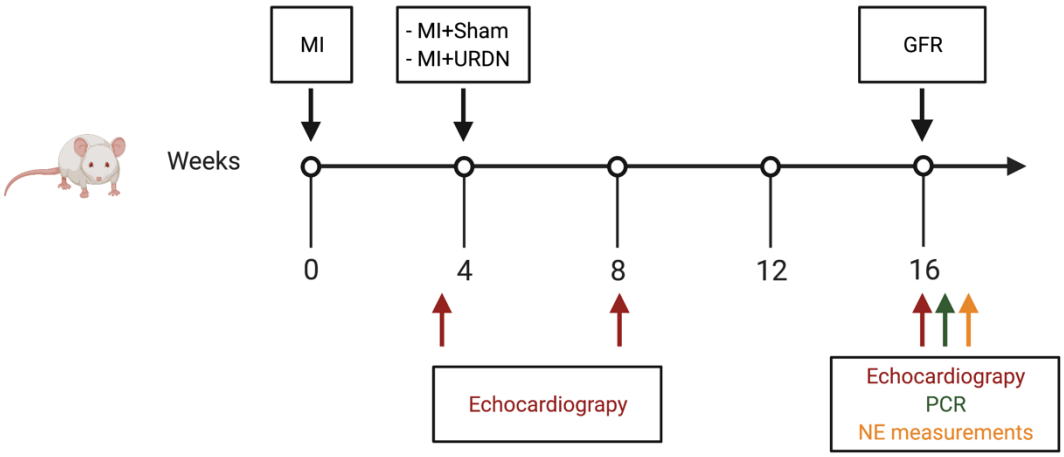

Figure 31. Schematic diagram of study design in Chapter 2.

Rat model of chronic heart failure and unilateral renal denervation

Myocardial infarction (MI)-induced CHF was produced by coronary ligation as previously described.[35] Four weeks after the MI procedure, rats were randomized to either the unilateral renal denervation group (URDN) or the sham surgery group. Under anesthesia with 3% isoflurane, the left renal arteries and veins were exposed by a left flank incision. All visible left renal nerve bundles were cut off followed by painting the left renal artery with 10% phenol absolute ethanol. The sham-operated rats received similar procedures with the exception that the renal nerves remained intact. Renal NE, DOPA, epinephrine, dopamine and serotonin were quantified with the help from Dr. Gregory Fink in the Department of Pharmacology and Toxicology at the Michigan State University.

At different time points, prior to URDN, 8 weeks post MI and 16 weeks post MI, echocardiography was performed to evaluate cardiac function. Detailed methods are described in Chapter 1.

GFR measurement

GFR was measured as previous described in Chapter 1, Blood sample was collected from a catheter that was placed through the right carotid artery into the left ventricle.

RT-PCR

Kidney tissues from left and right sides were harvested and dissected into cortex and medulla at 16-18 weeks post-MI. The mRNA expression of *Kim-1*, *Ngal*, *Il1b*, and *Il6* were measured by using the QuantiFast SYBR Green PCR Kit (Qiagen, Germantown, MD, USA). Primer sequences for RT-PCR and detailed methods are provided in Chapter 1.

Statistics

All data are expressed as the mean ± standard deviation (SD). Differences between groups were determined by a two-way ANOVA followed by Tukey's post hoc test. P-value < 0.05 was considered statistically significant.

Results

Morphological data and echocardiographic data

There was no difference in infarct sizes between CHF+Sham rats and CHF+URDN rats (36.4±7.8% in CHF+Sham group and 36.3±3.9% in CHF+URDN group; **Figure 32**). To evaluate the effects of URDN on cardiac remodeling of CHF rats, LV dimensions and volumes at different time points post-MI were performed (**Figure 33**). LV dimensions and volumes were increased in a temporal manner after MI, which was not observed in the CHF+URDN rats (**Figure 34 C-F**). At 18 weeks post-MI, the LVEF and FS of CHF+URDN were significantly improved in comparison with CHF+Sham, implying the preservation of LV contractility from URDN (**Figure 34 A-B**).

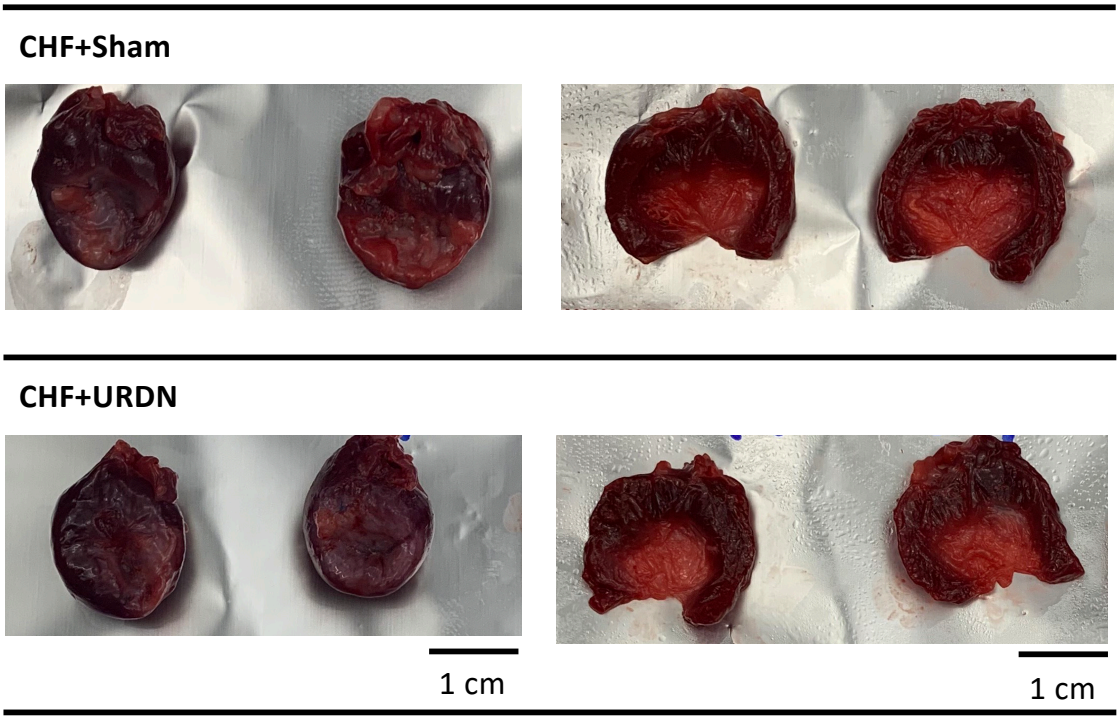

Figure 32 Gross morphology of infract hearts and infarct sizes of CHF rats treated with of Sham RDN surgery or URDN.

CHF+Sham

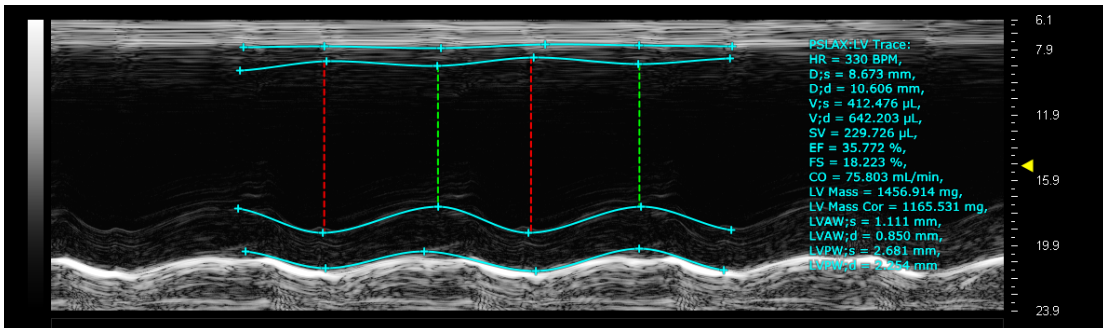

CHF+URDN

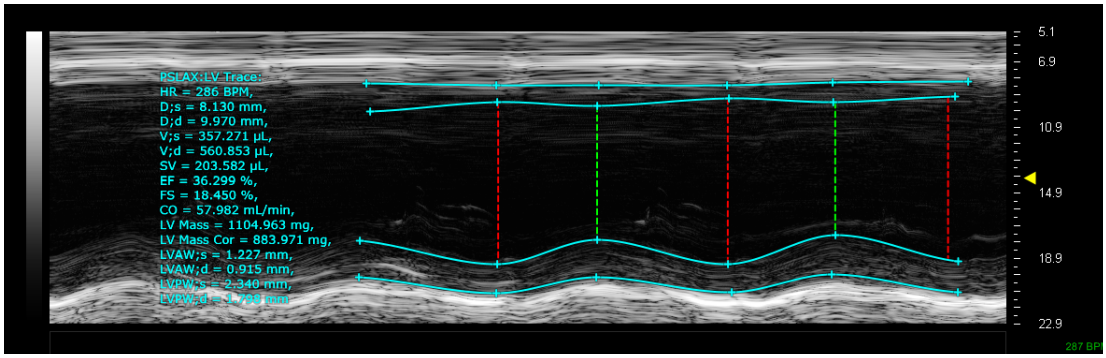

Figure 33 Representative M-mode, long-axis, and two-dimensional echocardiography images of the LV from CHF rats treated with of Sham RDN surgery or URDN at 18 weeks post-MI.

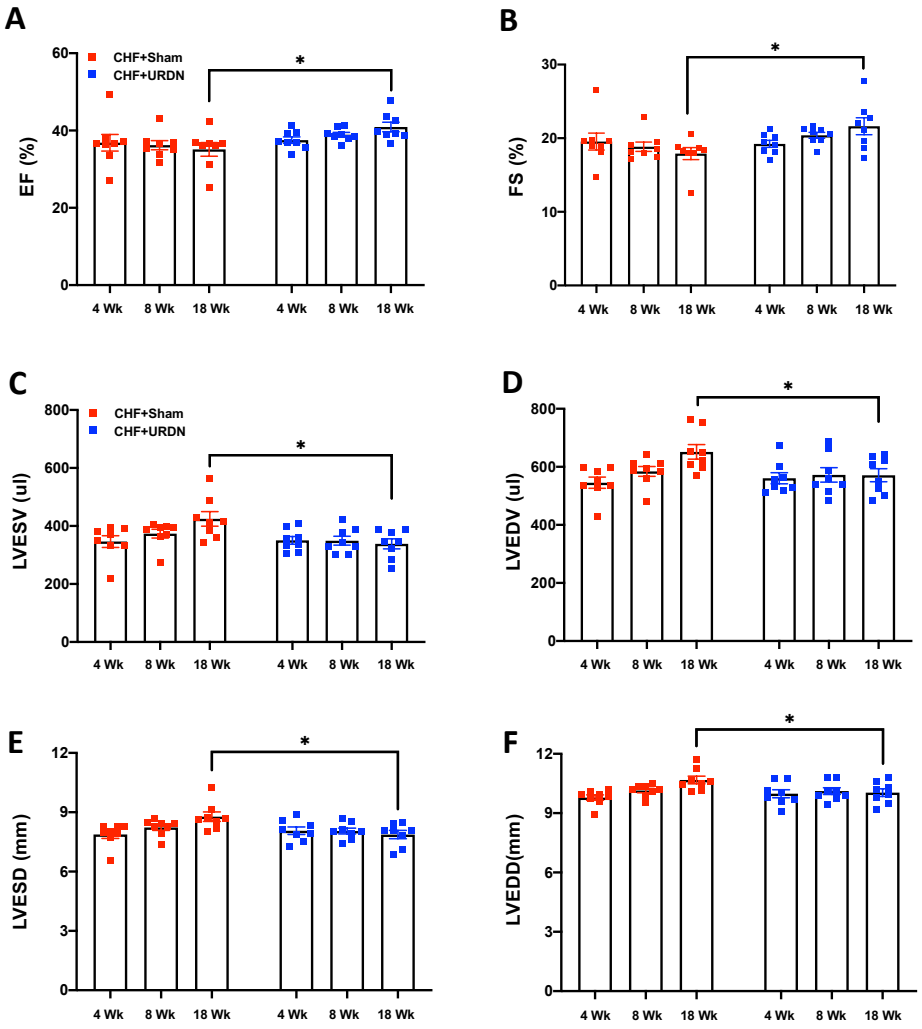

Figure 34. Echocardiographic measurements including EF (**A**), FS (**B**), LVESV (**C**), LVEDV (**D**), LVESD (**E**), and LVEDD (**F**) in CHF+Sham and CHF+URDN rats. EF, ejection fraction; FS, fractional shortening; LVESV, left ventricular end-systolic volume; LVEDV, left ventricular end-diastolic volume; LVESD, left ventricular end-systolic diameter; LVEDD, left ventricular end-diastolic diameter. *P<0.05 vs. CHF+Sham.

NE measurements

There was no difference in NE levels between the sham-operated kidneys and the non-operated kidneys of CHF rats (**Figure 35**). The renal NE levels of CHF rats were comparable with that in the control group. Compared with the non-operated kidneys in the CHF+URDN group, a reduction in NE of % 79.2% was found in denervated kidneys 12 weeks after URDN surgery, which was 16 weeks post MI.

No significant difference in the levels of DOPA or epinephrine were detected among the left and right kidneys from the control, CHF and CHF+URDN groups (**Figure 36 A, B**). The dopamine levels in the sham-operated kidneys and non-operated kidneys were higher than that in the control group. A decrease in the dopamine levels in the denervated kidneys was detected compared with that in the contralateral side (**Figure 36 C**). Interestingly, the serotonin level in the denervated kidneys was increased compared with those in the control group, CHF group and the non-operated side in the CHF+URDN group (**Figure 36 D**).

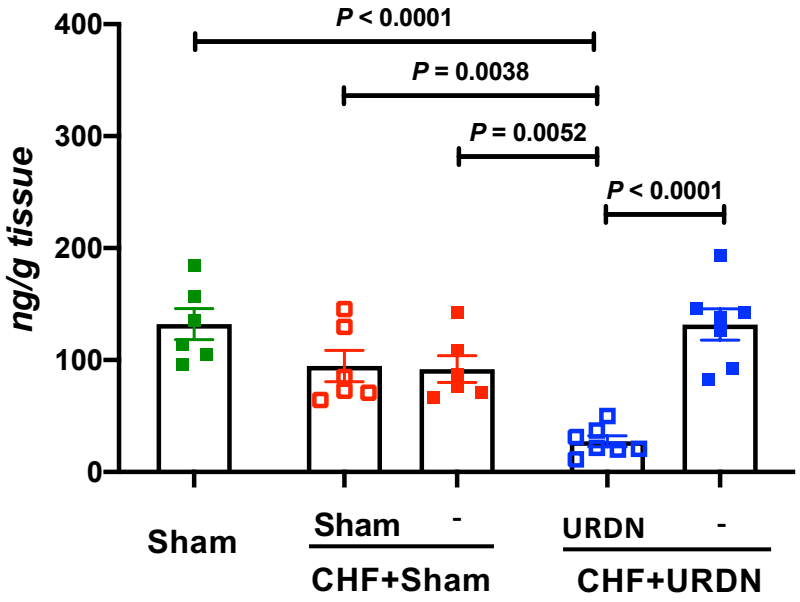

Figure 35. Unilateral renal denervation reduced the NE production in the denervated kidneys. CHF, chronic heart failure; URDN, unilateral renal denervation; NE, norepinephrine.

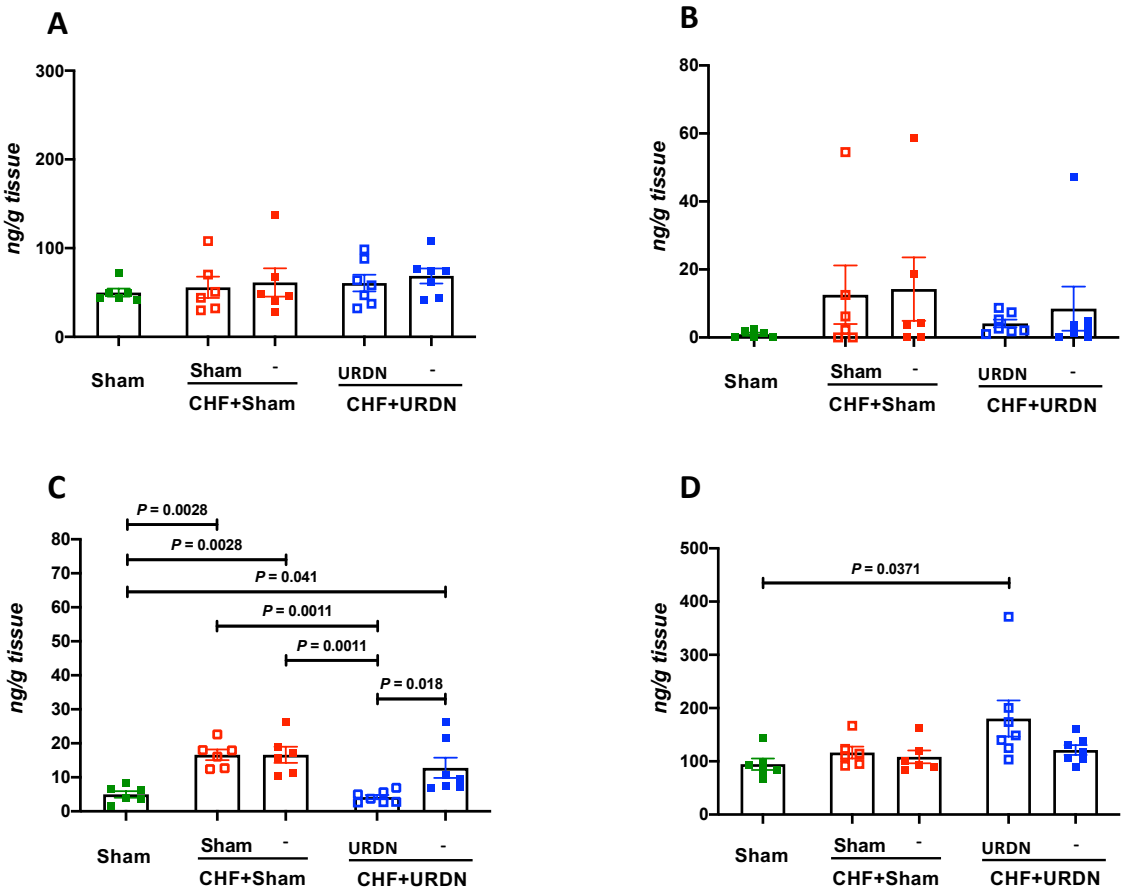

Figure 36. The effects of renal denervation on the production of DOPA (A), epinephrine (B), dopamine (C), and serotonin (D) in the kidneys. CHF, chronic heart failure; URDN, unilateral renal denervation.

GFR measurements

To evaluate kidney function, GFR values were measured at 16-18 weeks post MI. Compared with control animals, the GFR of CHF+Sham denervation animals was significantly reduced at 16 weeks post MI, which was improved in the CHF+URDN group (**Figure 37**).

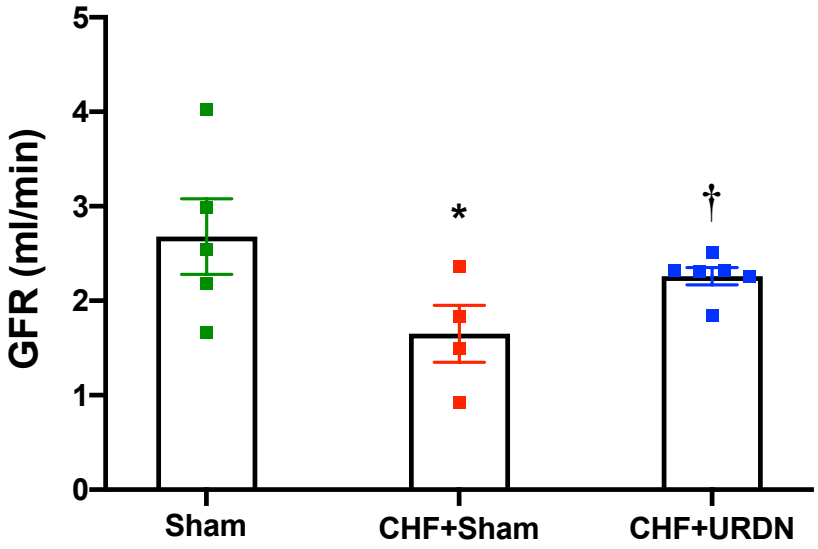

Figure 37. Unilateral renal denervation ameliorated renal dysfunction in chronic heart failure. CHF, chronic heart failure; URDN, unilateral renal denervation. *P<0.05 vs. Control. †P<0.05 vs. CHF+Sham.

PCR data of kidney damage, and inflammation markers

In the renal cortexes from the left and right kidneys of CHF+Sham rats, *Kim1* and *Ngal* mRNA levels were significantly increased, which were largely prevented by the unilateral denervation in the left renal cortexes of CHF+URDN rats (**Figure 38 A-D**). Similar trends were observed in the renal medulla (**Figure 38 A-D**). There was a tendency of the mRNA expression of *Il1b* and *Il6* in the left and right kidneys to increase, which was not attenuated by URDN (**Figure 38 E-F**).

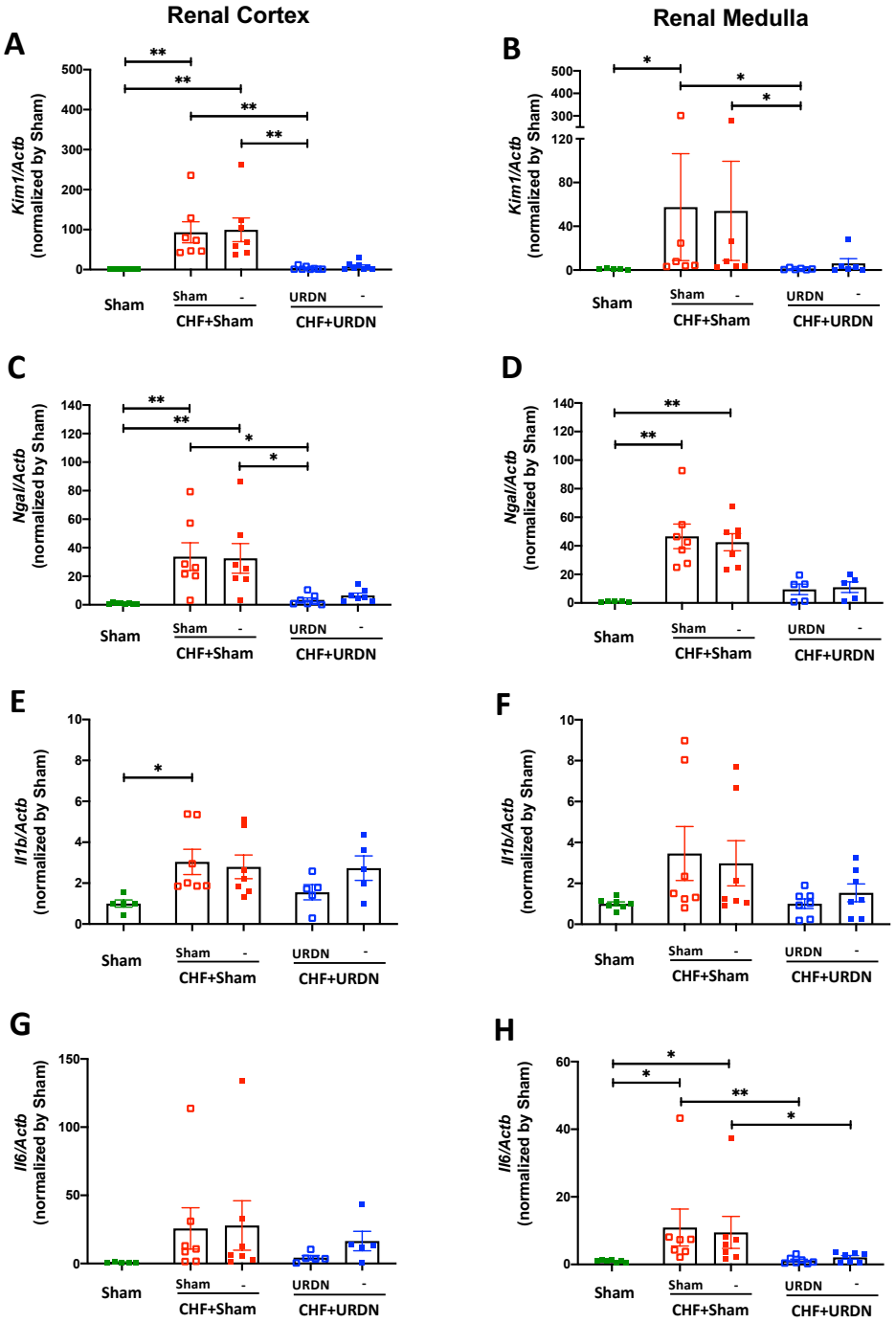

Figure 38. Real-time PCR data showing *Kim1*(**A, B**), *Ngal* (**C, D**), *Il1b* (**E, F**), and *Il6* (**G, H**) mRNA expressions in the renal cortex and medulla from sham, CHF+Sham, and CHF+URDN rats. Control group, n=5-8 for A-H; CHF+Sham group, n=6-7 for A-H; CHF+RTX group, n=5-8 for A-H. *Kim1*, kidney injury molecule-1; *Ngal*, neutrophil gelatinase-associated lipocalin; *Il6*, interleukin 6; *Il1b*, interleukin 1 beta; *Actb*, actin beta. *, $P<0.05$. **, $P<0.01$.

Discussion

In this study we hypothesized that unilateral renal denervation produces long-term improvements in renal function and cardiac function in a rat model of heart failure. The primary findings of this study include: 1) unilateral renal denervation mitigated renal dysfunction, as evidenced by preventing the deterioration of GFR and by attenuation of both enhanced KIM-1 gene expression and NGAL gene expression; 2) unilateral renal denervation improved cardiac function of CHF rats. This study suggests that in a rat model of MI-induced HF, unilateral renal denervation was efficacious to preserve renal function and cardiac function.

In the setting of decompensated HF, renal spinal afferents are sensitized and provide increased input to the central nervous system causing excessive sympathetic outflow to the heart, the kidneys, and the peripheral vasculature. Activation of renal efferent nerves leads to increased renal vascular resistance and activation of the renin-angiotensin-aldosterone system contributing to sodium and water retention. RDN, by reducing both afferent and efferent renal nerve activity, can affect global sympathetic tone and volume status. In this study, we observed that renal denervation mimics some of the same effects as CSAR ablation. It's well known that the presence of the renal nerves can activate molecular pathways involved in inflammation, fibrosis, renin release and vasoconstriction.[121-123] Studies have shown that renal denervation prevents the progression of CHF through attenuation of LV fibrosis, reduction in renal sympathetic activity, inhibition of RAAS, restoration of impaired natriuresis.[61, 124] However, the effects of renal denervation on the renal dysfunction in the setting of CHF and underlying mechanisms have not been extensively examined. Watanabe et al. evaluated the effects of RDN on renal damage in Dahl salt-sensitive hypertensive rats in the hypertrophic stage, demonstrating that β blocker and RDN similarly ameliorated the progression of cardiac and renal damage, which is associated with suppression of the gene expression of endothelin-1, renin and angiotensin-converting enzyme.[125] In a rabbit model of pacing-induced CHF, renal blood flow was reduced and renal angiotensin II type 1 receptors, which

were decreased by RDN at 2 weeks post-pacing.[64] In our current study, a rat model of MI-induced HF was used and URDN was performed at 4 weeks post MI. URDN mitigated renal dysfunction, and improved cardiac function of CHF rats, suggesting the efficacy in ameliorating renal dysfunction in the CHF state after CSAR ablation is mediated by a reduction in renal sympathetic nerve activity.

Furthermore, it should be notice that CSAR ablation reduces sympathetic tone to the kidneys through renal efferent, while renal denervation interrupts both efferent and afferent renal nerve fibers. Therefore, it is critical to differentiate the roles that afferents and efferent play in the renal dysfunction in CHF. Experiments to selectively denervate afferent fibers have shown efficacy in CHF.[126, 127] In future studies, experiments can be designed to use the capsaicin or RTX to selectively ablate renal afferents although the demonstration that renal efferent nerve activity is augmented in response to CSAR activation suggest that efferent responses are of major importance.

CHAPTER 3: SAFETY AND EFFICACY OF RENAL DENERVATION IN PATIENTS WITH HEART FAILURE WITH REDUCED EJECTION FRACTION

Introduction

HF is a prevalent, widespread, and costly disease. Each year in the United States, HF affects over 800,000 new patients, contributes to more than 300,000 deaths, and costs 30 billion dollars.[128] The progressive pathophysiology of heart failure is characterized by maladaptive sympatho-excitation which adversely affects the cardiovascular and renal systems. Endovascular RDN is a minimally invasive procedure that has been shown to effectively decrease BP in patients with refractory hypertension.[57] In addition, RDN has provided improvements in alleviating the symptoms of heart failure by reducing sympathetic nerve activity and attenuating adverse cardiac remodeling in both HF animal models and in patients,[56, 67, 129, 130] suggesting that RDN is a promising approach for the management of HF. Several clinical trials have been done to compare the effectiveness of RDN in the treatment of chronic HF, suggesting that RDN decreased N-terminal pro-B-type natriuretic peptide, increased in LVEF, and improved exercise tolerance in patients with chronic HF in RDN group over 6-month follow-up.[67, 71] Potential complications of RDN including renal artery stenosis or dissection, pseudoaneurysm at the femoral access site, and bradycardia are not common but require a concern. Given the lack of large clinical trials in HF patients, the relative benefits and harm of RDN in this patient population remain unclear. We therefore carried out a systematic analysis of clinical trials to in order to assess the effectiveness and risks of bilateral RDN in patients with chronic HFrEF.

Methods

Search strategy

This systematic review was performed according to the Preferred Reporting Items for Systematic Reviews and Meta-Analyses (PRISMA)[131] and the reporting Meta-Analyses of Observational Studies in Epidemiology (MOOSE)[132].

Studies that evaluated the effect of RDN in patients with HF published before December 21, 2019, were identified using PubMed and EMBASE databases, MEDLINE, and ClinicalTrials.gov. The following keywords were used: renal denervation, renal sympathetic denervation and heart failure. References of relevant articles were also reviewed for any additional studies. We searched for studies in any language in which adult patients with HF received bilateral RDN.

Study selection

Studies that met each of the following criteria were included:

(1) the study assessed the effectiveness of RDN in patients with HF who had reduced (< 50%) EF.

(2) the outcomes included NYHA class, six-minute walk test, B-type natriuretic peptide levels, LVEF, LVESD, LVEDD, and left atrium diameter (LAD), HR, systolic blood pressure (SBP), and diastolic blood pressure (DBP), GFR, and creatinine.

(3) the duration of follow-up was at least 6 months.

Data extraction

Two reviewers independently extracted data. Any disagreement in opinion was resolved through discussion with all investigators. The following data were extracted from the included studies: publication year, methodology, number of patients, patient population, intervention including drugs they received, and outcomes.

Primary outcomes were NYHA class, six-minute walk test, BNP levels, LVEF and other cardiac parameters including LVESD, LVEDD, and LAD. Secondary outcomes were HR, SBP, DBP, GFR, and creatinine.

NYHA class, six-minute walk test, BNP levels, LVEF, LVESD, LVEDD, LAD, HR, SBP, DBP, GFR, and creatinine were treated as continuous variables, of which mean differences (MDs) with 95% confidence intervals (CIs) were calculated.

Using the formula shown in Chapter 7 of the Cochrane Handbook for Systematic Reviews of interventions, we estimated the mean and variance of the trials in which only median, interquartile range (IQR), and size were reported.[133]

Quality assessment

The Newcastle-Ottawa Scale (NOS) was used to evaluate the quality of the included studies.[134] Assessment scores of 0-3, 4-6, and 7-9 were considered as poor, fair, and good, respectively. Disagreements were resolved by consensus.

Data analysis

All analyses were performed based on a random-effects model. Heterogeneity between studies was evaluated using a chi-squared test, and a P value of <0.10 was indicative of significant heterogeneity. Data analyses were done with Comprehensive Meta-analysis version 2.2. (Biostat Inc., Englewood, NJ)., and a P value of <0.05 was considered as significant in the analysis.

Results

Eligible studies

The initial search retrieved 52 publications. After excluding duplicates, 42 distinct articles were identified for title and abstract screen (**Figure 39**). Of these, 30 articles were excluded, of which three were studies about RDN for HF with preserved or normal EF, 22 were studies about HTN, renal diseases or Parkinson's disease, four were studies not mentioning RDN, and one was an animal study. Twelve studies were full-text read for further evaluation. The other five were excluded because of no defined endpoints reported or incomplete study details. Therefore, seven studies were included in this analysis (**Table 12**).[67-71, 135, 136]

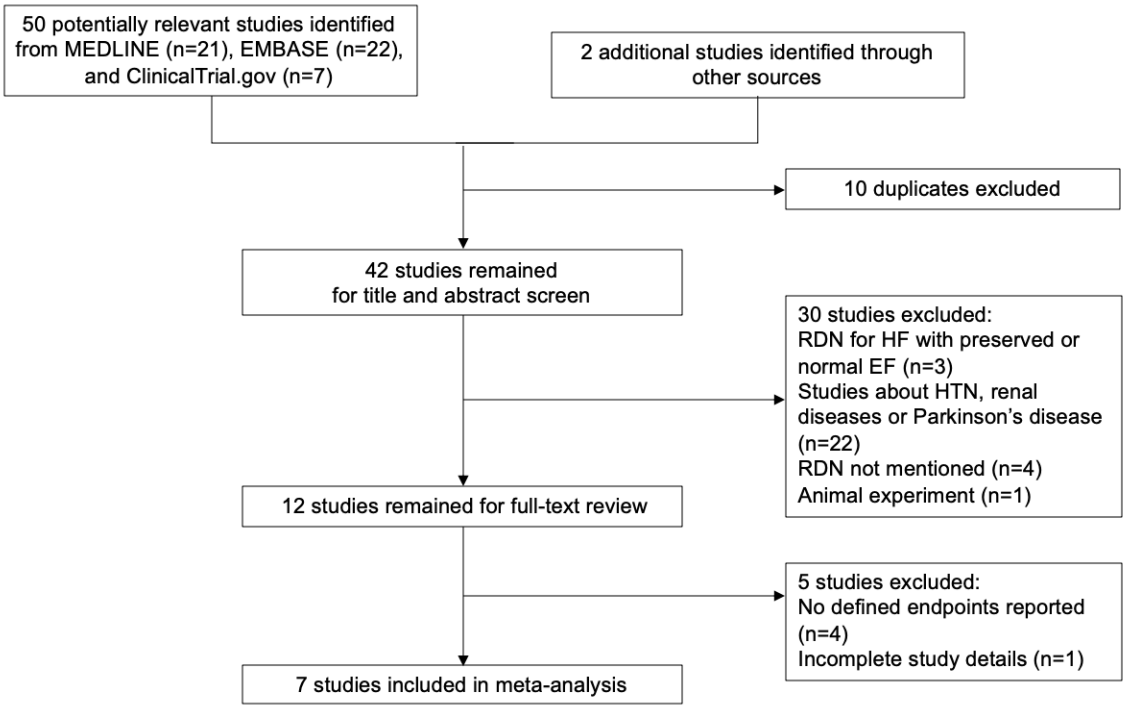

Figure 39. Flowchart of the literature search.

Table 12. Main characteristics of included studies.

No	Study	Country	Design	No. of Patients	Pt condition	Age, Mean (SD), y		Males, %		NYHA class	EF	Catheter type	Follow-up duration	NOS score
						RDN	Control	RDN	Control					
1	Gao et al (2019)	China	Single-center, RCT	60	Chronic systolic HF (65.0% hypertension, 58.3% coronal heart disease, 11.7% atrial fibrillation, and 25% type 2 diabetes)	59.0 (12.1)	61.3 (11.1)	83.3	73.0	II-III	< 40%	Stockert EP Shuttle radiofrequency generator (Johnson & Johnson Medical)	6 months	9
2	Drożdż et al (2019)	Poland	Open-label, RCT	20	Adult HF patients despite optimal medical treatment and resynchronization therapy (60% ischemic cardiomyopathy, and 40% dilated cardiomyopathy of unknown etiology)	75.0 (65.0-81.0)	71.0 (70.0-76.0)	80.0	70.0	II-III	< 35%	Symplicity catheter (Medtronic)	24 months	9
3	Chen et al (2017)	China	Single center, open label, RCT	60	CHF (25% hypertension, 57% cardiomyopathy, 18% ischemic cardiomyopathy).	48.5 (8.4)	50.5 (7.7)	73.30	80.0	ll-lV	≤ 40%	Thermocool catheter (Biosense Webster)	6 months	9
4	Gao et al (2017)	China	Open label, single-arm study	14	CHF (29% hypertension, 14% dilated cardiomyopathy, 57% coronary artery disease).	69.6 (5.7)	N/A	85.7	N/A	III-IV	< 45%	Stockert EP Shuttle radiofrequency generator (Johnson & Johnson Medical)	6 months	6

5	Hopper et al (2017)	8 study sites in Europe and Australia	Multi-center, open-label, single-arm study	39	Chronic systolic HF and renal impairment (62% ischemic heart failure)	65 (11)	N/A	87.0	N/A	II-III	< 40%	Symplicity Flex single-electrode catheter system (Medtronic)	12 months	6
6	Dai et al (2015)	China	Single center, open label, CT	20	CHF (40% dilated cardiomyopathy, 40% ischemic cardiomyopathy, 20% hypertensive cardiopathy).	63 (10)	64 (5)	80.0	70.0	III-IV	< 40%	NR	6 months	9
7	Davies et al (2013)	UK	Open-label, single-arm study	7	CHF (71% ischemic HF, 29% unknown etiology)	69 (7)	N/A	71.4	N/A	III-IV	< 40%	Symplicity catheter (Medtronic)	6 months	6

Characteristics of studies included in the meta-analysis

The main characteristics of the included studies are summarized in **Table 12**. All studies were published between 2013 to 2019. Patient follow-up duration ranged from 6 to 24 months. There were five randomized, control trails,[67-69, 71, 136] and two single-arm trails.[70, 135]

Primary outcomes

NYHA class

Four trials evaluated the effect of RDN on NYHA class (**Figure 40**).[67, 70, 71, 136] From baseline to 6 months after RDN, the pooled mean NYHA class decreased by 0.9, consistent with an amelioration of heart failure symptoms (MD, -0.9; 95% CI, -1.6 to -0.2; P = 0.018).

Six-minute walk test

Five trials reported the effect of RDN on the six-minute walk test (**Figure 40**).[67, 69-71, 136] Four reported mean (SD),[67, 69-71] and one reported median (IQR).[136] The mean six-minute walk test was increased by 79.5 meters (MD, 79.5 m; 95% CI, 26.9 to 132.1; P = 0.003).

BNP levels

Five trials reported the changes of BNP levels after RDN (**Figure 40**).[67, 68, 70, 71, 136] Four reported mean (SD),[67, 68, 70, 71] and one reported median (IQR).[136] The average BNP level was decreased by -436.8 pg/mL (MD, 436.8 pg/mL; 95% CI, -732.8 to -140.8; P = 0.004).

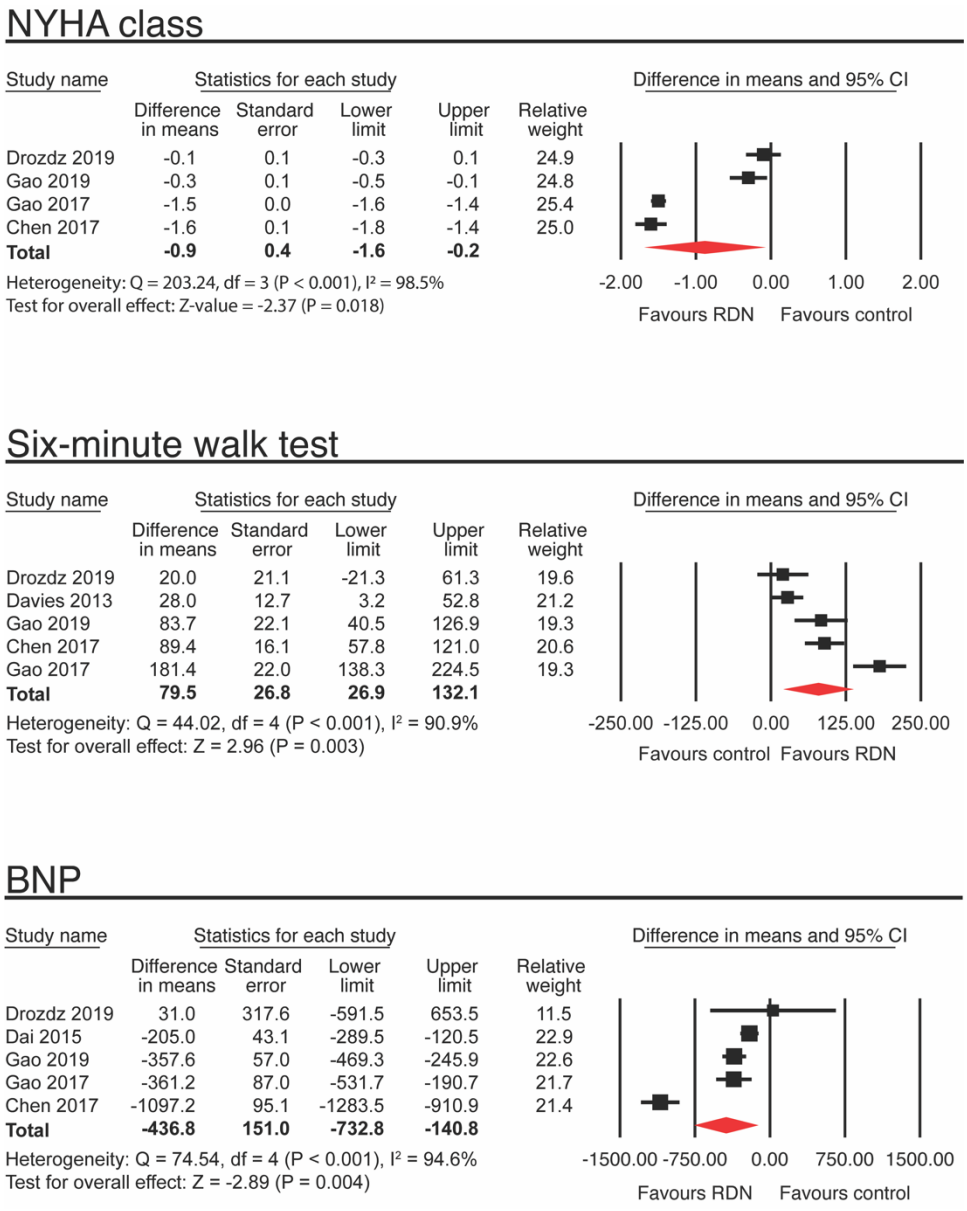

Figure 40. Effects of renal denervation on NYHA class, six-minute walk test, and B-type natriuretic peptide (BNP) levels.

Echocardiography

Six out of seven studies evaluated the effect of RDN on LVEF (**Figure 41**).[67-71, 136] The combined data showed that RDN increased LVEF by 5.7% (MD, 5.7%; 95% CI, 1.6 to 9.6; P = 0.004). Three studies evaluated the effect of RDN on LVESD.[69-71] The combined data showed that RDN significantly decreased the LVESD by 0.4 cm (MD, -0.4 cm; 95% CI, -0.5 to -0.2; P < 0.001). Four studies evaluated the effect of RDN on LVEDD.[67, 69-71] The combined data showed that RDN significantly decreased the LVEDD by 0.5 cm (MD, -0.5 cm; 95% CI, -0.6 to -0.3; P < 0.001).

Three studies evaluated the effect of RDN on LAD.[67, 69, 70] The combined data showed that the renal denervation significantly decreased the LAD by 0.4 cm (MD, -0.4 cm; 95% CI, -0.8 to 0; P = 0.045).

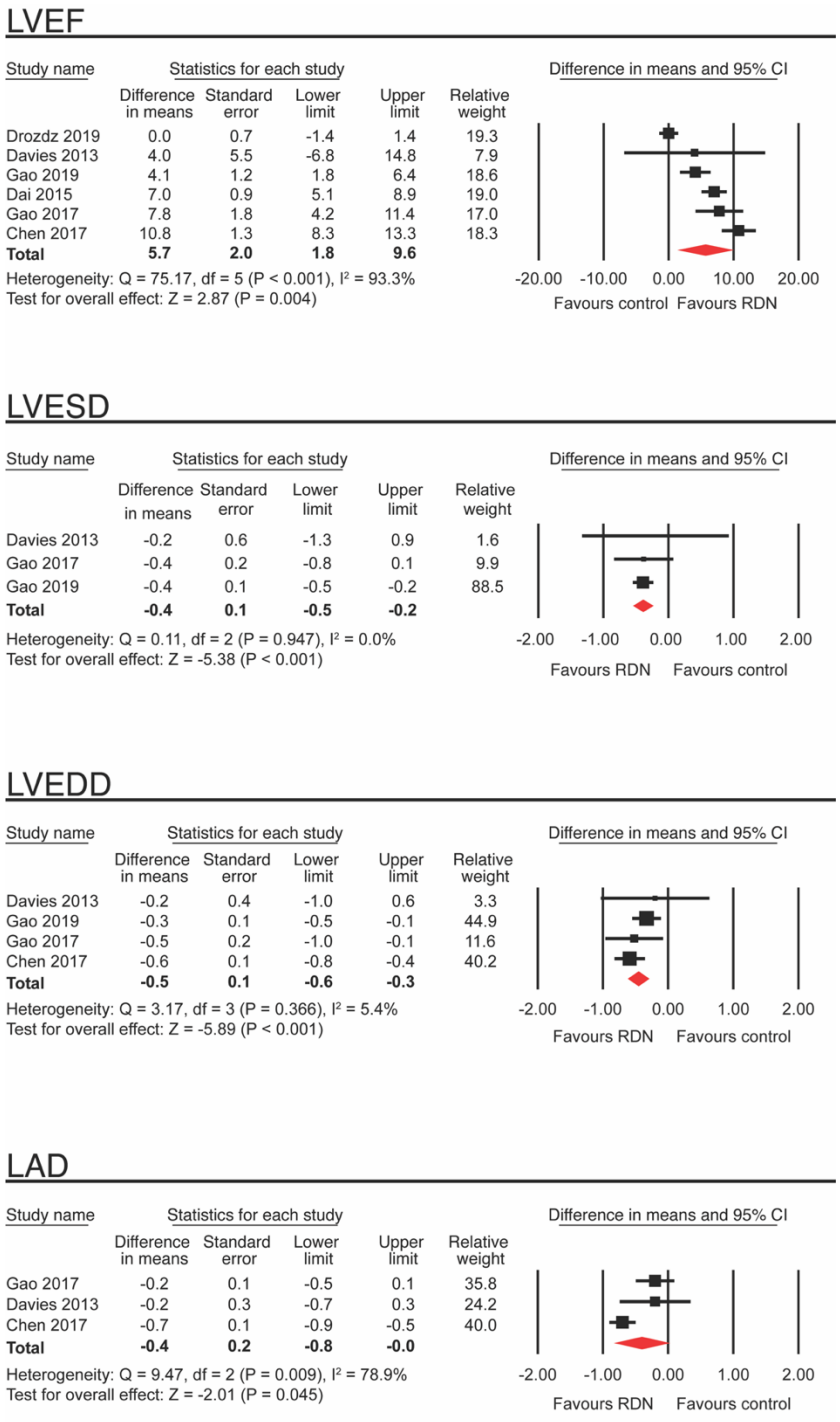

Figure 41. Effects of renal denervation on left ventricular ejection fraction (LVEF), left ventricular end-systolic diameter (LVESD), left ventricular end-diastolic diameter (LVEDD), and left atrium diameter (LAD).

Secondary outcomes

BP and HR

The changes of BP were examined in five studies (**Figure 42**).[67, 69-71, 136] The analysis demonstrated that RDN significantly decreased systolic BP by 9.4 mmHg (MD, -9.4 mmHg; 95% CI, -16.3 to -2.4; P = 0.008) and diastolic BP by 4.9 mmHg (MD, -4.9 mmHg; 95% CI, -9.5 to -0.4; P = 0.033). Four trials included changes of HR as an outcome of interest,[67, 69, 70, 136] showing that RDN was associated with a reduction in HR (MD, -4.5 bpm; 95% CI, -8.2to -0.9; P = 0.015).

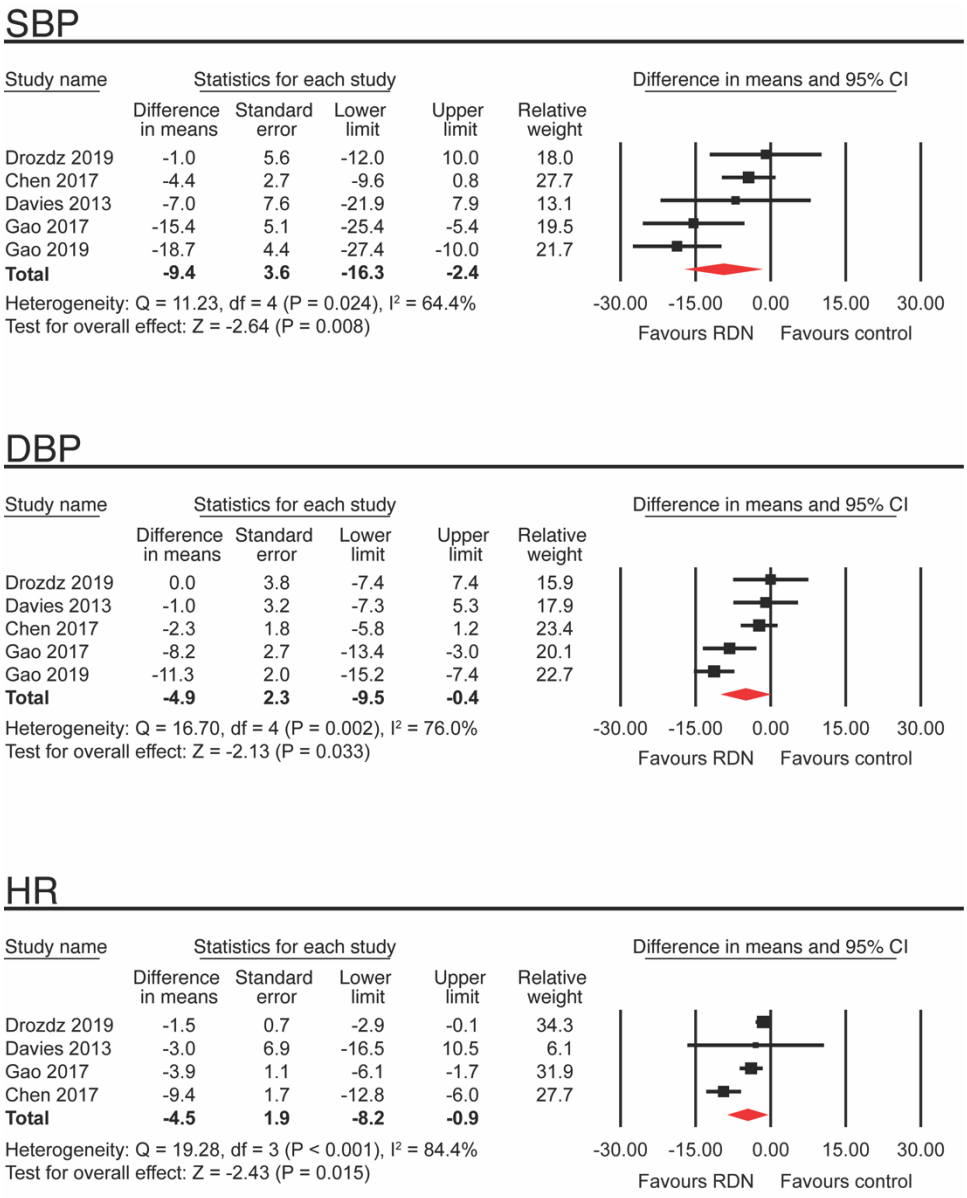

Figure 42. Effects of renal denervation on systolic blood pressure (SBP), diastolic blood pressure (DBP), and heart rate (HR).

GFR and creatinine

Three trials evaluated the effect of RDN on GFR (**Figure 43**).[67, 135, 136] The analysis did not demonstrate a statistically significant effect of RDN on GFR from baseline to 6-month post-RDN (MD, 4.9; 95% CI, -4.7 to 14.5; P = 0.315). Two trials reported the effect of RDN on serum creatinine levels.[69, 70] Similarly, mean creatinine levels did not change after RDN (MD, -7.2; 95% CI, -23.7 to 9.4; P = 0.397).

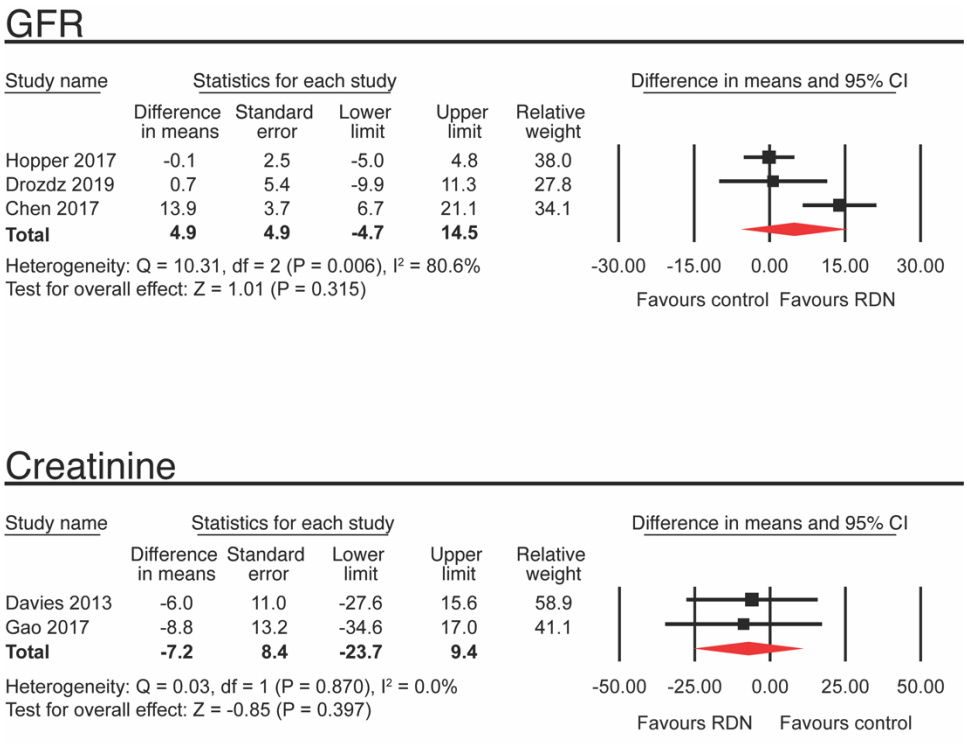

Figure 43. Effects of renal denervation on glomerular filtration rate (GFR), and creatinine.

Discussion

This meta-analysis showed that RDN significantly improved the symptoms of heart failure as evidenced by decreases in NYHA class and increased six-minute walk distances. This meta-analysis also showed echocardiographic improvements in left ventricular function (LVEF, LVESD) and congestion (LAD, LVEDD) after RDN, suggesting that these echocardiographic improvements could drive symptomatic improvement. Moreover, renal denervation decreased systolic and diastolic BP as well as HR without affecting renal function.

RDN was originally performed to treat patients with resistant hypertension. Initial clinical studies showed that RDN was efficient to decrease BP in patient with hypertension,[57, 137] which was not supported by the observation from the Symplicity HTN-3 study.[138] Later on, the DENERHTN trial demonstrated that RDN plus antihypertensive agents deceased BP more in comparison with pharmacotherapy alone.[139] Nowadays, CHF has also been proposed as another indication of RDN. A major problem in the development of HF is excessive sympatho-excitation that promotes cardiac dysfunction and affects other important organs such as the kidneys. Several animal experiments have shown that RDN improves cardiac function, decreases ventricular arrythmia and ameliorates renal damage, suggesting beneficial effects of RDN in chronic HF.[62, 63] However, whether RDN is effective in treating patients with chronic HF is still unclear. Our study shows that RDN significantly improved symptoms related to HF, suggesting an improvement in the quality of life. A possible mechanism is that RDN suppresses sympathetic tone and the renin-angiotensin-aldosterone system, leading to the amelioration of cardiac fibrosis and improvement cardiac contractility.

Our study reviewed two potential safety endpoints: hemodynamics and renal function. Our study suggests that bilateral RDN slightly decreased systolic and diastolic BP as well as HR in chronic HF; therefore, hemodynamics should be taken into consideration prior to and after the RDN procedure as hypotension and bradycardia may further compromise perfusion in these vulnerable

patients. In addition, renal denervation has been shown to improve renal function in patients with chronic kidney diseases.[140] Our analysis suggests that RDN neither harms nor ameliorates renal function in HFrEF patients. Several other included studies also evaluated the changes of sodium levels, potassium levels and BUN; however, whether renal denervation could improve kidney function requires future studies with this focus.

The current study has several limitations. One major limitation of the current study is the small sample sizes of the included studies. Second, the RDN procedure varies considerably due to high intrinsic procedural variability, interventionist and center experience, and catheter technology. In the included studies, details concerning the denervation procedure including the number of ablation points, the sites of denervation, the catheter types, and the operator experience were not extensively described. Liu et al used renal nerve stimulation to identify the nerve-enriched areas during RDN in order to improve the efficacy of the procedure in a dog model of hypertension, indicating that renal nerve stimulation could serve as a useful guide to locate the optimal ablation targets.[141] In addition, a recent study carried out in rabbits and pigs suggests that transfer function analysis of the coupling between renal blood flow and BP on a beat by beat basis may be beneficial in determining the completeness of RDN in the cath lab.[142] Additionally, none of the studies used hard endpoints like mortality, death from cardiovascular causes, or heart failure admissions that drive changes in the standard of care for heart failure patients. Large, multicenter, sham-controlled randomized trials with gold-standard endpoints are needed to definitively test the therapeutic potential of catheter-based RDN in chronic HF patients.

GENERAL DISCUSSION

Major findings of the dissertation

In summary, the major findings of this dissertation are:

1. In the setting of MI-induced CHF, CSAR-induced sympathetic activation impaired renal function through renal hypoperfusion and potentially through exacerbated renal venous congestion (Chapter 1).

2. Unilateral renal denervation was efficacious to preserve renal function and cardiac function, suggesting the efficacy in ameliorating renal dysfunction in the CHF state after CSAR ablation is mediated by a reduction in renal sympathetic nerve activity (Chapter 2).

3. Bilateral RDN appears safe and well-tolerated in patients with HF. RDN improved the signs and symptoms of HF and slightly decreased systolic and diastolic BP without affecting renal function in the clinical trials performed to date (Chapter 3).

Taken together, these findings demonstrate the CSAR plays a critical role in mediating the pathological development of renal impairment in the CRS type 2. The current study suggests that both CSAR ablation and RDN may have translational potential in the treatment of patients with CRS type 2.

Conclusion and Perspectives

Our data demonstrate that the CSAR plays a critical role in mediating the pathological development of renal impairment in the CRS type 2 (**Figure 44**). The CSAR is silent in the normal state but becomes tonically activated in CHF and contributes to a continuous sympathetically mediated vasoconstrictor tone to visceral vascular beds including the kidney, resulting in both chronic renal ischemia and potent peripheral vasoconstriction. The latter, in combination with the decreased intrinsic myocardial contractility causes a volume shift from the peripheral circulation

to the thorax, thus increasing CVP/renal venous pressure and contributing to renal venous congestion. Both CSAR-induced renal ischemia and venous congestion contribute to chronic kidney dysfunction. Cardiac afferent denervation by epicardial application of RTX at the time of MI benefits the kidneys in CHF through attenuation of renal hypoperfusion and venous congestion. RTX has been shown to produce analgesic effects in animal models of arthritis and chronic pain when delivered intra-articularly or intrathecally.[143, 144] The current study suggests that epicardial application of RTX may have potential in the treatment of patients with CRS type 2.

To further evaluate the translational potential of cardiac afferent denervation, we performed intra-stellate injection of RTX at 4 weeks post MI, observing a similar renal protective effect on renal function, suggesting that cardiac afferent denervation following heart failure still has the beneficial effect on the kidneys. However, the underlying mechanism of the beneficial effects of intra-stellate injection of RTX, the appropriate therapeutic window, dosage and volume, laterality (one side or both sides) remains questions for further investigations.

To discover the underlying mechanisms of the beneficial effects of CSAR ablation on renal function in CHF, unilateral renal nerve denervation was performed in CHF rats. Our result shows that unilateral renal denervation was efficacious to preserve renal function and cardiac function by attenuation renal sympathetic nerve activity. However, the mechanisms underlying the renal denervation do not seem to be exactly the same with that of CSAR, which requires further investigation. In the future, bilateral renal denervation should be performed to examine its effect on renal dysfunction in CHF to mimic the catheter based RDN in clinics.

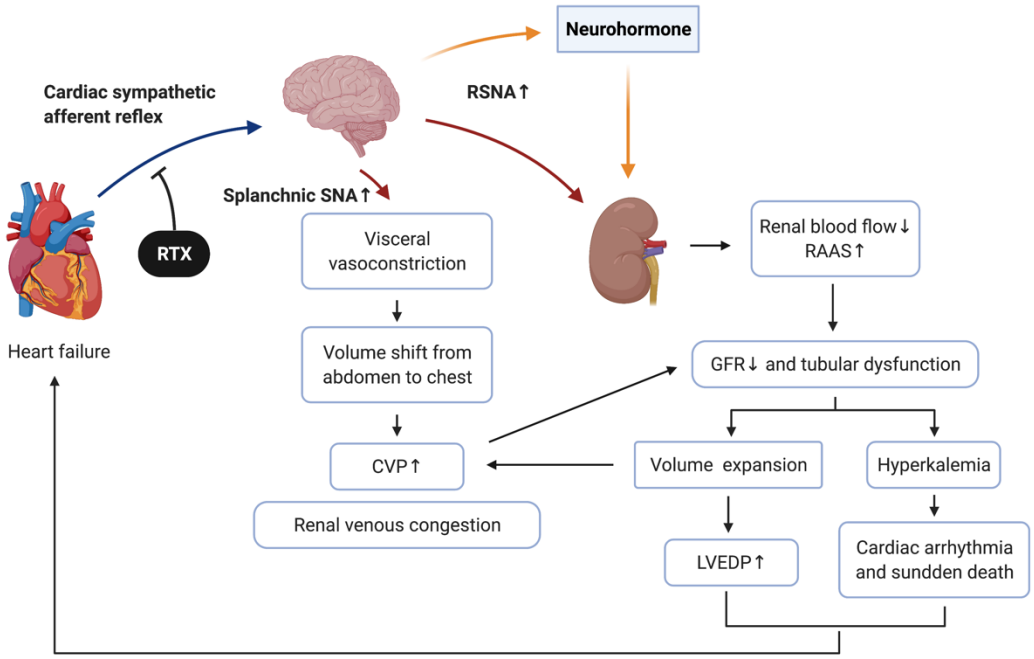

Figure 44. A schematic diagram showing direct neural crosstalk between the heart and kidney via the cardiac sympathetic afferent reflex in heart failure. CSAR-induced sympathetic activation impairs renal function through renal hypoperfusion and potentially through exacerbated renal venous congestion. AVP, vasopressin; CVP, central venous pressure; RAAS, renin-angiotensin-aldosterone system; RSNA, renal sympathetic nerve activity. LVEDP, left ventricular end-diastolic pressure.

BIBLIOGRAPHY

1. Virani SS, Alonso A, Benjamin EJ*, et al.* Heart Disease and Stroke Statistics-2020 Update: A Report From the American Heart Association. *Circulation* **141**, e139-e596 (2020).

2. Packer M, Bristow MR, Cohn JN*, et al.* The effect of carvedilol on morbidity and mortality in patients with chronic heart failure. U.S. Carvedilol Heart Failure Study Group. *The New England journal of medicine* **334**, 1349-1355 (1996).

3. Flather MD, Yusuf S, Køber L*, et al.* Long-term ACE-inhibitor therapy in patients with heart failure or left-ventricular dysfunction: a systematic overview of data from individual patients. ACE-Inhibitor Myocardial Infarction Collaborative Group. *Lancet* **355**, 1575-1581 (2000).

4. McMurray JJ, Ostergren J, Swedberg K*, et al.* Effects of candesartan in patients with chronic heart failure and reduced left-ventricular systolic function taking angiotensin-converting-enzyme inhibitors: the CHARM-Added trial. *Lancet* **362**, 767-771 (2003).

5. Hillege HL, Nitsch D, Pfeffer MA*, et al.* Renal function as a predictor of outcome in a broad spectrum of patients with heart failure. *Circulation* **113**, 671-678 (2006).

6. Palazzuoli A, Lombardi C, Ruocco G*, et al.* Chronic kidney disease and worsening renal function in acute heart failure: different phenotypes with similar prognostic impact? *European heart journal Acute cardiovascular care* **5**, 534-548 (2016).

7. Ponikowski P, Anker SD, Chua TP*, et al.* Depressed heart rate variability as an independent predictor of death in chronic congestive heart failure secondary to ischemic or idiopathic dilated cardiomyopathy. *The American journal of cardiology* **79**, 1645-1650 (1997).

8. White HD, Norris RM, Brown MA, Brandt PW, Whitlock RM, Wild CJ. Left ventricular end-systolic volume as the major determinant of survival after recovery from myocardial infarction. *Circulation* **76**, 44-51 (1987).

9. Cohn JN, Levine TB, Olivari MT*, et al.* Plasma norepinephrine as a guide to prognosis in patients with chronic congestive heart failure. *The New England journal of medicine* **311**, 819-823 (1984).

10. van den Broek SA, van Veldhuisen DJ, de Graeff PA, Landsman ML, Hillege H, Lie KI. Comparison between New York Heart Association classification and peak oxygen consumption in the assessment of functional status and prognosis in patients with mild to moderate chronic congestive heart failure secondary to either ischemic or idiopathic dilated cardiomyopathy. *The American journal of cardiology* **70**, 359-363 (1992).

11. McAlister FA, Ezekowitz J, Tonelli M, Armstrong PW. Renal insufficiency and heart failure: prognostic and therapeutic implications from a prospective cohort study. *Circulation* **109**, 1004-1009 (2004).

12. Löfman I, Szummer K, Dahlström U, Jernberg T, Lund LH. Associations with and prognostic impact of chronic kidney disease in heart failure with preserved, mid-range, and reduced ejection fraction. *European journal of heart failure* **19**, 1606-1614 (2017).

13. Di Lullo L, House A, Gorini A, Santoboni A, Russo D, Ronco C. Chronic kidney disease and cardiovascular complications. *Heart failure reviews* **20**, 259-272 (2015).

14. Husain-Syed F, McCullough PA, Birk HW*, et al.* Cardio-Pulmonary-Renal Interactions: A Multidisciplinary Approach. *Journal of the American College of Cardiology* **65**, 2433-2448 (2015).

15. Clementi A, Virzi GM, Brocca A*, et al.* Advances in the pathogenesis of cardiorenal syndrome type 3. *Oxidative medicine and cellular longevity* **2015**, 148082 (2015).

16. Palazzuoli A, Ruocco G. Heart-Kidney Interactions in Cardiorenal Syndrome Type 1. *Advances in chronic kidney disease* **25**, 408-417 (2018).

17. Jungbauer CG, Birner C, Jung B*, et al.* Kidney injury molecule-1 and N-acetyl-beta-D-glucosaminidase in chronic heart failure: possible biomarkers of cardiorenal syndrome. *European journal of heart failure* **13**, 1104-1110 (2011).

18. Schaub JA, Parikh CR. Biomarkers of acute kidney injury and associations with short- and long-term outcomes. *F1000Research* **5**, (2016).

19. Heerspink HJ, Gao P, de Zeeuw D*, et al.* The effect of ramipril and telmisartan on serum potassium and its association with cardiovascular and renal events: results from the ONTARGET trial. *Eur J Prev Cardiol* **21**, 299-309 (2014).

20. McCullough PA, Barnhart HX, Inrig JK*, et al.* Cardiovascular toxicity of epoetin-alfa in patients with chronic kidney disease. *Am J Nephrol* **37**, 549-558 (2013).

21. McCullough PA, Ali S. Cardiac and renal function in patients with type 2 diabetes who have chronic kidney disease: potential effects of bardoxolone methyl. *Drug Des Devel Ther* **6**, 141-149 (2012).

22. Chin MP, Wrolstad D, Bakris GL*, et al.* Risk factors for heart failure in patients with type 2 diabetes mellitus and stage 4 chronic kidney disease treated with bardoxolone methyl. *Journal of cardiac failure* **20**, 953-958 (2014).

23. Chapleau MW, Hajduczok G, Abboud FM. Mechanisms of resetting of arterial baroreceptors: an overview. *Am J Med Sci* **295**, 327-334 (1988).

24. Thrasher TN. Unloading arterial baroreceptors causes neurogenic hypertension. *American journal of physiology Regulatory, integrative and comparative physiology* **282**, R1044-1053 (2002).

25. de Leeuw PW, Bisognano JD, Bakris GL, Nadim MK, Haller H, Kroon AA. Sustained Reduction of Blood Pressure With Baroreceptor Activation Therapy: Results of the 6-Year Open Follow-Up. *Hypertension (Dallas, Tex : 1979)* **69**, 836-843 (2017).

26. Doumas M, Faselis C, Kokkinos P, Anyfanti P, Tsioufis C, Papademetriou V. Carotid baroreceptor stimulation: a promising approach for the management of resistant hypertension and heart failure. *Curr Vasc Pharmacol* **12**, 30-37 (2014).

27. Grassi G, Brambilla G, Pizzalla DP, Seravalle G. Baroreflex Activation Therapy in Congestive Heart Failure: Novel Findings and Future Insights. *Curr Hypertens Rep* **18**, 60 (2016).

28. Zucker IH, Hackley JF, Cornish KG*, et al.* Chronic baroreceptor activation enhances survival in dogs with pacing-induced heart failure. *Hypertension (Dallas, Tex : 1979)* **50**, 904-910 (2007).

29. Zile MR, Abraham WT, Lindenfeld J*, et al.* First granted example of novel FDA trial design under Expedited Access Pathway for premarket approval: BeAT-HF. *American heart journal* **204**, 139-150 (2018).

30. Sabbah HN, Gupta RC, Imai M*, et al.* Chronic electrical stimulation of the carotid sinus baroreflex improves left ventricular function and promotes reversal of ventricular remodeling in dogs with advanced heart failure. *Circ Heart Fail* **4**, 65-70 (2011).

31. Gronda E, Seravalle G, Brambilla G*, et al.* Chronic baroreflex activation effects on sympathetic nerve traffic, baroreflex function, and cardiac haemodynamics in heart failure: a proof-of-concept study. *European journal of heart failure* **16**, 977-983 (2014).

32. Abraham WT, Zile MR, Weaver FA*, et al.* Baroreflex Activation Therapy for the Treatment of Heart Failure With a Reduced Ejection Fraction. *JACC Heart Fail* **3**, 487-496 (2015).

33. Wang HJ, Rozanski GJ, Zucker IH. Cardiac sympathetic afferent reflex control of cardiac function in normal and chronic heart failure states. *The Journal of physiology* **595**, 2519-2534 (2017).

34. Malliani A, Montano N. Emerging excitatory role of cardiovascular sympathetic afferents in pathophysiological conditions. *Hypertension (Dallas, Tex : 1979)* **39**, 63-68 (2002).

35. Wang HJ, Wang W, Cornish KG, Rozanski GJ, Zucker IH. Cardiac sympathetic afferent denervation attenuates cardiac remodeling and improves cardiovascular dysfunction in rats with heart failure. *Hypertension (Dallas, Tex : 1979)* **64**, 745-755 (2014).

36. Zhu GQ, Xu Y, Zhou LM*, et al.* Enhanced cardiac sympathetic afferent reflex involved in sympathetic overactivity in renovascular hypertensive rats. *Exp Physiol* **94**, 785-794 (2009).

37. Du YH, Chen AF. A "love triangle" elicited by electrochemistry: complex interactions among cardiac sympathetic afferent, chemo-, and baroreflexes. *Journal of applied physiology (Bethesda, Md : 1985)* **102**, 9-10 (2007).

38. Karai L, Brown DC, Mannes AJ*, et al.* Deletion of vanilloid receptor 1-expressing primary afferent neurons for pain control. *The Journal of clinical investigation* **113**, 1344-1352 (2004).

39. Sapio MR, Neubert JK, LaPaglia DM*, et al.* Pain control through selective chemo-axotomy of centrally projecting TRPV1+ sensory neurons. *The Journal of clinical investigation* **128**, 1657-1670 (2018).

40. Shanks J, Xia Z, Lisco SJ*, et al.* Sympatho-excitatory response to pulmonary chemosensitive spinal afferent activation in anesthetized, vagotomized rats. *Physiological reports* **6**, e13742 (2018).

41. von Banchet GS, Schaible HG. Localization of the neurokinin 1 receptor on a subset of substance P-positive and isolectin B4-negative dorsal root ganglion neurons of the rat. *Neuroscience letters* **274**, 175-178 (1999).

42. Wang WZ, Gao L, Wang HJ, Zucker IH, Wang W. Interaction between cardiac sympathetic afferent reflex and chemoreflex is mediated by the NTS AT1 receptors in heart failure. *American journal of physiology Heart and circulatory physiology* **295**, H1216-h1226 (2008).

43. Glass DJ. Signalling pathways that mediate skeletal muscle hypertrophy and atrophy. *Nature cell biology* **5**, 87-90 (2003).

44. Sullivan MJ, Green HJ, Cobb FR. Skeletal muscle biochemistry and histology in ambulatory patients with long-term heart failure. *Circulation* **81**, 518-527 (1990).

45. Mancia G. Neurohumoral activation in congestive heart failure. *American heart journal* **120**, 1532-1537 (1990).

46. Malliani A, Lombardi F. Circulatory markers of nervous activation during myocardial ischemia. *The Canadian journal of cardiology* **Suppl A**, 40a-45a (1986).

47. Zucker IH, Wang W. Reflex control of renal sympathetic nervous activity in heart failure. *Herz* **16**, 82-91 (1991).

48. Mahfoud F, Lüscher TF, Andersson B*, et al.* Expert consensus document from the European Society of Cardiology on catheter-based renal denervation. *European heart journal* **34**, 2149-2157 (2013).

49. Kandzari DE, Böhm M, Mahfoud F*, et al.* Effect of renal denervation on blood pressure in the presence of antihypertensive drugs: 6-month efficacy and safety results from the SPYRAL HTN-ON MED proof-of-concept randomised trial. *Lancet* **391**, 2346-2355 (2018).

50. Azizi M, Schmieder RE, Mahfoud F*, et al.* Endovascular ultrasound renal denervation to treat hypertension (RADIANCE-HTN SOLO): a multicentre, international, single-blind, randomised, sham-controlled trial. *Lancet* **391**, 2335-2345 (2018).

51. Townsend RR, Mahfoud F, Kandzari DE*, et al.* Catheter-based renal denervation in patients with uncontrolled hypertension in the absence of antihypertensive medications (SPYRAL HTN-OFF MED): a randomised, sham-controlled, proof-of-concept trial. *Lancet* **390**, 2160-2170 (2017).

52. Kshatriya S, Kozman H, Siddiqui D*, et al.* The kidney in heart failure: friend or foe? *Am J Med Sci* **344**, 228-232 (2012).

53. Hasking GJ, Esler MD, Jennings GL, Burton D, Johns JA, Korner PI. Norepinephrine spillover to plasma in patients with congestive heart failure: evidence of increased overall and cardiorenal sympathetic nervous activity. *Circulation* **73**, 615-621 (1986).

54. Dzau VJ, Colucci WS, Hollenberg NK, Williams GH. Relation of the renin-angiotensin-aldosterone system to clinical state in congestive heart failure. *Circulation* **63**, 645-651 (1981).

55. Booth LC, May CN, Yao ST. The role of the renal afferent and efferent nerve fibers in heart failure. *Frontiers in physiology* **6**, 270 (2015).

56. Schiller AM, Pellegrino PR, Zucker IH. The renal nerves in chronic heart failure: efferent and afferent mechanisms. *Frontiers in physiology* **6**, 224 (2015).

57. Krum H, Schlaich M, Whitbourn R*, et al.* Catheter-based renal sympathetic denervation for resistant hypertension: a multicentre safety and proof-of-principle cohort study. *Lancet* **373**, 1275-1281 (2009).

58. Villarreal D, Freeman RH, Johnson RA, Simmons JC. Effects of renal denervation on postprandial sodium excretion in experimental heart failure. *The American journal of physiology* **266**, R1599-1604 (1994).

59. Villarreal D, Freeman RH, Johnson RA. Neurohumoral modulators and sodium balance in experimental heart failure. *The American journal of physiology* **264**, H1187-1193 (1993).

60. Souza DR, Mill JG, Cabral AM. Chronic experimental myocardial infarction produces antinatriuresis by a renal nerve-dependent mechanism. *Braz J Med Biol Res* **37**, 285-293 (2004).

61. Sharp TE, 3rd, Polhemus DJ, Li Z*, et al.* Renal Denervation Prevents Heart Failure Progression Via Inhibition of the Renin-Angiotensin System. *Journal of the American College of Cardiology* **72**, 2609-2621 (2018).

62. Sharp TE, 3rd, Polhemus DJ, Li Z*, et al.* Renal Denervation Prevents Heart Failure Progression Via Inhibition of the Renin-Angiotensin System.

63. Watanabe H, Iwanaga Y, Miyaji Y, Yamamoto H, Miyazaki S. Renal denervation mitigates cardiac remodeling and renal damage in Dahl rats: a comparison with β-receptor blockade.

64. Clayton SC, Haack KK, Zucker IH. Renal denervation modulates angiotensin receptor expression in the renal cortex of rabbits with chronic heart failure. *American journal of physiology Renal physiology* **300**, F31-39 (2011).

65. Polhemus DJ, Trivedi RK, Gao J*, et al.* Renal Sympathetic Denervation Protects the Failing Heart Via Inhibition of Neprilysin Activity in the Kidney. *Journal of the American College of Cardiology* **70**, 2139-2153 (2017).

66. DiBona GF, Sawin LL. Role of renal nerves in sodium retention of cirrhosis and congestive heart failure. *The American journal of physiology* **260**, R298-305 (1991).

67. Chen W, Ling Z, Xu Y*, et al.* Preliminary effects of renal denervation with saline irrigated catheter on cardiac systolic function in patients with heart failure: A Prospective, Randomized, Controlled, Pilot Study. *Catheter Cardiovasc Interv* **89**, E153-e161 (2017).

68. Dai Q, Lu J, Wang B, Ma G. Effect of percutaneous renal sympathetic nerve radiofrequency ablation in patients with severe heart failure. *Int J Clin Exp Med* **8**, 9779-9785 (2015).

69. Davies JE, Manisty CH, Petraco R*, et al.* First-in-man safety evaluation of renal denervation for chronic systolic heart failure: primary outcome from REACH-Pilot study. *International journal of cardiology* **162**, 189-192 (2013).

70. Gao JQ, Xie Y, Yang W, Zheng JP, Liu ZJ. Effects of percutaneous renal sympathetic denervation on cardiac function and exercise tolerance in patients with chronic heart failure. *Rev Port Cardiol* **36**, 45-51 (2017).

71. Gao JQ, Yang W, Liu ZJ. Percutaneous renal artery denervation in patients with chronic systolic heart failure: A randomized controlled trial. *Cardiol J* **26**, 503-510 (2019).

72. Armour JA. Cardiac neuronal hierarchy in health and disease. *American journal of physiology Regulatory, integrative and comparative physiology* **287**, R262-271 (2004).

73. Van Stee EW. Autonomic innervation of the heart. *Environ Health Perspect* **26**, 151-158 (1978).

74. Tzadok M, Harush A, Nissenkorn A, Zauberman Y, Feldman Z, Ben-Zeev B. Clinical outcomes of closed-loop vagal nerve stimulation in patients with refractory epilepsy. *Seizure* **71**, 140-144 (2019).

75. Kubota Y, Nakamoto H, Miyao S, Kawamata T. Efficacy of Vagal Nerve Stimulation for Pharmacoresistant Poststroke Epilepsy. *World Neurosurg* **133**, e448-e451 (2020).

76. Yuan H, Silberstein SD. Vagus Nerve and Vagus Nerve Stimulation, a Comprehensive Review: Part II. *Headache* **56**, 259-266 (2016).

77. Li M, Zheng C, Sato T, Kawada T, Sugimachi M, Sunagawa K. Vagal nerve stimulation markedly improves long-term survival after chronic heart failure in rats. *Circulation* **109**, 120-124 (2004).

78. Zhang Y, Popovic ZB, Bibevski S*, et al.* Chronic vagus nerve stimulation improves autonomic control and attenuates systemic inflammation and heart failure progression in a canine high-rate pacing model. *Circ Heart Fail* **2**, 692-699 (2009).

79. Springer J, Okonko DO, Anker SD. Vagal nerve stimulation in chronic heart failure: an antiinflammatory intervention? *Circulation* **110**, e34; author reply e34 (2004).

80. Premchand RK, Sharma K, Mittal S*, et al.* Autonomic regulation therapy via left or right cervical vagus nerve stimulation in patients with chronic heart failure: results of the ANTHEM-HF trial. *Journal of cardiac failure* **20**, 808-816 (2014).

81. Zannad F, De Ferrari GM, Tuinenburg AE*, et al.* Chronic vagal stimulation for the treatment of low ejection fraction heart failure: results of the NEural Cardiac TherApy foR Heart Failure (NECTAR-HF) randomized controlled trial. *European heart journal* **36**, 425-433 (2015).

82. Gold MR, Van Veldhuisen DJ, Hauptman PJ*, et al.* Vagus Nerve Stimulation for the Treatment of Heart Failure: The INOVATE-HF Trial. *Journal of the American College of Cardiology* **68**, 149-158 (2016).

83. Song JJ, Popescu A, Bell RL. Present and potential use of spinal cord stimulation to control chronic pain. *Pain Physician* **17**, 235-246 (2014).

84. Murphy DF, Giles KE. Dorsal column stimulation for pain relief from intractable angina pectoris. *Pain* **28**, 365-368 (1987).

85. Olgin JE, Takahashi T, Wilson E, Vereckei A, Steinberg H, Zipes DP. Effects of thoracic spinal cord stimulation on cardiac autonomic regulation of the sinus and atrioventricular nodes. *J Cardiovasc Electrophysiol* **13**, 475-481 (2002).

86. Lopshire JC, Zhou X, Dusa C*, et al.* Spinal cord stimulation improves ventricular function and reduces ventricular arrhythmias in a canine postinfarction heart failure model. *Circulation* **120**, 286-294 (2009).

87. Liu Y, Yue WS, Liao SY*, et al.* Thoracic spinal cord stimulation improves cardiac contractile function and myocardial oxygen consumption in a porcine model of ischemic heart failure. *J Cardiovasc Electrophysiol* **23**, 534-540 (2012).

88. Tse HF, Turner S, Sanders P*, et al.* Thoracic Spinal Cord Stimulation for Heart Failure as a Restorative Treatment (SCS HEART study): first-in-man experience. *Heart rhythm* **12**, 588-595 (2015).

89. Lloyd-Jones D, Adams R, Carnethon M*, et al.* Heart disease and stroke statistics--2009 update: a report from the American Heart Association Statistics Committee and Stroke Statistics Subcommittee. *Circulation* **119**, e21-181 (2009).

90. Schefold JC, Filippatos G, Hasenfuss G, Anker SD, von Haehling S. Heart failure and kidney dysfunction: epidemiology, mechanisms and management. *Nature reviews Nephrology* **12**, 610-623 (2016).

91. Nohria A, Hasselblad V, Stebbins A*, et al.* Cardiorenal interactions: insights from the ESCAPE trial. *Journal of the American College of Cardiology* **51**, 1268-1274 (2008).

92. Wang WZ, Gao L, Pan YX, Zucker IH, Wang W. AT1 receptors in the nucleus tractus solitarii mediate the interaction between the baroreflex and the cardiac sympathetic afferent reflex in anesthetized rats. *American journal of physiology Regulatory, integrative and comparative physiology* **292**, R1137-1145 (2007).

93. Zahner MR, Li DP, Chen SR, Pan HL. Cardiac vanilloid receptor 1-expressing afferent nerves and their role in the cardiogenic sympathetic reflex in rats. *The Journal of physiology* **551**, 515-523 (2003).

94. Boesen EI. ET(A) receptor activation contributes to T cell accumulation in the kidney following ischemia-reperfusion injury. *Physiological reports* **6**, e13865 (2018).

95. Martin M. Cutadapt removes adapter sequences from high-throughput sequencing reads. *EMBnetjournal* **27**, 10-12 (2011).

96. Dobin A, Davis CA, Schlesinger F*, et al.* STAR: ultrafast universal RNA-seq aligner. *Bioinformatics (Oxford, England)* **29**, 15-21 (2013).

97. Love MI, Huber W, Anders S. Moderated estimation of fold change and dispersion for RNA-seq data with DESeq2. *Genome Biol* **15**, 550 (2014).

98. Benjamini Y, Hochberg Y. Controlling the False Discovery Rate: A Practical and Powerful Approach to Multiple Testing. *Journal of the Royal Statistical Society: Series B (Methodological)* **57**, 289-300 (1995).

99. Bindea G, Mlecnik B, Hackl H*, et al.* ClueGO: a Cytoscape plug-in to decipher functionally grouped gene ontology and pathway annotation networks. *Bioinformatics (Oxford, England)* **25**, 1091-1093 (2009).

100. Blighe K, Rana S, Lewis M. EnhancedVolcano: Publication-ready volcano plots with enhanced colouring and labeling. R package version 1.4.0, https://github.com/kevinblighe/EnhancedVolcano. (2019).

101. Hahka TM, Xia Z, Hong J*, et al.* Resiniferatoxin (RTX) ameliorates acute respiratory distress syndrome (ARDS) in a rodent model of lung injury. *bioRxiv*, 2020.2009.2014.296731 (2020).

102. Gao L, Schultz HD, Patel KP, Zucker IH, Wang W. Augmented input from cardiac sympathetic afferents inhibits baroreflex in rats with heart failure. *Hypertension (Dallas, Tex : 1979)* **45**, 1173-1181 (2005).

103. Weir MR. Microalbuminuria and cardiovascular disease. *Clinical journal of the American Society of Nephrology : CJASN* **2**, 581-590 (2007).

104. van Deursen VM, Urso R, Laroche C*, et al.* Co-morbidities in patients with heart failure: an analysis of the European Heart Failure Pilot Survey. *European journal of heart failure* **16**, 103-111 (2014).

105. Lekawanvijit S, Kompa AR, Zhang Y, Wang BH, Kelly DJ, Krum H. Myocardial infarction impairs renal function, induces renal interstitial fibrosis, and increases renal KIM-1 expression: implications for cardiorenal syndrome. *American journal of physiology Heart and circulatory physiology* **302**, H1884-1893 (2012).

106. Toschi-Dias E, Rondon M, Cogliati C, Paolocci N, Tobaldini E, Montano N. Contribution of Autonomic Reflexes to the Hyperadrenergic State in Heart Failure. *Front Neurosci* **11**, 162 (2017).

107. Wang W, Zucker IH. Cardiac sympathetic afferent reflex in dogs with congestive heart failure. *The American journal of physiology* **271**, R751-756 (1996).

108. van Timmeren MM, van den Heuvel MC, Bailly V, Bakker SJ, van Goor H, Stegeman CA. Tubular kidney injury molecule-1 (KIM-1) in human renal disease. *J Pathol* **212**, 209-217 (2007).

109. Ajay AK, Kim TM, Ramirez-Gonzalez V, Park PJ, Frank DA, Vaidya VS. A bioinformatics approach identifies signal transducer and activator of transcription-3 and checkpoint kinase 1 as upstream regulators of kidney injury molecule-1 after kidney injury. *Journal of the American Society of Nephrology : JASN* **25**, 105-118 (2014).

110. Ruiz-Ortega M, Ruperez M, Lorenzo O*, et al.* Angiotensin II regulates the synthesis of proinflammatory cytokines and chemokines in the kidney. *Kidney Int Suppl*, S12-22 (2002).

111. Kawai M, Naruse K, Komatsu S*, et al.* Mechanical stress-dependent secretion of interleukin 6 by endothelial cells after portal vein embolization: clinical and experimental studies. *J Hepatol* **37**, 240-246 (2002).

112. Wang BW, Chang H, Lin S, Kuan P, Shyu KG. Induction of matrix metalloproteinases-14 and -2 by cyclical mechanical stretch is mediated by tumor necrosis factor-alpha in cultured human umbilical vein endothelial cells. *Cardiovasc Res* **59**, 460-469 (2003).

113. Colombo PC, Rastogi S, Onat D*, et al.* Activation of endothelial cells in conduit veins of dogs with heart failure and veins of normal dogs after vascular stretch by acute volume loading. *Journal of cardiac failure* **15**, 457-463 (2009).

114. Docherty NG, O'Sullivan OE, Healy DA, Fitzpatrick JM, Watson RW. Evidence that inhibition of tubular cell apoptosis protects against renal damage and development of fibrosis following ureteric obstruction. *American journal of physiology Renal physiology* **290**, F4-13 (2006).

115. Aboryag NB, Mohamed DM, Dehe L*, et al.* Histopathological Changes in the Kidney following Congestive Heart Failure by Volume Overload in Rats. *Oxidative medicine and cellular longevity* **2017**, 6894040 (2017).

116. Fine LG, Bandyopadhay D, Norman JT. Is there a common mechanism for the progression of different types of renal diseases other than proteinuria? Towards the unifying theme of chronic hypoxia. *Kidney Int Suppl* **75**, S22-26 (2000).

117. Veach RA, Wilson MH. CRISPR/Cas9 engineering of a KIM-1 reporter human proximal tubule cell line. *PLoS One* **13**, e0204487 (2018).

118. Ohashi R, Kitamura H, Yamanaka N. Peritubular capillary injury during the progression of experimental glomerulonephritis in rats. *Journal of the American Society of Nephrology : JASN* **11**, 47-56 (2000).

119. Goldsmith SR. Arginine vasopressin antagonism in heart failure: Current status and possible new directions. *J Cardiol* **74**, 49-52 (2019).

120. Affleck VS, Coote JH, Pyner S. The projection and synaptic organisation of NTS afferent connections with presympathetic neurons, GABA and nNOS neurons in the paraventricular nucleus of the hypothalamus. *Neuroscience* **219**, 48-61 (2012).

121. Kanazawa K, Adachi S, Yoshiya N, Honma S, Takahashi H, Takeuchi S. Establishment and characterization of a subline predisposed to pulmonary metastasis from a human gestational choriocarcinoma cell line in nude mice. *Acta Obstet Gynecol Scand* **68**, 429-434 (1989).

122. Mattson DL. Immune mechanisms of salt-sensitive hypertension and renal end-organ damage. *Nature reviews Nephrology* **15**, 290-300 (2019).

123. Wang M, Han W, Zhang M*, et al.* Long-term renal sympathetic denervation ameliorates renal fibrosis and delays the onset of hypertension in spontaneously hypertensive rats. *Am J Transl Res* **10**, 4042-4053 (2018).

124. Nozawa T, Igawa A, Fujii N*, et al.* Effects of long-term renal sympathetic denervation on heart failure after myocardial infarction in rats. *Heart Vessels* **16**, 51-56 (2002).

125. Watanabe H, Iwanaga Y, Miyaji Y, Yamamoto H, Miyazaki S. Renal denervation mitigates cardiac remodeling and renal damage in Dahl rats: a comparison with β-receptor blockade. *Hypertens Res* **39**, 217-226 (2016).

126. Zheng H, Katsurada K, Liu X, Knuepfer MM, Patel KP. Specific Afferent Renal Denervation Prevents Reduction in Neuronal Nitric Oxide Synthase Within the Paraventricular Nucleus in Rats With Chronic Heart Failure. *Hypertension (Dallas, Tex : 1979)* **72**, 667-675 (2018).

127. Foss JD, Wainford RD, Engeland WC, Fink GD, Osborn JW. A novel method of selective ablation of afferent renal nerves by periaxonal application of capsaicin. *American journal of physiology Regulatory, integrative and comparative physiology* **308**, R112-122 (2015).

128. Yancy CW, Jessup M, Bozkurt B*, et al.* 2013 ACCF/AHA guideline for the management of heart failure: a report of the American College of Cardiology Foundation/American Heart Association Task Force on Practice Guidelines. *Journal of the American College of Cardiology* **62**, e147-239 (2013).

129. Schirmer SH, Sayed MM, Reil JC*, et al.* Improvements in left ventricular hypertrophy and diastolic function following renal denervation: effects beyond blood pressure and heart rate reduction. *Journal of the American College of Cardiology* **63**, 1916-1923 (2014).

130. Schiller AM, Haack KK, Pellegrino PR, Curry PL, Zucker IH. Unilateral renal denervation improves autonomic balance in conscious rabbits with chronic heart failure. *American journal of physiology Regulatory, integrative and comparative physiology* **305**, R886-892 (2013).

131. Moher D, Liberati A, Tetzlaff J, Altman DG. Preferred reporting items for systematic reviews and meta-analyses: the PRISMA statement. *Ann Intern Med* **151**, 264-269, w264 (2009).

132. Stroup DF, Berlin JA, Morton SC*, et al.* Meta-analysis of observational studies in epidemiology: a proposal for reporting. Meta-analysis Of Observational Studies in Epidemiology (MOOSE) group. *Jama* **283**, 2008-2012 (2000).

133. Higgins JPT, Deeks JJe. Chapter 7: Selecting studies and collecting data. In: Higgins J.P.T., Green, S. (editors), Cochrane Handbook for Systematic Reviews of Interventions Version 5.1.0 (updated March 2011). The Cochrane Collaboration, 2011. Available from www.handbook.cochrane.org.

134. Wells G, Shea B, O'Connell D*, et al.* The Newcastle–Ottawa Scale (NOS) for Assessing the Quality of Non-Randomized Studies in Meta-Analysis. , (2000).

135. Hopper I, Gronda E, Hoppe UC*, et al.* Sympathetic Response and Outcomes Following Renal Denervation in Patients With Chronic Heart Failure: 12-Month Outcomes From the Symplicity HF Feasibility Study. *Journal of cardiac failure* **23**, 702-707 (2017).

136. Drozdz T, Jastrzebski M, Moskal P*, et al.* Renal denervation in patients with symptomatic chronic heart failure despite resynchronization therapy - a pilot study. *Adv Interv Cardiol* **15**, 240-246 (2019).

137. Esler MD, Krum H, Sobotka PA, Schlaich MP, Schmieder RE, Böhm M. Renal sympathetic denervation in patients with treatment-resistant hypertension (The Symplicity HTN-2 Trial): a randomised controlled trial. *Lancet* **376**, 1903-1909 (2010).

138. Bhatt DL, Kandzari DE, O'Neill WW*, et al.* A controlled trial of renal denervation for resistant hypertension. *The New England journal of medicine* **370**, 1393-1401 (2014).

139. Azizi M, Sapoval M, Gosse P*, et al.* Optimum and stepped care standardised antihypertensive treatment with or without renal denervation for resistant hypertension (DENERHTN): a multicentre, open-label, randomised controlled trial. *Lancet* **385**, 1957-1965 (2015).

140. Ott C, Mahfoud F, Schmid A*, et al.* Renal denervation preserves renal function in patients with chronic kidney disease and resistant hypertension. *J Hypertens* **33**, 1261-1266 (2015).

141. Liu H, Chen W, Lai Y*, et al.* Selective Renal Denervation Guided by Renal Nerve Stimulation in Canine. *Hypertension (Dallas, Tex : 1979)* **74**, 536-545 (2019).

142. Pellegrino PR, Zucker IH, Chatzizisis YS, Wang HJ, Schiller AM. Quantification of Renal Sympathetic Vasomotion as a Novel End Point for Renal Denervation. *Hypertension (Dallas, Tex : 1979)* **76**, 1247-1255 (2020).

143. Iadarola MJ, Sapio MR, Raithel SJ, Mannes AJ, Brown DC. Long-term pain relief in canine osteoarthritis by a single intra-articular injection of resiniferatoxin, a potent TRPV1 agonist. *Pain* **159**, 2105-2114 (2018).

144. Brown DC, Agnello K, Iadarola MJ. Intrathecal resiniferatoxin in a dog model: efficacy in bone cancer pain. *Pain* **156**, 1018-1024 (2015).